#01

ADVANCED DIAGNOSTIC TECHNIQUES FOR THREE-PHASE SLURRY BUBBLE COLUMN REACTORS (SBCR)

Annual Technical Progress Report No. 1
for the Period July 1, 1999 – June 30, 2000
DE-FG-26-99FT40594

Principal Investigators:

M.H. Al-Dahhan
Assistant Professor and Associate Director
Chemical Reaction Engineering Laboratory

Washington University
Department of Chemical Engineering
Campus Box 1198
One Brookings Drive
St. Louis, Missouri 63130
Fax: 314-935-4832
Phone: 314-935-7187
E-mail: muthanna@che.wustl.edu

M.P. Dudukovic
The Laura and William Jens
Professor and Chairman
Director, Chemical Reaction Engineering
Laboratory

Washington University
Department of Chemical Engineering
Campus Box 1198
One Brookings Drive
St. Louis, Missouri 63130
Fax: 314-935-4832
Phone: 314-935-6021
E-mail: dudu@wuche3.wustl.edu

L.-S. Fan
Distinguished University Professor
Chairman, Department of Chemical
Engineering

Ohio State University
Department of Chemical Engineering
140 West 19th Avenue-Room 125
Columbus, Ohio 43210-1180
Fax: 614-292-3769
Phone: 614-292-7907
E-mail: FAN@er6s1.eng.ohio-state.edu

Industrial Collaborator

B. Toseland — Air Products and Chemicals

Co-Investigators

Washington University: N. Rados, Dr. A. Kemoun, Dr. Y. Wu
Ohio State University: R. Lau, W. Peng

July 25, 2000

Prepared for the United States Department of Energy
Award No. DE-FG-26-99FT40594
Award Period: July 1, 1999 – June 30, 2002

Disclaimer

ADVANCED DIAGNOSTIC TECHNIQUES FOR THREE-PHASE SLURRY BUBBLE COLUMN REACTORS (SBCR)

Annual Technical Progress Report No. 1
for the Period July 1, 1999 – June 30, 2000
DE-FG-26-99FT40594

ABSTRACT

This report summarizes the accomplishment made during the first year of this cooperative research effort between Washington University, Ohio State University and Air Products and Chemicals. A technical review of the variables affecting SBCR performance, some aspects of bubble dynamics and hydrodynamics properties and physical properties of FT waxes and catalyst have been performed. The needed experimental facilities and measurement techniques have been evaluated and prepared. Exxon Norpar 14 has been suggested as a solvent to be used that mimics at room temperature and pressure up to 200 psi the hydrodynamics of FT waxes. A new correlation has been developed and tested to predict gas-liquid mass transfer coefficient at high pressure operation based on high pressure gas holdup and atmospheric data of gas-liquid mass transfer coefficient.

ADVANCED DIAGNOSTIC TECHNIQUES FOR THREE-PHASE SLURRY BUBBLE COLUMN REACTORS (SBCR)

Annual Technical Progress Report No. 1
for the Period July 1, 1999 – June 30, 2000
DE-FG-26-99FT40594

TABLE OF CONTENTS

LIST OF FIGURES

LIST OF TABLES

ADVANCED DIAGNOSTIC TECHNIQUES FOR THREE-PHASE SLURRY BUBBLE COLUMN REACTORS (SBCR)

Annual Technical Progress Report No. 1
for the Period July 1, 1999 – June 30, 2000
DE-FG-26-99FT40594

EXECUTIVE SUMMARY

The objective of this cooperative research effort between Washington University, Ohio State University and Air Products and Chemicals is to advance the understanding of the hydrodynamics of Fischer-Tropsch (FT) Slurry Bubble Column Reactors (SBCR) via advanced diagnostics techniques. The emphasis during this first year was: i) on technical review of the variables affecting SBCR performance, some aspects of bubble dynamics and hydrodynamic properties and the physical properties of FT waxes and catalyst, ii) on preparation of the experimental facilities and the advanced measurement techniques, iii) on identifying the solvent that mimic FT waxes at FT operating conditions and the gas and solid phase to be used in the hydrodynamics investigation, v) on development of a new procedure to estimate the mass transfer coefficient at high pressure based on atmospheric pressure data.

This report summarizes the accomplishments made during the first year of this project. The report is organized in individual sections. Each section represents a distinct task.

Section 1 provides an introduction, a review of the objectives and tasks set for the project, list of accomplishments during the first year and plans for the second year.

Section 2 summarizes the technical review made. However, the detailed review of the aspects of high-pressure phenomena of bubbles in liquids and liquid-solid suspensions is discussed in Appendix A.

Section 3 describes the preparation made for the advanced techniques that will be used in the hydrodynamic investigations and for the in-situ physical properties (density, viscosity and surface tension) measurement of the selected solvent that mimic the FT waxes at FT operating conditions.

In section 4, the suggested system of air-Exxon Norpar 14-glass beads has been identified. Exxon Norpar 14 mimics at room temperature and pressure up to 200 psi the hydrodynamics of FT waxes.

Section 5 discusses the development of a new correlation to predict gas-liquid mass transfer coefficient at high pressure operation based on high pressure gas holdup and atmospheric data of gas-liquid mass transfer coefficient. This is part of the attempt to improve the scale-up procedure of bubble column reactors.

1. INTRODUCTION AND MOTIVATION

Synthesis gas (mixture of carbon monoxide and hydrogen) from coal is one of the most abundant and reliable sources of energy and chemicals. Fischer-Tropsch (FT) Chemistry is an acknowledged route for clean utilization of coal-derived synthesis gas in production of fuels and chemicals. Based on reaction engineering considerations and economics (i.e., from the heat transfer and high volumetric productivity viewpoints), slurry bubble column reactors (SBCR) operated at high gas velocities in churn turbulent flow regime are the preferred reactors for commercialization of FT synthesis.

Reliable data and tested models or theory for design and scale-up of SBCR for FT synthesis are currently not available. In response to this need, the Department of Energy (DOE) initiated the Hydrodynamics Initiative which focuses on advancing the state of the art in understanding the fluid dynamics of slurry bubble columns and replacing empirical design methods with a more rational approach.

As a part of this initiative DOE has awarded the DE-FG-26-99FT40594 grant for a collaborative effort between Washington University (WU), Ohio State University (OSU) and Air Products and Chemicals, Inc. (APCI) to advance the knowledge and understanding of the hydrodynamics of FT SBCR. The overall goals of this grant are: to search and select a system that simulate the microstructure of FT waxes and mimic their hydrodynamics at low temperature and pressure up to 10 atm, to study the microstructure of the gas-liquid-solid mixtures in a comparable fluid to FT waxes in 2 inch diameter column and develop a fundamental understanding as to how important the physical and fluid dynamic properties can be "finger-printed" via various diagnostic techniques (such as particle image velocimetry, PIV) or laser doppler anemometry (LDA), optical probe, dynamic gas disengagement (DGD) and differential pressure fluctuation technique) and to measure large scale hydrodynamic parameters at high pressure and high gas velocity in a 6 inch diameter slurry bubble column using computed tomography (CT) and computer automated radioactive particle tracking (CARPT) . CARPT and CT are the only non-invasive techniques that can provide information on slurry velocity and density profiles in the whole column. Such data provides a firm scientific and engineering basis for scale-up and design of FT SBCR. The resulting findings can be utilized as a benchmark to validate the computational fluid dynamic codes.

This grant enables a unique integration of the expertise of the two universities (WU and OSU) and industry (APCI) towards achieving the goals set as a part of the DOE Hydrodynamics Initiative. This study complements well the work in progress at CREL-WU, OSU, Iowa State University (ISU) and Sandia National Laboratory, Contract No. DE-FC-22-95PC95051, related to the LaPorte Advanced Fuels Demonstration Unit (AFDU) operated by Air Products with the Department of Energy funding.

1.1 Slurry Bubble Column Reactors (SBCR)

A slurry bubble column reactor (SBCR) is a cylindrical vessel in which gas is sparged through a batch slurry (liquid and small particles) or a flowing slurry (Figure 1.1). The gas superficial velocities are order of magnitude larger than those of the liquid so that it is the gas that governs the fluid dynamics of the system. Small slurry particles follow the liquid phase in SBCR. It is well known that fluid dynamics (phase velocities and holdup distribution) affect the phase mixing and transport (gas-liquid interfacial area, transport coefficients) between the phases, and hence, to a large extent affect the conversion and selectivity as shown in Figure 1.1. If the reaction involves phase volume changes (e.g. gas is either consumed or produced), the phase mixing, and transport parameters are affected along the column. Thus quantitative knowledge of fluid dynamics is essential for rational and predictive reactor design and scale-up.

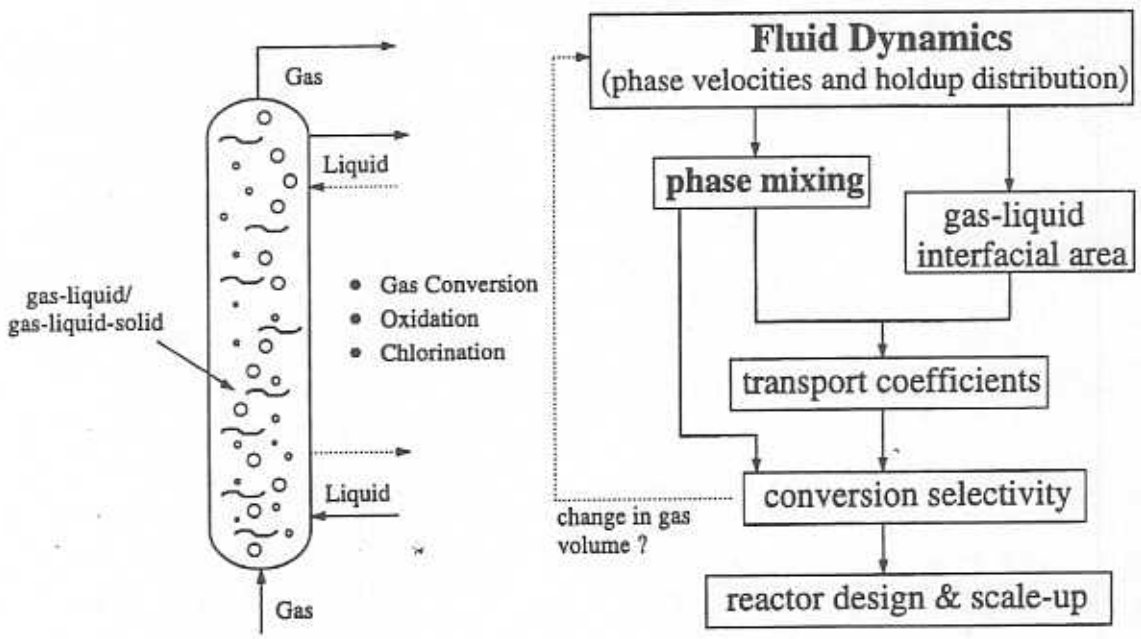

Figure 1.1. Slurry bubble column and the integrated effects of the phase mixing and transport on the reactor design and scale-up.

1.2 Overall Objectives

The overall objectives of this cooperative university (WU and OSU)-industry (APCI) research is to advance the understanding of the hydrodynamics of FT SBCR via advanced diagnostics techniques. The goals set for these projects are as follows:

TASK 1: Literature Review
- Physicochemical properties and their effect on the hydrodynamics of bubble columns.
- Models used to predict FT reactor performance.

TASK 2: Based on Task 1, identify the range of intrinsic properties (density, viscosity and surface tension) of the fluids used for the FT synthesis.
- Identify a solvent that, at room temperature and pressure up to 200 psig, will mimic the hydrodynamics of FT wax (at FT reaction conditions).
- Measure the intrinsic properties (density, surface tension, viscosity) of the identified solvent at room temperature and pressure up to 200 psig in a 2" diameter column.
- Identify the particle type and size to be used.

TASK 3: Using the identified system (solvent-particle-air), perform the following investigation on the hydrodynamics in a 2" diameter column:
- Using Laser Doppler Anemometer (LDA) or Particle Image Velocimetry (PIV) investigate the effect of reactor pressure on the flow field and turbulent parameters.
- Using Δp fluctuation measurements to identify the flow regime transition and investigate the effect of reactor pressure on the flow regime transition.
- Overall gas holdup.
- Bubble size and bubble rise velocity using optical probe.

TASK 4: Using the identified system in Task 2, investigate the hydrodynamics in a 6" diameter column via CT and CARPT techniques. The following will be measured:
- Phase distribution profiles using CT/CARPT/ Δp
- Flow field and turbulent parameters using CARPT
- Overall gas holdup

TASK 5: Evaluate scale-up procedure for slurry bubble column. Develop additional correlations, if needed.

TASK 6: As a case study, examine the available CFD and mechanistic models against the newly obtained data.

TASK 7: Final report.

1.3 Accomplishments During the First Year

The first year was dedicated to the technical review preparation of the experimental facilities and the advanced measurement techniques. A new correlation was developed to predict the liquid-solid mass transfer coefficient in high pressure bubble column based on the atmospheric pressure data. The accomplishments were as follows:

1. Technical review of the variable affecting SBCR performance, some aspects of bubble dynamics and hydrodynamic properties and the physical properties of FT waxes and catalyst have been performed.
2. Preparation of the experimental facilities and the advanced measurement techniques. The preparation includes the following units:
   - High pressure (up to 3000 psi) and high temperature (up to 250°C) 2-inch diameter slurry bubble column set-up.
   - High pressure (up to 200 psi) 6-inch diameter slurry bubble column set-up. Two facilities will be used; one for computer automated radioactive particle tracking (CARPT) and computed tomography (CT) techniques and another one for pressure drop measurements. The later facility consists of a 6-inch diameter column equipped with 6- windows and 15 ports along the column.
   - Particle Image Velocimetry (PIV) and Laser Doppler Anemometry (LDA) for 2" slurry bubble column facility.
   - CARPT and CT for 6-inch slurry bubble column facility.
   - Techniques to measure in situ the intrinsic density, viscosity and surface tension of the liquid phase that will be used for hydrodynamics investigation which mimic the hydrodynamics of FT waxes.
3. Identify the solvent that mimic FT waxes at FT operating conditions and the gas and solid phases to be used in the hydrodynamics investigation.
4. Development of a new procedure to estimate the mass transfer coefficient at high pressure based on atmospheric pressure data.

1.4 Plan for the Next Year

The following represents an outline of the tentative plan set for the next year (July 1, 2000 to June 30, 2001).

- Measure in situ the intrinsic properties (density, viscosity, surface tension) of the identified solvent that has properties within the range of FT waxes properties.
- Initiate the experimental investigations of the hydrodynamics using the identified system in 2-inch diameter column via LDA or PIV, optical probe and dynamic pressure drop measurements.
- Initiate the experimental investigation of the hydrodynamics using the identified system in 6"-inch diameter column via CARPT, CT and dynamic pressure drop measurements.
- Continue the hydrodynamic parameters modeling and initiate the computational fluid dynamic (CFD) work using the available codes (e.g. CFDLIB, Fluent).

2. TECHNICAL REVIEW

2.1 Variables Affecting Slurry Bubble Column (SBCR) Performance

A slurry bubble column reactor (SBCR) is usually a cylindrical vessel in which gas (containing one or more reactants, e.g. synthesis gas for FT processes) is sparged through the liquid (containing liquid reactant(s) and products), and a finely dispersed catalyst. As long as the operating liquid superficial velocity (in the range of 0 to 2 cm/s) is an order of magnitude smaller than the superficial velocity of the gas (1 to 30 cm/s), and the catalyst particles are small (less than 50 μm) and not excessively heavy, the gas dominates the hydrodynamics and, by buoyancy forces resulting from the nonuniform cross-sectional gas holdup distribution induces liquid velocities order of magnitude larger than the liquid superficial velocity. The finely dispersed catalyst follows the motion of the liquid.

Interpretation of SBCR performance must rely on an appropriate model which properly accounts for the events on the molecular scale (e.g. kinetics and catalyst particle performance, etc.), micro-scale (e.g. transport of reactants and products to and from the catalyst particle and of reactants from gas bubbles to the liquid) and macro-scale (e.g. liquid backmixing) on heat transfer and reactor performance. We know that numerous design and operating variables, listed in Figure 2.1, and physicochemical and thermodynamic properties of the fluid affect the many highly interactive phenomena in SBCR. All of these in turn affect reactor performance.

A slurry bubble column reactor for FT synthesis and other syngas processes in order to be economically successful, must operate at high volumetric productivity which requires high activity catalyst, high catalyst loading of the slurry, large gas flow rate and high gas conversion. The ability to achieve complete catalyst suspension and the desired flow pattern (degree of backmixing) of the liquid phase are crucial to the targeted reactor performance. In order to accomplish these an improved understanding and quantification of the key hydrodynamic phenomena is required.

We focus here our attention on properly describing the liquid (slurry) circulation and turbulence in SBCR for Fischer Tropsch synthesis because it is the liquid mixing that affects catalyst distribution, bubble coalescence, gas-liquid interfacial area, mass transfer coefficients and heat transfer from the reactor. We first summarize our current understanding of flow regimes and gas holdup, and their effect on liquid backmixing.

Flow regime affects gas holdup and holdup distribution. The available standard flow maps (e.g. Shah et al., 1982) are old and not very reliable in identifying the flow regime in FT SBCRs. It is commonly assumed, based on evidence of multiple bubble sizes (Patel et al., 1990; De Swart, 1996), that churn-turbulent flow occurs in FT waxes at superficial gas velocities above 5 cm/s. This needs additional verification. Information on characteristic bubble size as well as reliable diagnostic of the flow regime are needed.

Gas holdup is the fraction of the column occupied by gas. As Fan (1989) illustrates, existing older correlations cannot predict holdup accurately and no agreement regarding holdup is reached for Fischer Tropsch waxes (Quicker and Deckwer, 1981). Kemoun *et al.* (2000) studied the effect of pressure on gas holdup and its cross-sectional distribution using γ-ray Computed Tomography (CT) in air-water system at elevated pressures up to

0.7 MPa. The cross-sectional average gas holdup was calculated using the collected data and compared with various correlations found in the literature. Their main findings are:

- At atmospheric pressure, the correlation of Idogawa *et al.* (1985) was in the best agreement with experimental data except for U_G = 0.05 m/s. This operating condition is near the transition point, and the correlation and data may not belong to the same flow regime.
- At higher pressures and over the entire superficial gas velocity range investigated (2 to 30 cm/s), the correlation of Hammer *et al.* (1984) gives the best prediction of gas holdup data (average error of 12-17%) followed by Wilkinson *et al.* (1992; average error of 14-18%) and Idogawa *et al.* (1987; average error of 18-20%).
- At higher pressures and high superficial gas velocity ($U_G > 0.1$ m/s), in addition to the correlations of Idogawa *et al.* (1987), and Hammer *et al.* (1984), the correlation of Krishna *et al.* (1996) and Luo *et al.* (1999) also seem to provide reasonable predictions of the measured gas holdup.

They also concluded that they were not able to find any correlation that consistently predicted their experimental data well under all process conditions, which indicates the need for better characterization of the levels of liquid recirculation and turbulence which are needed for development of a more fundamentally based model for prediction of gas holdups (Fan, 1989).

Radial gas holdup distribution drives liquid recirculation as originally shown by Hills (1974). This distribution depends on operating conditions, physical properties of the system and distributor type (e.g. Chen et al., 1999; Rice and Geary, 1990). It has not been determined in FT SBCRs.

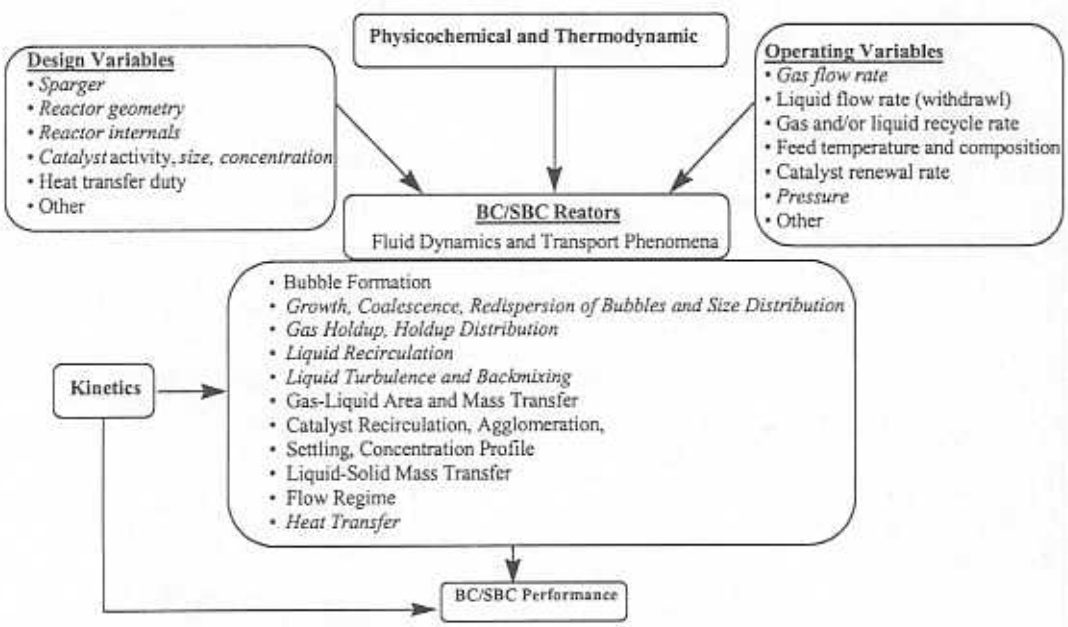

Figure 2.1: Variables that affect SBCR performance

Quantification of liquid backmixing is essential for reactor design, scale-up and interpretation of reactor performance. This is most commonly done by the use of the axial dispersion model. Fan (1989) compares the predictions for the liquid axial dispersion coefficient obtained from various correlations at different gas velocities and in columns of different diameter for the air-water system. The agreement leaves a lot to be desired, which is not surprising since the model assumes a flat velocity profile with eddy axial dispersion superimposed on it. However, the axial liquid velocity profile in a bubble column is anything but flat and, therefore, the axial dispersion coefficient has to account for a variety of mixing mechanisms, including non-uniform velocity, convective transport, bubble wake turbulence, liquid axial and radial turbulence, etc. The dominant mixing mechanism is due to liquid recirculation with contribution from wake and eddy dispersion. Therefore, the correlations reported in the literature, and summarized by Fan (1989), form a poor basis for design/scale-up.

Recently, Degaleesan (1997) has shown that the effective axial dispersion coefficient can be related to liquid recirculation and radial eddy diffusivity via Taylor type diffusivity and to the axial eddy diffusivity. She proposed a scale-up procedure to estimate the fluid dynamic parameters of industrial systems needed for prediction of their performance. The validity of the model proposed by Degaleesan (1997) for evaluation of these parameters on FT systems needs experimental verification.

Liquid recirculation in bubble columns (BC) has been observed and documented by Hills (1974), Rice and Geary (1990) and Devanathan (1991). A novel noninvasive experimental technique, based on monitoring the motion of a single radioactive particle, was used to demonstrate (Devanathan, 1991; Degaleesan 1997) that multiple stationary circulation cells, as proposed by Joshi and Sharma (1979), do not exist. Some preliminary data on slurry recirculation has been reported by Sannaes et al. (1995), Grevskott et al. (1996) and Rados (1999). Additional data in more concentrated slurries is needed.

Mean bubble size and bubble size distribution are also important parameters for SBCR performance, which depends on the flow regime and properties of the system. Insufficient information exists for SBCR in general and for FT systems in particular in spite of the recent work by de Swaart (1996).

2.2 Some aspects of bubble dynamics and hydrodynamic properties

The critical review of high-pressure phenomena of bubbles in liquid and liquid-solid suspension is discussed in Appendix A attached (Fan, et al., 1999). In this section some aspects of bubble dynamics and hydrodynamic properties that are reported in Appendix A are summarized.

2.2.1 Bubble Dynamics

Single bubble rise velocity

In liquid-solid suspensions under elevated pressure and temperature conditions, the bubble rise velocity is discussed in light of both the apparent homogeneous (or effective) properties of the suspension and the recently evolved numerical prediction based on a computational model for gas-liquid-solid fluidization systems. In the literature, it is found that the single bubble rise velocity does not depend on the gas density over the range of

0.1 to 30 kg/m^3. The effects of pressure and temperature, or more directly, the effects of physical properties of the gas and liquid phases on the variation of bubble rise velocity (u_b) with bubble diameter (d_b) could be represented or predicted most generally by the Fan-Tsuchiya equation (Fan and Tsuchiya, 1990) among three predictive equations. The other two are the modified Mendelson's wave-analogy equation (Mendelson, 1967) and a correlation proposed by Tomiyama et al. (1995).

In general, the bubble rise velocity decreases with an increase in pressure for a given solids holdup. A more drastic reduction in u_b can arise from the addition of solid particles. While the particle effect is small at low solids holdup, the effect is appreciable at high solids holdup, especially for high liquid viscosity. The reduction of the bubble rise velocity with an increase in pressure can lead to a significant increase in the gas holdup of three-phase fluidized beds. By comparing the pressure effect on the gas holdup with that on the bubble rise velocity, the increase in gas holdup with pressure is a consequence of the decreases in both the bubble size and the bubble rise velocity.

Heterogeneous approach: Discrete-phase computation

A two-dimensional discrete-phase simulation model for gas-liquid-solid fluidization systems has been developed recently (Jean and Fan, 1990; Luo, et al., 1997; Zhang et al., 1998a,b) to provide a much more thorough scheme of prediction of a single bubble rising in a liquid-solid fluidized bed. In this model, the volume-averaged method, the dispersed particle method (DPM) and the volume-of-fluid (VOF) method are used to account for the flow of liquid, solid, and gas phases, respectively. A bubble induced force (BIF) model, a continuum surface force (CSF) model, and Newton's third law are applied to account for the couplings of particle-bubble (gas), gas-liquid, and particle-liquid interactions, respectively. A close distance interaction (CDI) model is included in the particle-particle collision analysis, which considers the liquid interstitial effects between colliding particles.

The motion of a particle in a flow field can be described in Lagrangian coordinates with its origin attached to the center of the moving particle. The motion of a single particle can be described by its acceleration and rotation in a nonuniform flow field. The forces acting on a particle include interface forces between the fluid and particle, and forces imposed by external fields. The total force acting on a particle is composed of all applicable forces, including drag, added mass, gravity/buoyancy, Magnus force, Basset force, and other forces. The general scheme of a stepwise molecular dynamic (MD) simulation (Tildesley, 1987), based on a predictor-corrector algorithm, is used to compute the particle motion. The hard sphere approach is used for the collision dynamics. The collinear collision model is used to determine the normal velocity and momentum changes of colliding particles. The model includes the detailed close-range particle-fluid and particle-particle interactions during the entire process of particle collision. The tangential velocity and momentum changes are formulated and calculated based on a sticking/sliding model (Zhang et al., 1998a).

Bubble formation, initial bubble size, and jetting

Among various factors that affect the bubble formation, the wettability of the orifice surface is an important factor, which affects the initial size of the bubble formed on the

orifice. It is found that initial bubble size increases significantly with the contact angle between the bubble and the orifice surface when the contact angle exceeds the threshold value of 45°. The high-pressure studies indicated that an increase in gas density reduces the size of bubbles formed from a single orifice. A mechanistic model is described to predict the initial bubble size in liquid-solid suspensions at high-pressure conditions (Luo, et al., 1998c). The model considers various forces induced by the particles. During the expansion and detachment stages, particles collide with the bubble and stay on the liquid film. The particles and the liquid surrounding the bubble are set in motion as the bubble grows and rises. The model is applied to simulate the bubble formation process under constant flow conditions, which are characterized by constant gas flow rate through the orifice. When the volume of the gas chamber is small, the bubble formation can normally be assumed under constant flow conditions.

Bubble coalescence

For gas-liquid systems, the experimental results available in the literature indicate that an increase of pressure retards the bubble coalescence. It is known that surface tension decreases and liquid viscosity increases with increasing pressure. In addition, particle sphericity ϕ increases with pressure. These variations contribute to the reduction of the film thinning velocity, and hence, the bubble coalescence rate, as pressure increases. As a result, the time required for two bubbles to coalesce is longer and hence the rate of overall bubble coalescence in the bed is reduced at high pressures. Moreover, the frequency of bubble collision decreases with increasing pressure. An important mechanism for bubble collision is bubble wake effects (Fan and Tsuchiya, 1990). When the differences in bubble size and bubble rise velocity are small at high pressures, the likelihood of small bubbles being caught and trapped by the wakes of large bubbles decreases. Therefore, bubble coalescence is suppressed by the increase in pressure, due to the longer bubble coalescence time and the smaller bubble collision frequency.

Bubble breakup and maximum stable bubble size

There are many models proposed in the past that predicts the maximum stable bubbles size but they all do not account for the internal circulation of the gas. The internal circulation velocity is of the same order of magnitude as the bubble rise velocity. A centrifugal force is induced by this circulation, pointing outwards toward the bubble surface. This force can suppress the disturbances at the gas-liquid interface and thereby stabilizing the interface. On the other hand, the centrifugal force can also disintegrate the bubble, as it increases with an increase in bubble size. The bubble breaks up when the centrifugal force exceeds the surface tension force, especially at high pressures when gas density is high.

An analytical criterion for the bubble breakup is derived by considering a single large bubble rising in a stagnant liquid or slurry at a velocity of u_b, without any disturbances on the gas-liquid interface. The bubble is subjected to breakup when its size exceeds the maximum stable bubble size due to the circulation-induced centrifugal force (Luo et al., 1998a).

2.2.2 *Macroscopic Hydrodynamics*

Hydrodynamic similarity

Numerous studies have been conducted to investigate the effect of pressure on the gas holdup of bubble columns and three-phase fluidized beds. Further, empirical correlations have been proposed for gas holdup in bubble columns operated at elevated pressure and temperature (Fan et al., 1999; Kemoun et al., 2000). A similarity rule has been developed to simulate the hydrodynamics of industrial reactors which requires hydrodynamic similarity of the following dimensionless groups to be the same: U_g/u_{max}, Mo_m, and ρ_g/ρ_m.

Heat transfer characteristics

A consecutive film and surface renewal model is used to analyze the heat transfer behavior. The model assumes that a thin liquid film exists surrounding the heating surface; and liquid elements are forced to contact the outer surface of the film, due to the passage of bubbles. The liquid elements contact the film for a short time, t_c, and then, are replaced by fresh liquid elements. The heat is transferred to the bulk liquid through conduction by the liquid film and unsteady state conduction by the liquid elements. The heat transfer coefficient is expressed in terms of the physical properties of the liquid, the film thickness, and the contact time of the liquid elements (Wason and Aluwalia, 1969). By considering the pressure effects on the physical properties of liquid and bubble characteristics, such as bubble size and bubble rise velocity, this model may be used to analyze the heat transfer behavior in a high-pressure system.

2.3 *Models used for FT reactor performance prediction*

The use of slurry bubble column reactors (SBCR) provides an attractive alternative to traditional vapor-phase processes. Fischer-Tropsch (FT) synthesis has been recognized as a promising method for environmentally benign, indirect, coal utilization. Advantages of the three phase slurry FT synthesis process include: nearly isothermal operation, high catalyst effectiveness factor due to the smaller catalyst particle sizes, lower rate of catalyst deactivation and low pressure drop. Hence, SBCR is the favored reactor for commercialization of FT synthesis. However, one of the disadvantages of FT SBCR is the uncertainty of its design and scale-up in addition to the need for liquid-catalyst separation, catalyst attrition, etc. In addition to the mentioned advantages, slurry FT synthesis process doesn't require high hydrogen/carbon monoxide ratio syngas compared to fluidized or fixed bed reactor processes and hence, it can use the low hydrogen/carbon monoxide ratio syngas that is produced by the new generation of coal gasifiers. The chemical reaction of the FT synthesis (Paraffin synthesis) is as follows:

$$CO + (1 + \frac{m}{2n})H_2 \longrightarrow \frac{1}{n}C_nH_m + H_2O \qquad , m=2n+2 \qquad (2.1)$$

In processes that utilize iron catalyst and/or low hydrogen/carbon monoxide inlet ratio water gas shift reaction (WGS) should also be considered (Stern et al., 1985, Prakash, 1993; van der Laan et al., 1999):

$$CO + H_2O \longrightarrow CO_2 + H_2 \qquad (2.2)$$

Detailed kinetics that is probably needed for the accurate FT process modeling should at least also include methane ($n=1$), olefin ($m=2n$) synthesis and Boudouard's reaction:

$$2CO \longrightarrow C_{(s)} + CO_2 \qquad (2.3)$$

The basic paraffin synthesis kinetics (i.e., FT synthesis kinetics) have been almost exclusively used in the published FT models. Paraffin synthesis kinetics have been found to be of a Langmuir-Hinshelwood (L-H) type (Van der Laan, et al., 1999). However at hydrogen conversion below 60 % first order hydrogen kinetics (FTS 1st) has been shown to be a reasonable approximation (Dry, 1976; Huff and Satterfield, 1984). Table 2.1 lists the kinetic types used in FT SBCR performance modeling.

Due to the lack of understanding of the hydrodynamics of churn-turbulent slurry bubble column, most of the models assumed uniform concentration of the catalyst throughout the reactor. Following the work of Kato et al. (1972) some of the models calculated the catalyst axial concentration profile by using sedimentation and dispersion model (SDM) (Deckwer et al., 1982; Mills et al., 1996). These models have shown that in spite of small particle size and churn turbulent regime solids phase concentration is the highest at the bottom of the column and exponentially drops with height for batch slurry operation. However, the profiles of solids distribution in co-current and counter-current modes of operation strongly depend on the direction and magnitude of slurry inlet velocity (Mills et al., 1996).

Fisher-Tropsch process is highly exothermic and hence, one would naturally consider modeling the energy balance. However, results of several models (Deckwer et al., 1982; Mills et al., 1996) predict nearly isothermal operation of the FT slurry reactor. Turner and Mill's (1990) model predicted a slight temperature axial gradient (with local temperature within 20% from wall temperature). They related it to catalyst concentration axial profiles (SDM). In the mentioned models, the energy balance axial convection, reaction heat, wall convection and axial dispersion are included. However, all of these models neglected latent heat of evaporation whose contribution may be expected to be appreciable.

All published models on FT process treated the solids and liquid as one pseudo homogeneous slurry phase (SL). Slurry phase is the most often modeled as completely mixed (CM) (Bukur, 1983; Maretto and Krishna, 1999; van der Laan, 1999) or using axial dispersion model (ADM) (Deckwer et al., 1982; Mills et al., 1996; De Swart et al., 1997). Leib et al. (1995) used multi cell model for both liquid (completely mixed) and gas phase (plug flow, PF) so that the extent of backmixing has been varied by changing the number of mixing cells. Turner and Mills (1990) compared the predictions of mixing cell model (MCM) and axial dispersion model (ADM) and concluded that mixing cell model is more realistic approach although both models predicted the same performance of FT slurry reactor when number of cells (MCM) and Peclet number (ADM) were matched using a proposed correlation. Gas phase (G) has been traditionally modeled as a single phase in plug flow (PF) or with axial dispersion. Last few years several models appeared that described gas phase using two bubble class approach. In this approach small bubbles phase (SB) is modeled as completely mixed (as slurry phase), while large bubbles phase

(LB) is in plug flow (Maretto and Krishna, 1999; van der Laan et al., 1999), or alternatively, both of the gas phases are modeled using ADM (De Swart et al., 1997).

Table 2.1 shows a summary of the most relevant studies on the modeling of FT slurry bubble column reactors. The stoichiometry of the Fischer-Tropsch synthesis (eq. 2.1) is such that more moles reacts than it is produced. Because of this the amount of gas phase decreases along the FT slurry reactor with experimentally determined contraction factor α of about –0.5. Because of this effect valid model of the FT process must include a closure for the superficial gas velocity (SGV) axial profile. Classical approach assumes linear relationship between SGV and conversion of syngas (Deckwer et al., 1982):

$$U_G = U_G^i(1+\alpha X_{H_2+CO}) \tag{2.4}$$

Overwhelming number of different models is adopting this relationship (Table 2.1) although strictly this is valid only in steady state when axial mixing and convection in the liquid phase can be neglected (Stern et al., 1985). More accurate, rigorous modeling of the SGV axial profile is based on the overall gas phase mass balance (Prakash, 1993; Stern et al., 1985) which requires knowledge of the concentration profiles of all gaseous species. The drawback of this approach is obviously larger number of equations that have to be solved compared to classical Deckwer's approach.

Model for the prediction of the Fischer-Tropsch slurry reactor performance is needed which properly should include detailed kinetics with all relevant species, mixing pattern of different phases (e.g., the phenomenological multi cell recirculation model (Degaleesan et al., 1997)), change in SGV, solids axial profile, (e.g., the mechanistic model (Murray and Fan, 1989)), etc. In addition the present energy balance modeling may need to be improved by accounting for the latent heat of evaporation. In order to achieve this, detailed understanding of the hydrodynamics of FT slurry bubble column reactor via advanced diagnostic techniques is needed which is the focus of the tasks set for this grant.

Table 2.1. Summary of models for prediction of the Fischer-Tropsch process performance.

Model	Kinetics	Accounted species	Phase degree of mixing	Gas velocity profile	Solids profile	Energy balance	Steady state model
van der Laan et al., 1999	FTS, L-H WGS, L-H	H_2, CO, H_2O, CO_2 n products	SB-CM LB-PF SL-CM	f(X,α)	uniform	Yes	Yes
Maretto and Krishna, 1999	FTS, L-H	H_2, CO	SB-CM LB-PF SL-CM	uniform	uniform	iso-thermal	Yes
De Swart et al., 1997	FTS, 1st	H_2	SB-AD LB-AD SL-AD	f(X,α)	SDM	Yes	dynamic
Mills et al., 1996	FTS, 1st	H_2	G-AD SL-AD	f(X,α)	SDM	Yes	Yes
Leib et al., 1995	FTS, 1st	H_2	G-nCM or nPF L-nCM	f(X,α)	uniform	iso-thermal	Yes
Prakash, 1993	FTS, L-H WGS, L-H	H_2, CO, H_2O, CO_2	G-AD SL-AD	overall gas MB	SDM	Yes	Yes
Truner and Mills, 1990	FTS, 1st	H_2	G-nCM or nPF L-nCM , G-AD L-AD	f(X,α)	SDM	Yes	Yes
Kuo, 1983	FTS, L-H WGS, L-H	H_2, CO, H_2O, CO_2	G-PF SL-PF , CMorAD	f(X,α)	uniform	iso-thermal	Yes
Stern, et al., 1985	FTS, 1st WGS, 2nd	H_2, CO H_2O, CO_2 C_nH_m	G-AD SL-AD	overall gas MB	SDM	iso-thermal	Yes
Bukur, 1983	FTS, 1st	H_2	G-PF SL-CM	f(X,α)	uniform	iso-thermal	Yes
Deckwer et al., 1982	FTS, 1st	H_2	G-AD SL-AD	f(X,α)	SDM	iso-thermal	Yes

2.4 Physical Properties of FT Systems

2.4.1 Fischer-Tropsch waxes and solvent

It is known that the hydrodynamics of Fischer-Tropsch Synthesis process is greatly affected by the fluid physical properties of the waxes. Due to the high temperature and high pressure operating conditions for Fischer-Tropsch Synthesis, it is hard to conduct experiments at the matching conditions of Fischer-Tropsch Synthesis. Therefore, other hydrocarbons with similar physical properties as Fischer-Tropsch waxes under the operating conditions have been used to simulate the actual waxes to study the hydrodynamics of Fischer-Tropsch Synthesis. Several studies have been reported in the literature about the physical properties of different Fischer-Tropsch waxes and solvents used for the mimicking purpose (Gormley, et al., 1997; Marano and Holder, 1997; Patel, et al., 1990; Soong, et al., 1997). Table 2.2 shows the reported values of Fischer-Tropsch waxes and solvents. It can be observed that the density of reported Fischer-Tropsch waxes range from 645-849 kg/m^3. The viscosity of waxes on the other hand ranges from 0.41 to

71.9 cP. In general, the viscosity of most of the waxes used is around 2 to 4 cP. The range of surface tension stays reasonably constant between 16 and 28 dyne/cm.

Other than experimental data, models have been developed to predict the physical properties of Fischer-Tropsch liquids. Tables 2.3 and 2.4 show the asymptotic behavior correlations developed by Marano and Holder (1997) to estimate the properties of n-paraffins. The molar volume information derived from the correlation can be converted into density information by dividing the molar volume with the molecular weight of the n-paraffins used.

Table 2.2. The Physical Properties of Fischer Tropsch Waxes (Gormley, et al., 1997; Marano and Holder, 1997; Patel, et al., 1990; Soong, et al., 1997).

Fischer Tropsch Wax	Temperature (°C)	Density (kg/m3)	Viscosity (cp)	Surface Tension (dyne/cm)
ACPI wax	121	-	1.7	-
Arge wax	121	-	5.7	-
	150	-	4.2	24
	200	-	2.9	20
	230	-	2.5	19
	265	-	-	16
C28H58	110	-	20	-
	130	-	19.8	-
	150	-	5.6	-
d. Allied-AC-1702	110	-	-	-
	130	-	71.9	-
	150	-	46.3	-
Drakeol-10 Oil	20	849	38.13	28.3
	100	806	3.38	23.9
	175	-	-	19.9
	200	743.9	0.892	-
	265	698	0.55	-
FT-200 Wax	150	-	4.4	-
	200	-	2.8	-
	230	-	2.4	-
	149	-	4.4	-
	204	-	2.2	-
	260	-	1.7	24
FT-300 Wax	150	-	6.4	24
	200	722	4.2	21
	230	-	-	19
	265	681	2.7	17
F-T lt. Cut	25	-	-	23
F-T med. Cut	25	-	2.36	26
	100	-	0.842	-
	150	-	0.555	-
Kogasine	145	-	0.41	18
Krupp wax	200	-	3.0	-
	230	-	2.2	-
	260	-	1.6	-
Mobil run 3	149	-	2.8	-
	204	-	1.7	-
	260	-	-	26-27
Mobil run 4	149	-	6.1	-

	204	-	4.3	-
	260	-	3.4	26-27
Mobil run 5	149	-	17.6	-
	204	-	8.5	-
	260	-	5.5	28
Mobil run 7	149	-	8.2	-
	204	-	4.1	-
	260	-	2.3	26-27
Mobil comp	150	-	6.5	-
	200	-	3.8	-
	230	-	3.1	-
Mobil Wax	121	-	9.5	-
	200	716	3.8	-
	265	674	2.3	
Mobil FT Wax	110	-	26.6	-
	130	-	19.4	-
	150	-	17.2	-
P & W wax	100	-	1.829	-
	150	-	0.995	-
Paraflint	121	-	9.5	-
Paraffin wax	145	-	13.0	29.1
	175	-	8.1	27.0
	200	-	5.7	25.2
	220	-	4.0	24.0
	250	-	2.8	21.8
	260	-	2.0	21.2
	275	-	1.8	20.4
	300	-	1.2	19.8
Polywax-655	110	-	20.6	-
	130	-	14.5	-
	150	-	10.6	-
Sasol Wax	200	701	2.9	-
	265	655	2.0	-
UCC wax	121	-	2.8	-
n-Paraffins	0-300°C	See Table 2		

Table 2.3. Temperature-Independent Parameters for Properties of *n*-Paraffins

$Y = Y_{\infty,0} + \Delta Y_{\infty}(n - n_0) - \Delta Y_0 \exp(-\beta(n \pm n_0)^{\gamma})$

$(n + n_0)$ for molar volume, $(n - n_0)$ for all others

	Molar volume (cm3/gmol)	ln viscosity (cP)	Surface tension
n_0	-1.388524	-2.293981	0.264870
ΔY_0	a	a	a
$Y_{,0}$	0	57.8516	a
ΔY	a	a	0
β	0.183717	2.476409	2.511846
γ	0.753795	0.0112117	0.201325

[a] See Table 3

Table 2.4. Temperature-Dependent Parameters for Properties of *n*-Paraffins

$\Delta Y = A + B/T + C\ln T + DT^2 + E/T^2$ for $\ln\mu_L$

ΔY or $Y = A + BT + CT^2 + DT^3$ for V_L, σ

	Molar volume (cm3/gmol)		ln viscosity (cP)		Surface tension (dyne/cm)	
	ΔY_0	ΔY	ΔY_0	ΔY	ΔY_0	ΔY
A	8592.30	12.7924	-602.688	0.0290196	627.213	73.8715
B	-85.7292	0.0150627	77866.8	-241.023	-0.882888	-0.177123
C	0.280284	-130794×10^{-5}	198.006	0.0440959	0.00268188	1.54517×10^{-4}
D	-4.48451×10^{-4}	1.59611×10^{-4}	-4.18077×10^{-7}	-1.84891×10^{-7}	0	0
E			-2.49477×10^{6}	56561.7		
ΔT	0-300°C	0-300°C	0-300°C	0-300°C	0-150°C	0-150°C

2.4.2 Solid Phase (Catalyst)

Sabatier and Sanderson found in 1902 that methane can be obtained when hydrogen and carbon monoxide react over nickel or cobalt catalyst (Storch et al., 1951). Fischer and Tropsch in 1923 obtained a high yield of liquid products by using iron based alkali promoted catalyst. Process was later studied using iron, cobalt and nickel catalysts. First industrial scale and all pre and during WWII processes in Germany used cobalt based catalyst, 100Co:5ThO:8MgO:200Kieselguhr, because of its high activity. Due to the shortage in supply of Cobalt during WWII new iron based catalysts were developed. Ruhrchemie company developed a series of iron based catalysts, 100Fe:xCu:yK:zSiO2. South African commercial, ARGE, process still uses this type of a catalyst (x:y:z=4.3:4.1:25). Iron although less active is much cheaper and more easily available than cobalt. Srivastava et al. (1990) and Rao et al. (1992) reviewed various iron based FT catalysts. Nickel has been the most often used in combination with some other active component, such as cobalt. Ruthenium is the forth originally proposed Fisher-Tropsch

(FT) catalyst. However, ruthenium has been similarly as nickel mostly used in combination catalysts because it is expensive (two orders of magnitude more expensive than cobalt) and has much higher range of optimum working pressures compared to iron or cobalt. Until today thousands of different catalyst formulations have been tested and hundreds of active catalysts have been proposed with iron and cobalt based catalysts being the most common commercially. Recently more studies have been directed toward the cobalt based FT catalysts because of their high activity and modular selectivity. Iglesia (1997) and Oukachi et al. (1999) reviewed various cobalt based FT catalysts. Since catalyst activity and selectivity (which are affected by catalyst porosity, tortuosity, density which is usually greater than 5 gm/cm^3, surface composition and structure, wetability, etc.) are determined by catalyst chemical composition, type of carrier (catalyst support), catalyst preparation process, activation procedure, etc. The FT catalyst properties vary noticeably.

Traditionally the most often used support (binder) of FT catalysts have been silica (SiO_2) and alumina (Al_2O_3) (density between 1.5 to 3 gm/cm^3). Some early German catalysts used the Kieselguhr. In addition to these supports, titania (TiO_2), magnesia (MgO), active carbon and zeolits (e.g. ZSM-5) have been somewhat less frequently used (Storch et al., 1951).

Hence, hydrodynamics obtained using one catalyst may not represent a general information for all the catalyst types. Using only FT catalyst supports for hydrodynamics investigation does not either provide representative information due to the difference in the particle physical and mechanical properties. Therefore, in the open literature, most of the investigations on the hydrodynamics of cold-flow model slurry bubble column reactors have been performed using glass beads of different sizes and air-water/hydrocarbon system (Ong et al., 2000).

3. PREPARATION OF THE EXPERIMENTAL FACILITIES AND THE ADVANCED MEASUREMENT TECHNIQUES

Preparation has been made to the experimental facilities and to the measurement techniques that will be used for the hydrodynamics investigation of the FT slurry bubble column reactors. These facilities, techniques and their preparation are summarized below.

3.1 High pressure and high temperature 2" diameter slurry bubble column

The schematic diagram of the high pressure and high temperature slurry bubble column is shown in Figure 3.1. The actual photo of the column is shown in Figure 3.2. The column is made of stainless steel and is 80 cm in height and 8.08 cm in diameter. Three pairs of plane windows made of quartz are installed on the column; each window is 15 mm wide and 180 mm long. These windows allow viewing throughout the entire test section of the column. The present experiments are conducted at pressures up to 21 Mpa and temperatures up to 180°C. The pressure is controlled by a back pressure regulator installed at the outlet of the bed. The set-up has been tested for leakage and operation.

3.2 High pressure 6 inch diameter slurry bubble column

High pressure 6" slurry bubble column experimental setup (Figure 3.3) is designed to support the maximum operating pressure of 200 psig at room temperature. Compressed air is used as gas phase and is supplied from the compressor with working pressure of 185 psig at the maximum flowrate of 310 SCFM. Air passes through an air filter, pressure regulator, flowmeter setup (4 rotameters of increasing range in parallel) and enters through a check valve (to prevent liquid/slurry phase back flow) into distributor chamber of the bubble column. Air exits the column through a demister, passes through the back pressure regulator (that controls column operating pressure) and vents to atmosphere. A laboratory scale 16.15 cm (6") diameter stainless steel bubble column is used in all experiments. Column design enables easy removal of the distributor chamber and sparger replacement. Two similar column designs are used to suit all the needed experiments. The first one, designed for CARPT/CT experiments, is a smooth 6" column equipped with just two probe ports (1") at each end of the column. The second one (Figure 3.4), for probe measurements, is the same 6" column equipped with an array of additional 15 probe ports (1") and 6 (12"H x 1½"W) view ports. View ports mounted by three at radially opposite sides are staggered to cover the middle and the top part of the column. The batch of slurry constitutes of the selected solvent as the liquid phase and the selected solid phase.

Both 6" columns have been installed and tested.

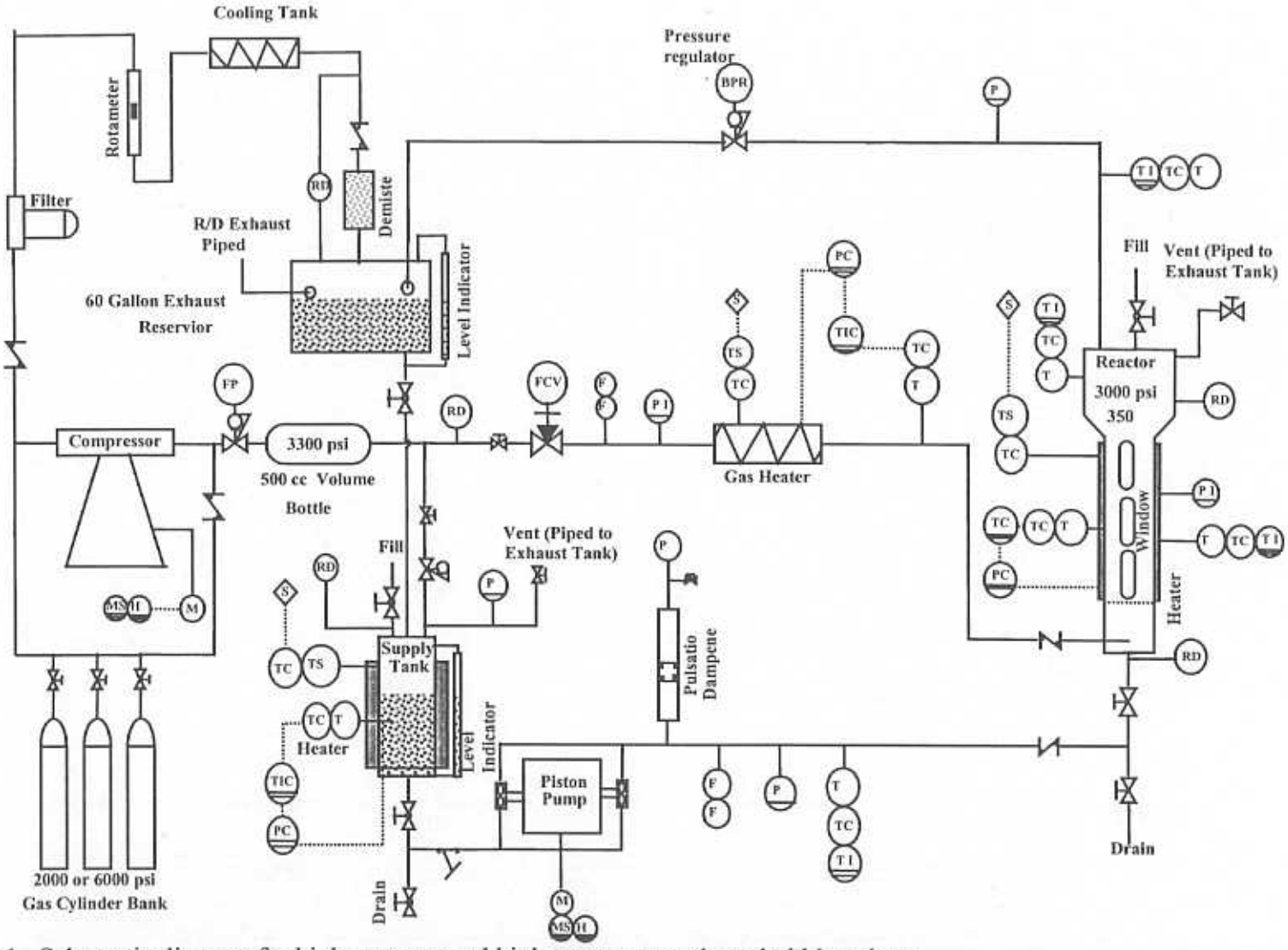

Figure 3.1. Schematic diagram for high pressure and high temperature slurry bubble column.

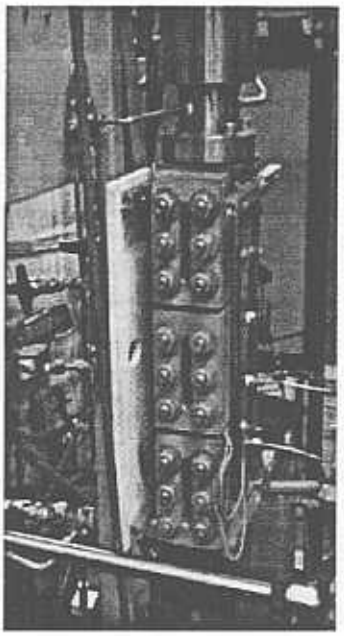

Figure 3.2. Photo of high pressure and high temperature 2" diameter slurry bubble column.

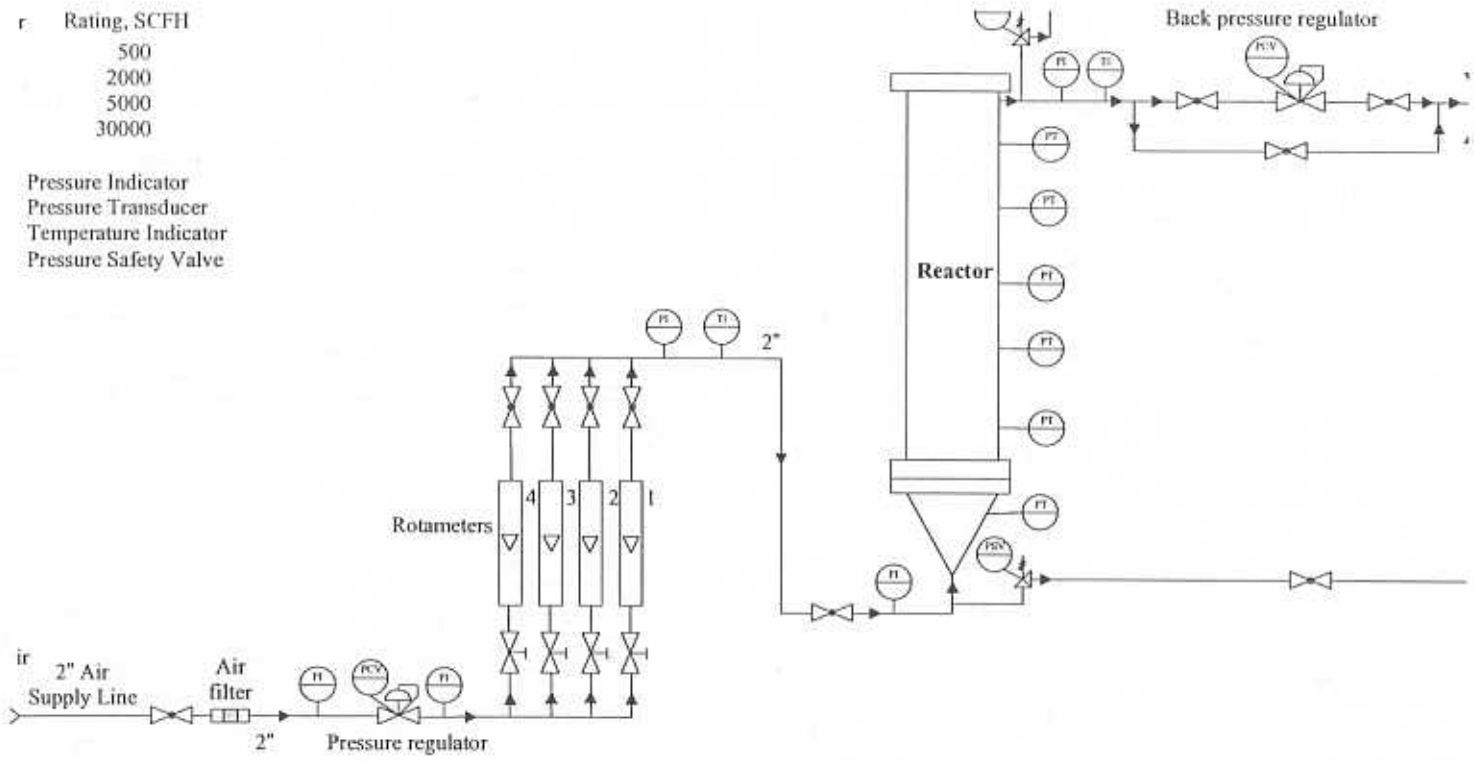

Figure 3.3. Gas flowsheet for the high pressure 6 inch diameter bubble column

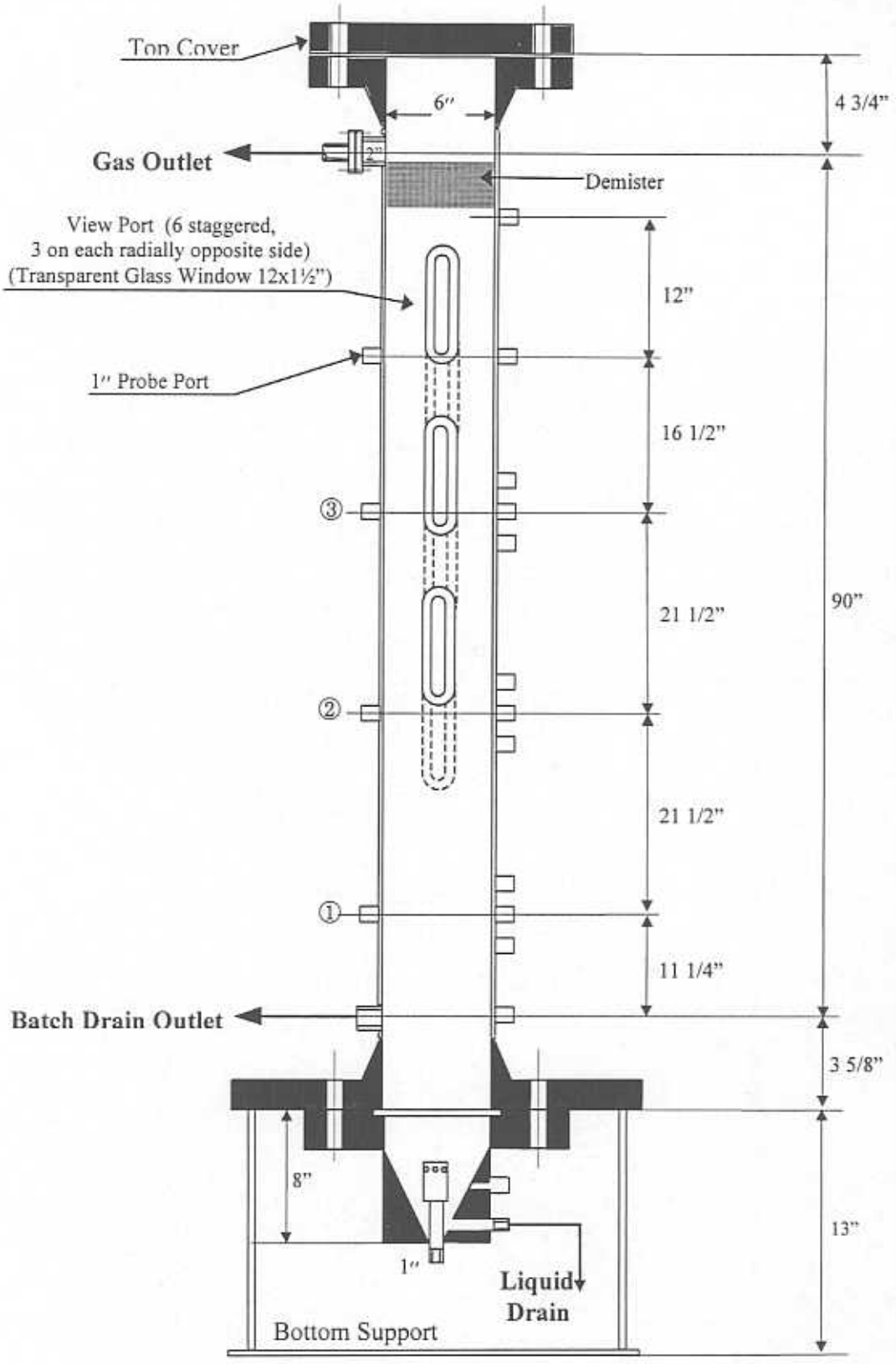

Figure 3.4. High pressure bubble column (probe measurement variation) design.

3.3 Particle Image Velocimetry (PIV)

The high speed PIV or LDA system, will be used in this project. Figure 3.5 shows a schematic diagram of the PIV system. The CCD image pick-up on the high frame rate camera features 765 pixels across by 246 lines. Camera speed can be selected up to 480 pictures per second. The camera is equipped with an asynchronous variable electronic shutter ranging from 1/60 second to 1/10000 second. The CCD image from the high frame rate camera can be simultaneously digitized by the high frame rate / high capacity frame grabber. The frame grabber is equipped with 40 MHz max pixel clock and 256 MB on board memory. Moreover, the high frame rate camera can be connected the high frame rate video recorder (240 pictures per second) for further study. A 4-watt argon ion laser system is utilized as a light source. A fiber optic cable is used to carry the laser light from the laser source to the test column. A cylindrical lens arrangement attached to the end of the fiber optic cable creates a laser sheet of thickness 5 mm.

3.4. Laser Doppler Anemometer (LDA)

The Laser Doppler Anemometer was invented by Yeh and Cummins in 1964. It is capable of non-intrusive velocity measurements in fluid dynamics in both gas and liquid phases. It has up to three velocity components with high accuracy and high spatial resolution due to small measurement volume. The basic components of an LDA include a continuous wave laser, a traverse system, transmitting and receiving optics and a signal conditioner and a signal processor. Figures 3.6 and 3.7 show the setup of the LDA system and the transmitting optics on the traverse system respectively. A 300-mW air-cooled argon-ion laser and a beam separator are used to generate two pairs of beams of known wavelengths of 514.5 and 480 nm. The light is transmitted through a fiber optic cable and a probe with 3.40 and 3.22 μm and measurement volumes of 0.164 X 0.164 X 2.162 mm and 0.156 X 0.156 X 2.05 mm for the 514.5 and 480-nm wavelengths respectively. The scattered light is collected with a detector and processed with a signal processor.

The principle of the operation follows that when a particle passes through the intersection volume formed by the two coherent laser beams, the scattered light received by a detector has components from both beams. The components interfere on the surface of the detector. Due to changes in difference between optical path lengths of the two components this interference produces pulsating light intensity as the particle moves through the measurement volume.

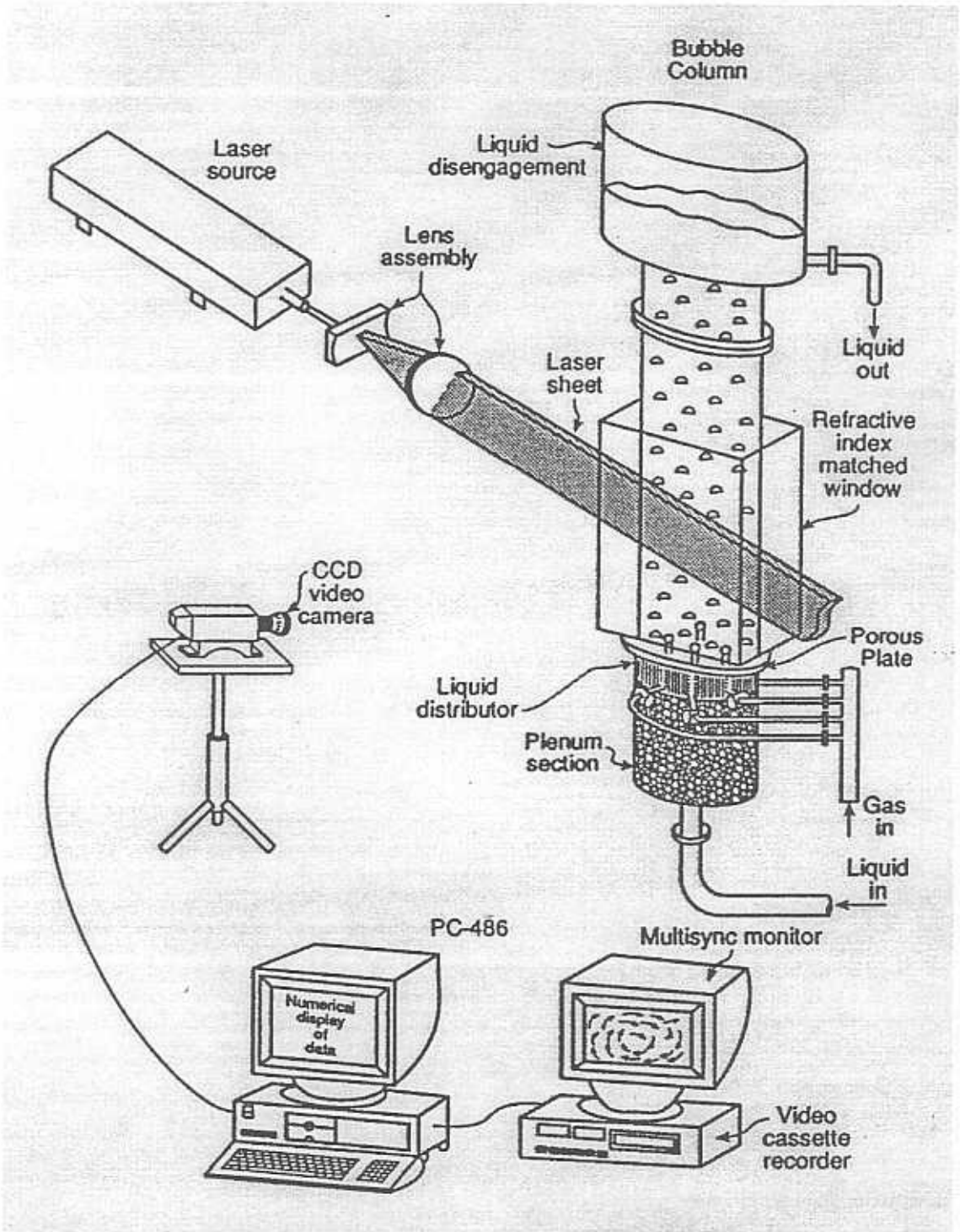

Figure 3.5. Schematic diagram of PIV system

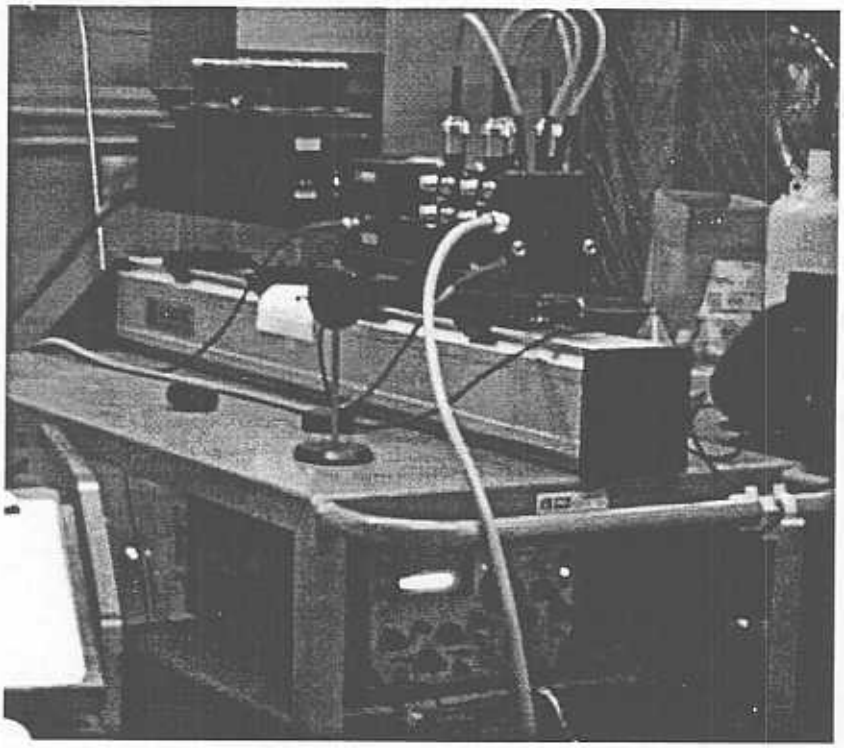

Figure 3.6. Laser Doppler Anemometer Setup.

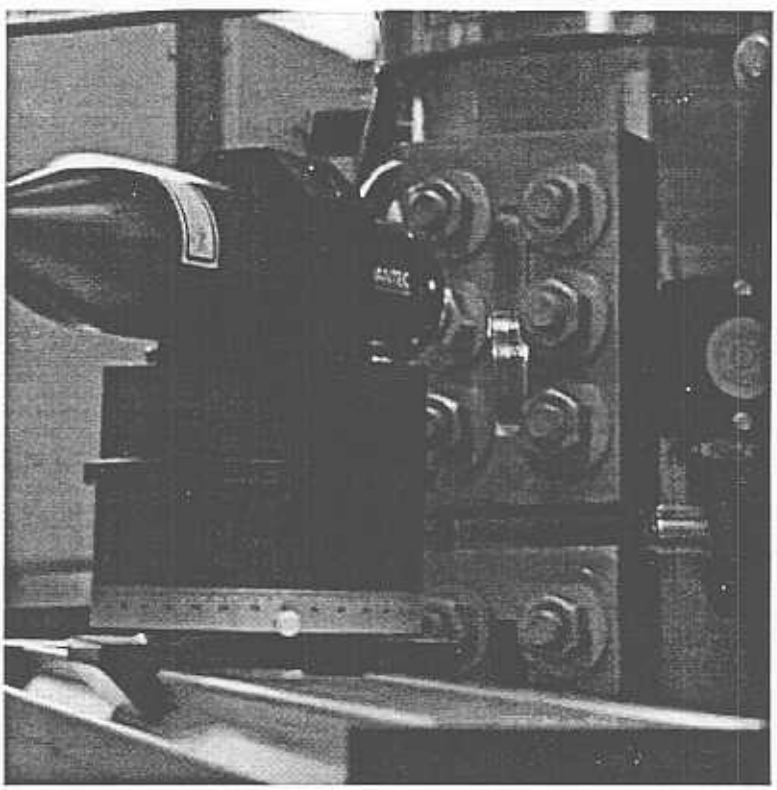

Figure 3.7. Transmitting optics applied on traverse system

3.5 Computer Automated Radioactive Particle Tracking (CARPT)

CARPT is a technique for tracking of a single radioactive tracer particle by detecting the intensity distribution of emitted γ-rays (Figure 3.8). It consists of a number of scintillation detectors (16-32) to monitor the motion of a single small radioactive particle in multiphase systems. This technique has been used extensively at Washington University (Chemical Reaction Engineering Laboratory) to measure in a non-invasive manner the flow pattern and turbulent parameters of different multiphase flow reactors. A fully wettable, neutrally buoyant particle is used to simulate the motion of the liquid in gas-liquid system and particle of the size and density of the solids used is employed for monitoring the motion of solids in two and three phase fluidized beds and other multiphase systems. Scandium 46 at activities of about 200 – 500 μci is used in a composite made tracer particle. Collected data for the tracer particle location in time is used to compute the tracer particle velocity and "turbulent" parameters. Precise calibration and good radioactive particle tracking are essential in obtaining accurate and reproducible CARPT data. In this work the assessment of solids velocities and "turbulent" parameters in a FT slurry bubble column is sought. Thus, the radioactive tracer particle should, as closely as possible, track the solids present in the system. To accomplish this the tracer particle should be comparable in size and density to the solid phase particles. Scandium is a highly reactive rare earth metal whose reactivity increases with increase in surface area per unit volume (decrease of diameter). To resolve the issue of the reacting scandium tracer particle we have developed a new technique for coating and protecting the minute size tracking particles. A tracer scandium Sc45 particle of required diameter is protected with a thin coating of Parylene N, an extremely inert derivative of poly p-xylene with excellent thermal and mechanical properties. The coated Scandium particle is then irradiated in a nuclear reactor. The resulting radioactive scandium Sc46 particle (strength of up to 200 μCi and half-life of 83 days) with a total diameter within the solid phase particle size range is thus used as a tracer particle. Since the density of Parylene N is 1.11 g/cm^3, application of different coating thickness lower the overall particle density from 2.99 g/cm^3 (of pure scandium) to about 2 g/cm^3.

A detailed experimental setup and calculation procedure for CARPT experiments is given by Degaleesan (1997). In-situ calibration of detectors will be performed under the desired operating conditions using a calibration device that is operated under high pressure. CARPT data (tracer particle position in time) acquired over sufficiently long time, to insure enough particle occurrences in each column cell and good time/ensemble averaging, is used for calculation of the time averaged solids:

a) velocities,
b) "Reynolds" stresses,
c) "turbulent" kinetic energy and
d) eddy diffusivities.

A sample of the CARPT results in an air-water-glass beads system in a 6" bubble column is presented in Figure 3.9 (Rados, 1999).

This unique technique is essential for validation of hydrodynamic models used in design and scale-up and testing the effect of different design and operation variables (e.g. pressure, gas velocity, distributor design, internals, etc.) on the flow patterns in FT slurry bubble column reactors.

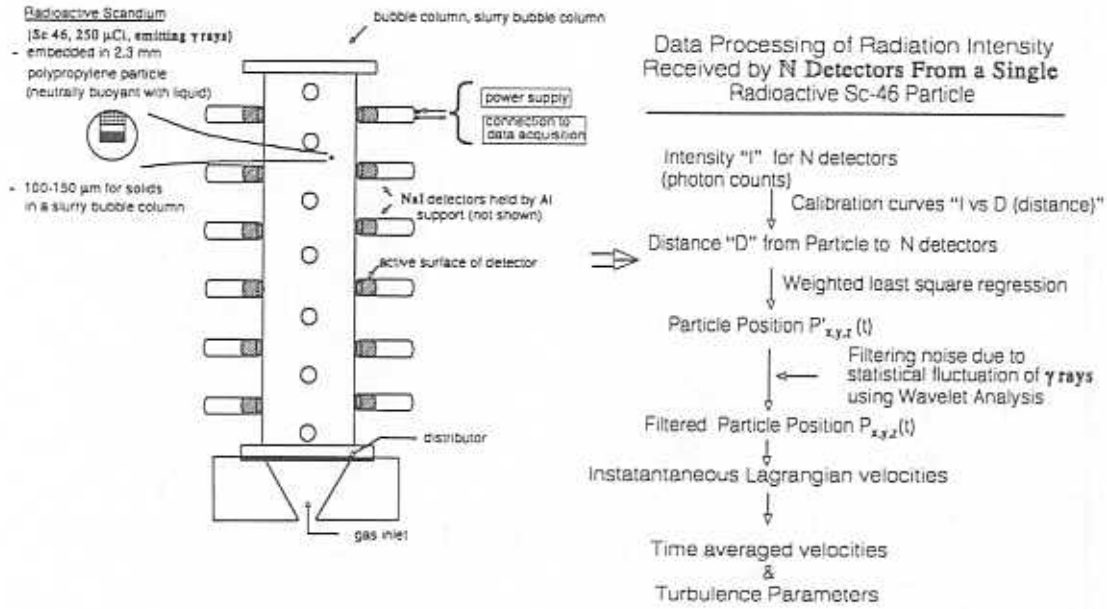

Figure 3.8. Configuration of the CARPT experimental setup.

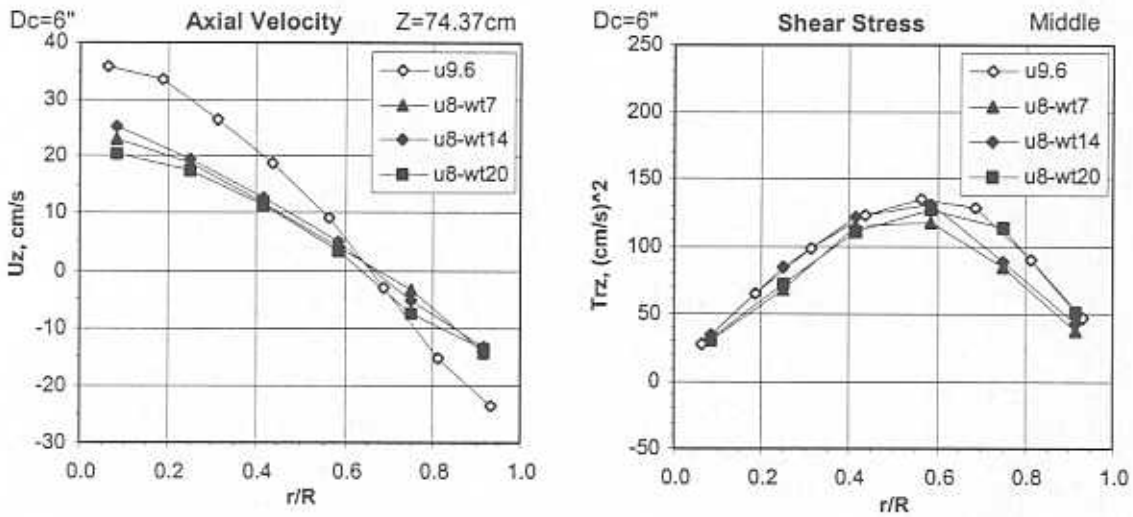

Figure 3.9. Time and azimuthally averaged axial velocity and shear stress radial profiles.
u8-wt14 denotes gas velocity of 8 cm/s and 14 wt.% solids loading. (Sannaes, 1997).

3.6 *Computed Tomography (CT)*

CT is a technique for measurement of the cross-sectional phase holdup distribution in multiphase systems (Figure 3.10).

The CT technique has been extensively implemented at Washington University on various multiphase flow systems. It consists of an array of detectors and an opposing source rotate together around the object to be scanned. The scanner uses a cesium-137 encapsulated γ–ray source with activity of ~ 85 mCi. The array of detectors and the source are mounted on a gantry which can be rotated about the object to be scanned through a step motor. The entire system is completely automated to acquire the data required for the reconstruction of the phase distribution in a given cross-section. The Estimation-Maximization algorithm for image reconstruction has been implemented. It is based on maximum likelihood principles and takes into account the stochastic nature of the projection measurements.

Single source CT is used for phase holdup reconstruction in two phase (e.g., gas-liquid) systems. Theoretically, dual source CT is capable of resolving the holdups in three phase systems (e.g., gas-liquid-solid). However, because of numerical error accumulation dual source CT reconstruction of holdup profiles is still not practical (Daly et al., 1996). In this work we utilize a new combination of measurement techniques CT/DP/CARPT that can be used to calculate holdup profiles of all three phases in a slurry system at all operating conditions including high pressure, high SGV and high solids loading (Rados, 1999).

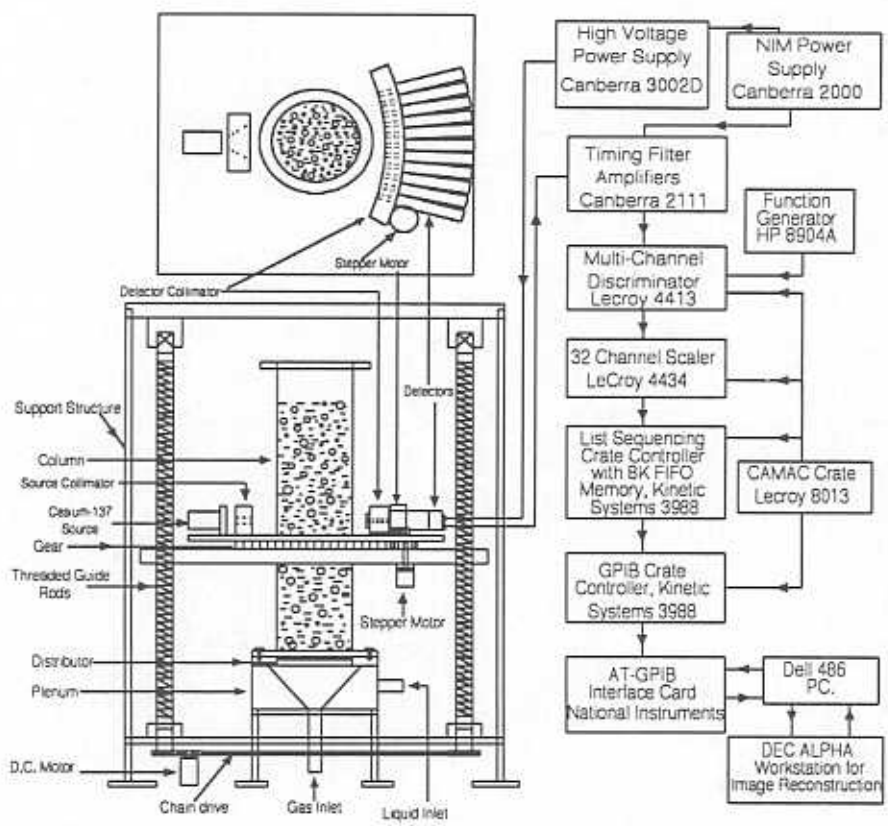

Figure 3.10: Configuration of the CT experimental setup (Kumar, 1994).

For a single γ radiation source, absorbance A over the path l is equal to:

$$A = -\ln\frac{I}{I_0} = \sum_l (\rho\mu)_{ij} l_{ij} \tag{3.1}$$

where I_0 is the intensity of radiation emitted by the source, I is the intensity of radiation received by the detector. Σ indicates the summation of the volumetric attenuation $(\rho\mu)_{ij}$ of each cell ij multiplied by the path length in that cell l_{ij} along the path l, through which the radiation beam passes on its way from the source to the detector. If sufficiently large number of the scans of the operating column are taken from different directions (projections) then the volumetric attenuation in each cell $(\rho\mu)_{ij}$ can be calculated. To get the holdup distribution we have to measure the absorbance A_K for an empty column (K=G), for a column filled with liquid (K=L), for a column with solids and gas in voids between solid particles (K=GS) and for a column in operation with the gas-liquid-solid slurry (K=GLS). For each of these situations the detected intensity of radiation I_K and hence the measured absorbance A_K is different. Since the flow is time dependent larger number of acquired projections than cells (#equations >> #unknowns, over sampling) will yield more accurate time averaged attenuation coefficients (better statistics). In general I_0 is unknown and because of that the intensity of radiation I_K must be normalized with the intensity of radiation detected in the column containing only the gas phase I_G. In addition the intensity I_K must be corrected for the background (room) radiation intensity $I_{K,bck}$. This yields the following equation for A_K:

$$A_K = -\ln\frac{I_K - I_{K,bck}}{I_G - I_{G,bck}} = \sum_l \left[(\rho\mu)_{K,ij} - (\rho\mu)_{G,ij}\right] l_{ij} \tag{3.2a}$$

One defines relative volumetric attenuation as:

$$R_{K,ij} = (\rho\mu)_{K,ij} - (\rho\mu)_{G,ij} \tag{3.2b}$$

For the column containing packed bed of solids (uniform holdup of ε_S^0) and gas in voids between the solids particles the volumetric attenuation coefficient in cell ij is equal to:

$$(\rho\mu)_{GS,ij} = (\rho\mu)_{S,ij}\varepsilon_S^0 + (\rho\mu)_{G,ij}\left(1-\varepsilon_S^0\right) \tag{3.3}$$

Substitution of eq. (3.2b) into eq. (3.3) (written for the gas-solid system, K = GS) after some manipulation yields the local solids volumetric attenuation coefficient:

$$(\rho\mu)_{S,ij} = \frac{R_{GS,ij} + (\rho\mu)_{G,ij}\varepsilon_S^0}{\varepsilon_S^0} \tag{3.4}$$

Similarly, for a slurry system:

$$(\rho\mu)_{GLS,ij} = (\rho\mu)_{G,ij}\varepsilon_{G,ij} + (\rho\mu)_{L,ij}\left(1-\varepsilon_{G,ij}-\varepsilon_{S,ij}\right) + (\rho\mu)_{S,ij}\varepsilon_{S,ij} \tag{3.5}$$

Eq. (3.5) combined with eq. (3.2b) (written for liquid, K=L and slurry, K=GLS) and eq. (3.4) yields the expression for local gas holdup (cell ij):

$$\varepsilon_{G,ij} = \frac{R_{GS,ij}\dfrac{\varepsilon_{S,ij}}{\varepsilon_S^0} + R_{L,ij}\left(1-\varepsilon_{S,ij}\right) - R_{GLS,ij}}{R_{L,ij}} \tag{3.6}$$

Clearly in order to close the system of equations we need one more equation for local solids holdup $\varepsilon_{S,ij}$. In dual source CT one more equation of the form (3.2) can be written for the other γ source. In this work the additional equation is generated from DP and CARPT measurements:

$$-\frac{1}{g}\frac{\Delta P}{\Delta z} = \rho_G\overline{\varepsilon_G} + \rho_L\left(1-\overline{\varepsilon_G}-\overline{\varepsilon_S}\right) + \rho_S\overline{\varepsilon_S} \qquad \text{DP} \qquad (3.7)$$

$$\varepsilon_{S,ij} = n_{S,ij}\frac{\overline{\varepsilon_S}}{\overline{n_S}} \qquad \text{CARPT} \qquad (3.8)$$

DP equation (3.7) assumes fully developed flow, no axial holdup profiles and negligible wall shear stress in the section Δz. Fully developed flow in slurry systems is usually reached at heights above two column diameters. Axial holdup profiles can be neglected over small Δz distances and the wall shear stress has been shown to be negligible compared to the pressure drop (Fan, 1989, less than 1%). CARPT equation (3.8) states that the volume averaged number of radioactive tracer particle occurances in the specific cell $n_{S,ij}$ is proportional to the solids holdup in that cell assuming that the radioactive tracer particle completely resembles solid phase particles and that all cells in considered cross plane are well perfused and readily accessible to the radioactive tracer particle (Moslemian et al., 1992). This assumption is justified in churn turbulent regime. Finally, the combination of eq. (3.7) and (3.8) yields the expression for the local solids holdup (cell ij):

$$\varepsilon_{S,ij} = \frac{-\dfrac{1}{g}\dfrac{\Delta P}{\Delta z} - \rho_G\overline{\varepsilon_G} - \rho_L\left(1-\overline{\varepsilon_G}\right)}{\rho_S-\rho_L} \times \frac{n_{S,ij}}{\overline{n_S}} \tag{3.9}$$

Using the following iterative procedure the holdup profiles of all three phases can be calculated.

1) Guess the cross-sectional average solids holdup. The initial guess is based on the calculation of the cross-sectional average solids holdup from the overall gas holdup measurements and nominal solids loading (v_{S0}, volume of solids per volume of slurry suspension initially charged into the column) using the equation $\overline{\varepsilon_S} = v_{S0}(1-\overline{\varepsilon_G})$.
2) Using eg. (3.8) calculate the solids holdup in each cell.
3) Using eq. (3.6) calculate the gas holdup in each cell.
4) Calculate the cross-sectional average gas holdup.
5) Using eq. (3.9) calculate the solids holdup in each cell.
6) Calculate the cross-sectional average solids holdup.
7) Compare the calculated and previous values (initial guess in the first iteration) of the cross-sectional average solids holdup.
8) Using the solids holdups in each cell recalculated in step 5 repeat the steps 3 through 7 until specified tolerance is achieved (convergence).

3.7 *Physical properties measurements techniques*

Most industrial processes are operated at extreme conditions with high temperatures and pressures, while most research reports have been focused on ambient conditions. It is known that the bubble formation process will be affected by the properties of gas and liquid, the diameter of nozzle, gas chamber pressure and the gas flow rate. The bubble interaction is function of the initial bubble size, bubble rise velocity and bubble breakup and coalescence. However, all of these are relative to gas and liquid physical properties. It is essential to know how the physical properties change with pressure and temperature for an individual system. Therefore, it is possible to characterize the transport phenomena of bubble columns operated under high pressure and high temperature based on the physical properties of the phases rather than the operating pressure and temperature.

3.7.1. *Density measurement*

The hydrostatic weighing method is adopted to measure the liquid density at elevated pressures and temperatures. A cylindrical aluminum tube of 0.305 m in length and 7.14 mm in outside diameter, shown in Figure 3.11, is submerged in the liquid. The volume of the tube above the liquid surface varies with the liquid density. Specifically, the liquid density relates to the tube volume above the liquid surface based on the Archimedes principle:

$$S[\rho_l l_1 + \rho_g (l - l_1)] = (W_1 + W_2) + S_1 \rho_g l_2 \qquad (3.10)$$

where W_1 and W_2 are the mass of the aluminum tube and metal weight respectively; ρ_l and ρ_g are the densities of liquid and pressurized nitrogen gas respectively; and S and S_1 are the cross-sectional areas of the tube based on the outer and inner diameters respectively.

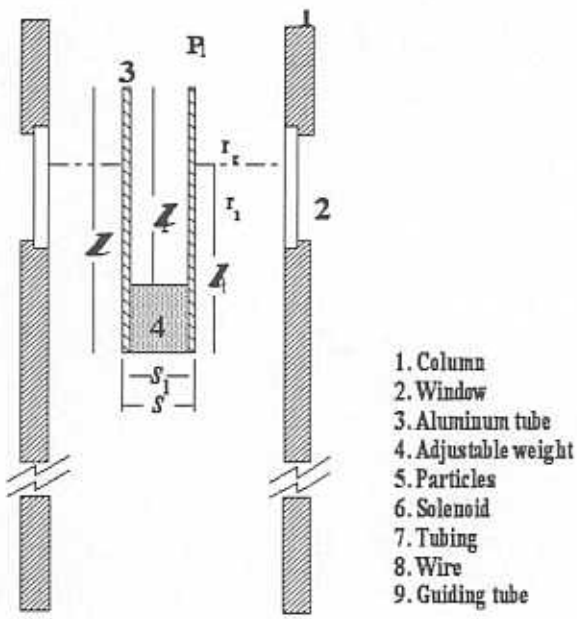

Figure 3.11. Density measurement apparatus setup.

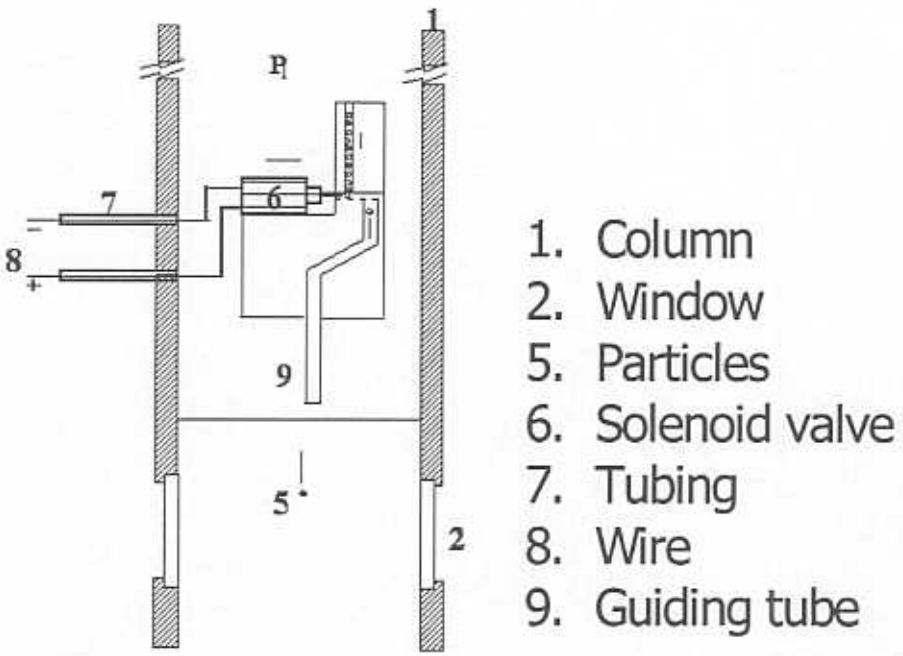

Figure 3.12. Viscosity measurement apparatus setup.

3.7.2. Viscosity measurement

The viscosity of the liquid under elevated pressures and temperatures is determined using the falling ball technique shown in Figure 3.12. A ball dropping device is used to release spherical particles into the column. The falling process is recorded by a CCD camera with an infinity lens situated outside the window. At steady state, the terminal velocity of the falling ball can be calculated from the falling distance (L) and the elapsed time (Δt). The particle size is selected in such a way that the Reynolds number is within the Stokes or intermediate region.

3.7.3. Surface tension measurement

The bubble emergent method is applied to measure the surface tension at varying pressures (up to 21 MPa) and temperatures (up to 250°C). A steel tube is inserted vertically into the column and submerged in the liquid, as shown in Figure 3.13. Video of the bubble generation process is recorded by a high resolution (800 X 490 pixel) CCD camera with an infinity lens. The gas-liquid boundary in Cartesian coordinates of the bubble before detachment is determined. The boundary coordinates are then submitted into the program developed by Jennings and Pallas (1988), from which the surface tension is calculated.

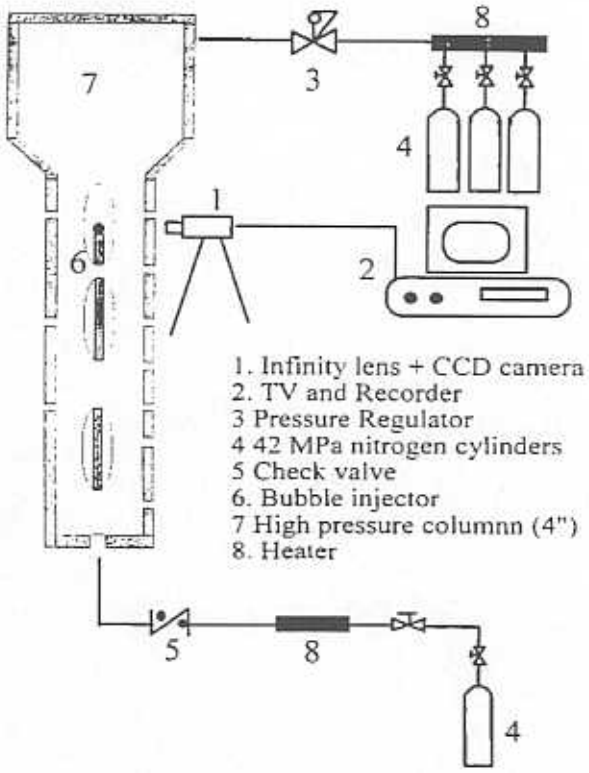

Figure 3.13. Surface tension measurement apparatus setup.

4. SUGGESTED SYSTEM TO BE USED

The gas-liquid-solid system that will be used in the hydrodynamics investigations of slurry bubble column has been selected based on the physical properties of the FT waxes reviewed in section 2 for liquid phase and based on the capabilities of the available experimental facilities and measurement techniques discussed in section 3 for the gas and solids phases. According to the discussion below, the selected system that will be used to conduct the needed hydrodynamics investigations in 2-inch and 6-inch diameter slurry bubble column reactors is air-Exxon Norpar 14-glass beads.

Liquid phase:

As discussed in section 2, a wide range of FT wax properties have been used. Table 4.1 list the range of density, viscosity and surface tension of the FT waxes used at FT reaction conditions.

Table 4.1. Range of FT waxes properties used

Temperature C°	Density Kg/m^3	Viscosity cP	Surface Tension dyne/cm
25 – 300	655 – 849	0.55 – 38.13	16 – 29.1

Accordingly, Exxon Norpar 14 at room temperature has been selected since it would mimic the hydrodynamics of FT waxes at FT operating conditions. The physical properties of Exxon Norpar 14 at room temperature are as follows:

Density: 770 kg/m^3
Viscosity: 2.2 cP
Surface tension: 25 dyne/cm

Gas phase:

As discussed in section 3, the high pressure 6" inch diameter slurry bubble column facility can be operated at pressure up to 200 psig at room temperature. It is equipped with an air compressor which provides up to 310 SCFM at these conditions. The facility has been designed to implement CARPT and CT techniques at high pressure and high superficial gas velocity. Since CARPT and CT have not been used to investigate the effect of high pressure and high gas velocity on the flow pattern, turbulent parameter and phase distribution in 6 inch slurry bubble column and since the implementation of these techniques at these conditions is not trivial, CARPT and CT will be used first to investigate at room temperature the effect of pressure and high gas velocity in slurry bubble column using air compressor. Accordingly, air has been selected as the gas phase. It is noteworthy that we have obtained in the Chemical Reaction Engineering Laboratory (CREL) – Washington University an extensive database of CARPT and CT in air-water system. By using air-Exxon Norpar 14 system, we will study the effect of the physical properties on the measure hydrodynamic parameters.

Solids phase:

CARPT technique will be used to monitor the solids flow pattern and to measure in a non-invasive manner the solids recirculation velocity and turbulent parameters. By combining CARPT/CT/Δp measurements the three phase distribution will be measured radially and axially. As mentioned earlier, CARPT relies on tracking a radioactive tracer particle of the same size and density of the solids used. In our laboratory we have used composite particles of scandium, polypropylene and air of sizes between 2 mm and 2.5 mm as the tracer particles. During this year we have evaluated the possibility of using a scandium radioactive particle with a size similar or close to the FT catalysis size. We found that a scandium particle of 300-150 μm diameter can be obtained (density = 2.99 g/cm^3). Since scandium is a highly reactive metal a nonreactor thin layer of coating is required. A parylene N has been selelcted to coat scandium particles since it has desirable thermal and mechanical properties (density = 1.11 gm/cm^3). According to the density of these materials, a spherical particles of 300 – 150 μm can be obtained with a density range between 2 – 2.8 gm/cm^3 based on the thickness of the coating. Therefore, a density and shape of glass beads particles (~2.4 gm/cm^3) can be matched with scandium coated by N parylene. Hence, in order to implement CARPT technique successfully for the first time in slurry bubble column operated under high pressure and high gas velocity and to obtain for the first time the flow pattern, turbulent parameters and phase distribution, glass beads particles of 150 μm to 300 μm diameter have been selected as the solids system.

5. PREDICTION OF MASS TRANSFER COEFFICIENT IN BUBBLE COLUMNS OPERATED AT HIGH PRESSURE BASED ON ATMOSPHERIC PRESSURE DATA

The liquid volumetric mass transfer coefficient is considered an important design parameter for bubble columns. Consequently, many authors have experimentally determined the values of mass transfer coefficient and developed empirical equations for their estimation (Akita and Yoshida, 1973; Hikita et al., 1981; Hammer et al., 1984; Ozturk et al., 1987). However, these published empirical equations do not account for the effect of pressure, in spite of the fact that the increase in gas hold up and decrease in bubble size with increased pressure leads to a higher interfacial area and mass transfer coefficient. Therefore, the mass transfer coefficient in a high-pressure bubble column will be underestimated by the published empirical correlations. Thus, an accurate estimation of the volumetric mass transfer coefficient for high pressure conditions requires experiments at high pressure, which are more complicated than those at atmospheric pressure.

Very few studies of the mass transfer coefficient at high pressure condition have been reported in the literature. Letzel et al., (1999) measured the mass transfer coefficient in bubble column reactors at elevated pressure by using the dynamic oxygen desorption method. They found that the ratio of volumetric mass transfer coefficient to gas holdup (k_La / ε_g) is constant and equal to approximately one half up to system pressure of 1.0 MPa. However when gas hold up is larger than 35%, the scatter in k_La increases due to the problems with the probe. Kojima et al., (1997) measured the volumetric mass transfer coefficient in bubble columns under pressurized conditions with different liquid phases and with different diameters of the single nozzle used as gas disperser. An empirical correlation was obtained for volumetric mass transfer by considering the effect of pressure and diameter of single nozzle with four empirical constants as fitted parameters, in addition, gas hold up correlation is needed to calculate the mass transfer coefficient. Dewes and Schumpe (1997) reported very strong effects of gas density on gas-liquid mass transfer and the gas density effect increased with the gas velocity. The pressure range in their study was similar to that used by Letzel (1999) and Kojima (1997).

The objective of this study is to develop a procedure for prediction of the volumetric mass transfer coefficient at any pressure based on atmospheric pressure data.

5.1. Procedure development

Wilkinson (1991) recommended accounting for the pressure effect by using the following equation:

$$\frac{(k_L a)_P}{(k_L a)_a} = [\frac{(\varepsilon_G)_P}{(\varepsilon_G)_a}]^M \qquad (5.1)$$

where subscript P means pressure conditions and a indicates atmospheric conditions. This allow one to calculate k_La in pressurized bubble columns from atmospheric data for k_La and gas hold up, provided the gas hold up at elevated pressure is also known. However, due to the complex hold up structure, M depends on physical properties and flow regime (Deckwer et al.,1993). Therefore, the approach suggested by Wilkinson is of limited applicability (Grund et al., 1992). To improve the procedure recommended by Wilkinson, a correlation for M was developed by considering physical properties, column dimension and operation conditions. The following approach was used :

a. Chose proper correlations for the quantities in equation (5.1).

At atmospheric conditions, Akita and Yoshida's correlation is chosen for k_La calculation since it has been proven to be applicable for scale up (Deckwer et al.,1993)

$$\frac{k_L a D^2}{D_L} = 0.6\left(\frac{\mu_L}{\rho_L D_L}\right)^{0.5}\left(\frac{g\rho_L D^2}{\sigma}\right)^{0.62}\left(\frac{g\rho_L^2 D^3}{\mu_L^2}\right)^{0.31}\varepsilon_G^{1.1} \qquad (5.2)$$

To predict gas holdup the correlation of Luo et al.(1999) was used at both low pressure and high pressure since it can cover a wide range of operating conditions and systems of different physical properties,

$$\frac{\varepsilon_G}{1-\varepsilon_G} = 2.9\frac{\left(\frac{U_G^4\rho_G}{\sigma g}\right)^{\alpha}\left(\frac{\rho_G}{\rho_L}\right)^{\beta}}{[\cosh(Mo_L)^{0.054}]^{4.1}} \qquad (5.3)$$

Where $Mo_L = g\mu_L^4 / (\rho_L - \rho_G)\sigma^3$, $\alpha = 0.21Mo_L^{0.0079}$ and $\beta = 0.096Mo_L^{-0.011}$

Substituting equations (5.2) for $(k_La)_a$ to equation (5.1), and assuming $(\varepsilon_G^{1.1}/\varepsilon_G^M)_{atm} = 1$ to simplify the problem, one can obtains the following equation:

$$\frac{k_L a D^2}{D_L} = 0.6Sc^{0.5}Eo^{0.62}Ga^{0.31}(\varepsilon_G)_P^M \qquad (5.4)$$

where $(\varepsilon_G)_P$ can be evaluated from equation (5.3).

b. Develop a correlation for M

In equation (5.4) parameter M depends on physical properties and flow regime which is associated with the operating conditions and column dimensions as mentioned above. To account for these factors, a correlation was developed by Wu et al.(1999):

$$n = 2.188\times10^3\,\mathrm{Re}^{-0.598}Fr^{0.146}M_{oL}^{-0.004} \qquad (5.5)$$

for prediction of the exponent n in the gas radial gas hold up profile which is usually represented by

$$\varepsilon_G = \widetilde{\varepsilon}_G(\frac{n+2}{n})[1-c(r/R)^n]$$

n indicates the steepness of hold up profile and reflect the intensity of liquid circulation. It is depends on flow characteristics and nature of system used as well. n and M must be somehow related. Then M= f (n) can be obtained by fitting part of the experimental data reported in the literature using equation (5.1). We have obtained 155 sets of experimental data available from the literature and chosen 65% of the points to obtain the M dependence on n as follows:

$$M = 0.3\ln(n) + 0.044 \qquad (5.6)$$

Now one can predict the mass transfer coefficient based on gas hold up data only by using equations (5.3)-(5.6). We have compared the model predictions with experimental data at the range of pressure 0.1MPa -1.1MPa. Some of results are shown below.

5.2. Comparison of model prediction and experimental data

At elevated pressure, experimental data has been reported by Letzel (1999) at 0.1MPa to 1.0 MPa system pressure with column diameter equal to 0.15 m using dynamic oxygen desorption method. The comparison of model prediction and the reported experimental data by Letzel (1999) at 0.2MPa system pressure is shown in Figure 1. From Figure 1 one can see that the model predicts the experimental data well. The prediction by the correlation of Akita (1973) under-estimates the experimental data even if using hold up data at 0.2MPa. This correlation usually provides for a conservative estimate as reported by Deckwer et al.(1993). For the pressure at 0.3, 0.4 MPa or higher, the comparison of model prediction and experimental data is similar to what is discussed above and mass transfer coefficient increases with increasing system pressure due to small bubble size and an increase in the number of small bubbles which results in higher gas hold up. In addition, parameter M in equation (5.1) was reported by Wilkinson(1992, 1994) to be equal to 1-1.2. If M is set equal to 1.1, one can apply equation (5.2) and (5.3) in equation (1), then the correlation of Akita returns the same formula except that the hold up needs to be calculated by the correlation obtained at elevated pressure condition. From this point of view, one can argue that the procedure suggested by Wilkinson does not predict the experimental data well without considering the dependence of M on physical properties and flow regime. When the dependence of M on physical properties and flow regime, as suggested by Deckwer et al.(1993), is accounted for the prediction for k_La is good. In this study M was found to vary from 0.4 to 1.1 depending on system pressure and superficial gas velocity.

The other sets of experimental data for volumetric mass transfer coefficient at high pressure was obtained by Kojima (1997) using oxygen electrode (Oxi-96WTW) to measure dissolved oxygen. The column diameter used was small (0.045 m) and the

system pressure range employed was 0.1-1.1 MPa. The comparison of model prediction and experimental data at 0.6 MPa is shown in Figure 5.2. From Figure 5.2, it is clear that the model proposed in this work can predict experimental observation well. Again either Akita's correlation or equation (1) with M=1.1 predicts a lower mass transfer coefficient than experimental data.

The comparison of additional experimental data and model prediction is shown in Figure 5.3. From Figure 5.3, one can see that for most of the available experimental data the error between predicted mass transfer coefficient by this work and experimental data reported in the literature is less than 20% within the pressure range 0.1 to 1.1 MPa. There is another set of experimental results reported by Dewes et al.(1997), The data was not included in Figure 5.3 due to insufficient information on physical properties to be used in the proposed model. However, Dewes et al.(1997) reported that $k_L a \propto \rho_G^{0.45-0.5}$ and this is comparable with this work regarding the dependence of mass transfer coefficient on gas density.

5.3. *SUMMARY*

Based on the approach that mass transfer coefficient and gas hold up data obtained at lower pressure and gas hold up obtained at high pressure conditions can be used to predict the mass transfer coefficient at high pressure, we have chosen the widely accepted mass transfer correlation and newly reported gas hold up correlation which covers wide operating pressure conditions to form a new correlation for the prediction of mass transfer coefficient at wide range of operating conditions. The correlation can be used to predict the mass transfer coefficient up to 1.1 MPa system pressure with error within 20%.

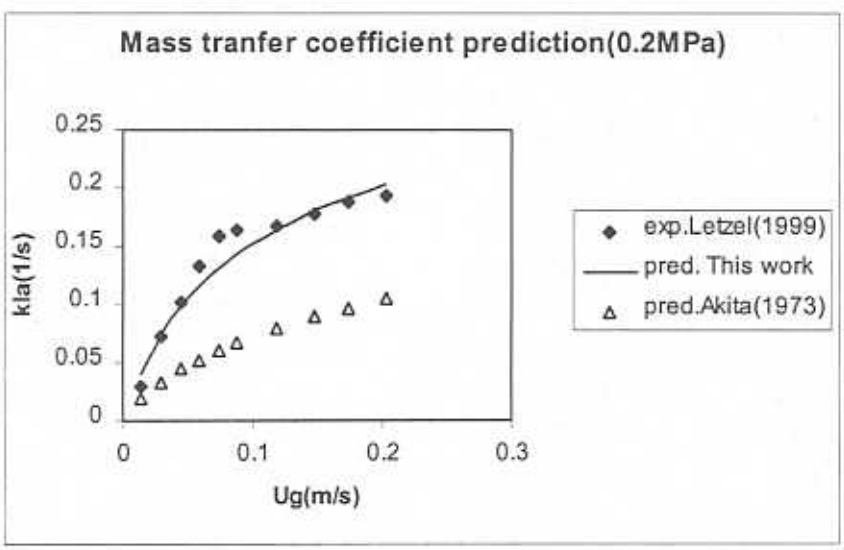

Figure 5.1 Comparison of model prediction and experimental data of Letzel (1999)

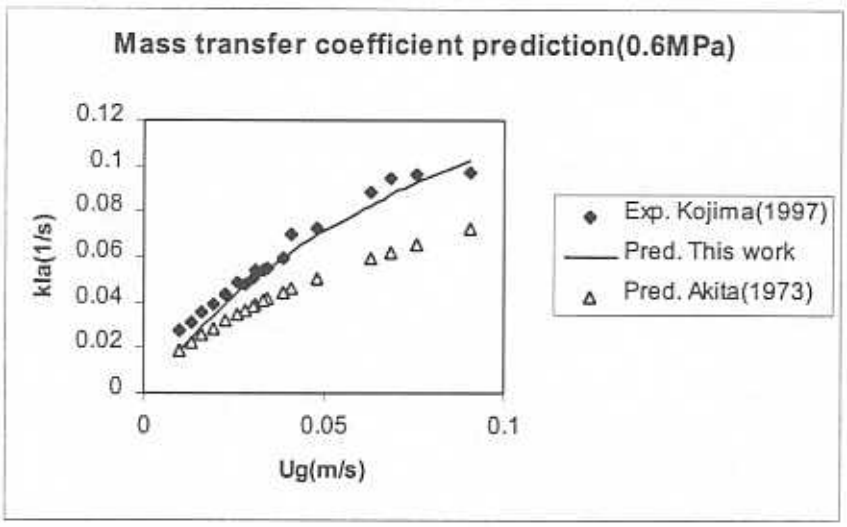

Figure 5.2 Comparison of model prediction and experimental data by Kojima(1997)

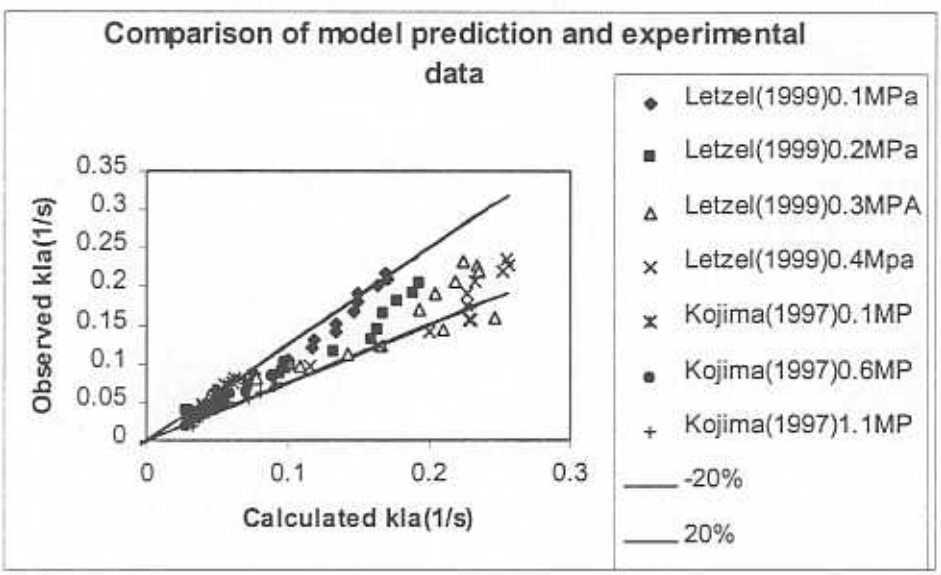

Figure 5.3 Comparison of predicted $k_L a$ and observed $k_L a$

5.4 *NOMENCLATURE*

a	special interfacial area, m^2/m^3
D	Column diameter, m
D_L	Molecular diffusivity, m^2/s
Eo	Eotvos number, dimensionless
Fr_g	Gas Froude number, dimensionless
g	Acceleration due to gravity, m/s^2
Ga	Galieo number, dimensionless
k_La	Volumetric mass transfer coefficient, 1/s
Mo_L	Liquid Morton number, dimensionless
n	Parameter in Eq(5)
Re_G	Reynolds number, dimensionless
Sc	Schmidt number, dimensionless
U_{Sg}	Superficial gas velocity, m/s

Greek letters

ε_G	Cross-sectional average gas hold up
μ_L	Liquid viscosity, Pa.s
ρ_G	Gas density, kg/m^3
ρ_L	Liquid density, kg/m^3
σ_L	Liquid surface tension, N/m

6. REFERENCES

Akita, K.,and F. Yoshida, Gas holdup and volumetric mass transfer coefficient in bubble columns, Ind. Eng. Chem. Proc. Des. Dev., 12, 76, 1973.

Allen, M. P. and D. J. Tildesley. *Computer Simulation of Liquids*, Clarendon Press, Oxford, 1987.

Bukur, D.B., Models for Fischer-Tropsch reaction in slurry bubble column reactors, *Chem. Eng. Sci.*, 38(3), 441, 1983.

Chen, J., A. Kemoun, M.H. Al-Dahhan, M.P. Dudukovic, D.J. Lee, L.S. Fan. Comparative hydrodynamics study in a bubble column using CARPT/CT and PIV. *Chem. Eng. Sci*, 1999.

Chen, J., F. Li, S. Degaleesan, M.H. Al-Dahhan, M.P. Dudukovic, B. Toseland. Fluid dynamic parameters in bubble columns with internals. *Chem. Eng. Sci*, 1999.

Daly, J.G., Patel, S.A. and Bukur, D.B., Measurements of gas holdups in a three phase bubble column by gamma-ray densitometry, *Fluidization VIII*, 647, 1996.

de Swart, J.W.A, Krishna, R., Sie, S.T., Selection, design and scale up of the Fischer-Tropsch reactor, *Stud. Surf. Sci. Catal.*, 107(Natural Gas Conversion IV), 213, 1997.

de Swart, J.W.A. Scale-up of a Fischer-Tropsch slurry reactor. Ph.D. Thesis, University of Amsterdam, The Netherlands. 1996

Deckwer W.-D and A. Schumple, Improved tools for bubble column reactors design and scale up, Chem. Eng. Sci., 48, 889-911, 1993.

Deckwer, W.-D., Serpemen, Y, Ralek, M. and Schmidt B., Modeling the Fischer-Tropsch Synthesis in the slurry phase, *Ind. Eng. Chem. Process Des. Dev.*, 21, 231, 1982.

Degaleesan, S., Dudukovic, M.P., Toseland, B.A. and Bhatt, B.L., A two-compartment convection-diffusion model for slurry bubble column, *Ind. Eng. Chem. Res.*, 36, 4670, 1997.

Degaleesan, S., Turbulence and liquid mixing in bubble columns, *D.Sc. Thesis*, Washington University, St. Louis, MO, 1997.

Devanathan, N. Investigation of liquid hydrodynamics in bubble columns via computer automated radioactive particle tracking (CARPT). D.Sc Thesis, Washington University, St. Louis, 1991.

Dewes I. And A. Schumpe, Gas density effect on mass transfer in the slurry bubble column, Chem. Eng. Sci., 52, 4105-4109, 1997.

Dry, M.E., Advances in Fisher-Tropsch chemistry, *Ind. Eng. Chem. Prod. Res. Dev.*, 15, 282, 1976.

Fan, L.-S., Gas-liquid-solid fluidization engineering, *Butterworths Series in Chemical Engineering*, Boston, 1989.

Fan, L.-S. and K. Tsuchiya. *Bubble Wake Dynamics in Liquids and Liquid-Solid Suspensions*. Butterworth-Heinemann, Stoneham, MA, 1990.

Fan, L.-S., G.Q. Yang, D.J. Lee, K. Tsuchiya and X. Luo. Some aspects of high-pressure phenomena of bubbles in liquids and liquid-solid suspensions. *Chem. Eng. Sci.*, 54, 4681, 1999.

Gormley, R.J., Zarochak, M.F., Deffenbaugh, P.W. and Rao, K.R.P.M., Effect of initial wax medium on the Fishcer-Tropsch slurry reaction, *Applied Catalysis*, 161, 263-279, 1997.

Grevskott, S., B.H. Sannaes, M.P. Dudukovic, K.W. Hiarbo, and H.F. Svendsen. Liquid circulation, bubble size distribution and solids movements in two- and three-phase bubble columns. *Chem. Eng. Sci.*, 51, 1703-1713, 1996.

Grund, G., A. Schumpe and W.D. Deckwer. Gas-liquid mass transfer in a bubble column with organic liquids, Chem. Eng. Sci., 47, 3509-3516, 1992.

Hammer, H, H. Schrag, K. Hektor, K. Schonau, W. Kuster, A. Soemarno, U. Sahabi, and W. Napp, New subfunctions on hydrodynamics, heat and mass transfer for gas/liquid and gas/liquids/solid chemical and biochemical reactors, Front. Chem. Reac. Eng., 464, 1984.

Hikita, H., H. Sasai, K.Tanigawa, K. Segawa,and M. Kitao, The volumetric liquid phase mass transfer coefficient in bubble columns, Chem. Eng. J., 22,61, 1981.

Hills, J.H. Radial non-uniformity of velocity and voidage in a bubble column. *Trans. Inst. Chem. Engrs.*, 52, 1-9, 1974

Huff, G.A.Jr. and Satterfield, C.N., Intrinsic kinetics of the Fischer-Tropsch synthesis on a reduced fused-magnetite catalyst, *Ind. Eng. Chem. Process Des. Dev.*, 23(4), 696, 1984.

Idogawa, K., Ikeda, K., Fukuda, T., and Morooka, S., 'Effect of Gas and Liquid Properties on the Behavior of Bubbles in a Bubble Column under High Pressure,' *Kag. Kog. Ronb.*, 11, 432, 1985.

Idogawa, K., Ikeda, K., Fukuda, T., and Morooka, S., 'Effect of Gas and Liquid Properties on the Behavior of Bubbles in a Column under High Pressure,' *Int. Chem. Eng.*, 27, 93-99, 1987.

Iglesia, E., Design, synthesis, and use of cobalt-based Fischer-Tropsch sythesis catalysts, *Appl. Catal.*, 161(1-2), 59, 1997.

Jean, R.-H. and L.-S. Fan. Rise velocity and gas-liquid mass transfer of a single large bubble in liquids and liquid-solid fluidized beds. *Chem. Eng. Sci.,* 45, 1057, 1990.

Jennings, J.W.,Jr. and Pallas, N. R.., An efficient method for the determination of interfacial tensions from drop profiles, *Langmuir*, 4(4), 959, 1988.

Joshi, J.B. and M.M. Sharma. A circulation cell model for bubble columns. *Trans. Inst. Chem. Engrs*, 57, 244-251, 1979.

Kato, Y., Nishiwaki, A., Fukuda, T. and Tanaka, S., The behavior of suspended solid particles and liquid in bubble columns, *J. Chem. Eng. Japan*, 5, 112, 1972.

Kemoun, A., Ong, B. C., Gupta, P., Al-Dahhan, M. H., and Dudukovic', M. P., 'Gas Holdup in Bubble Columns at Elevated Pressure via Computed Tomography,' To be published in *International J. of Multiphase Flows*, 2000.

Kojima H., J. Sawai and H. Suzuki, Effect of pressure on volumetric mass transfer coefficient and gas hold up in bubble columns, *Chem. Eng. Sci.*, 52, 4111-4116, 1997.

Krishna, R., and Ellenberger, J., 'Gas Holdup in Bubble Column Reactors Operating in the Churn-Turbulent Flow Regime,' *AIChE J.*, 42, 9, 2627-2634, 1996.

Kumar, S.B., Computed tomography measurements of void fraction and modeling of the flow in bubble columns, *Ph.D. Thesis*, Florida Atlantic University, Boca Raton, 1994.

Kuo, J.C.W., Slurry Fischer-Tropsch/Mobil two-stage process of converting syngas to high octane gasoline, *U.S. DOE Final Report*, DOE/PC/30022-10, 1983.

Leib, T.M., Mills, P.L., Lerou, J.J. and Turner, J.R., Evaluation of Neural Networks for simulation of three-phase bubble column reactors, *Trans. Inst. Chem. Eng. (Part A)*, 73, 690, 1995.

Letzel, H.M., J.C. Schouten, R.Krishna, C.M. van den Bleek, Gas hold up and mass transfer in bubble column reactors operated at elevated pressure, Chem. Eng. Sci., 54, 2237-2246, 1999.

Luo, X., P. Jiang, and L.-S. Fan. High pressure three-phase fluidization: hydrodynamics and heat transfer. *AIChE J.*, 43, 2432, 1997a.

Luo, X., J. Zhang, J., K. Tsuchiya, and L.-S. Fan. On the rise velocity of bubbles in liquid-solid suspensions at elevated pressure and temperature. *Chem. Eng. Sci.*, 52, 3693, 1997b.

Luo, X., D. J. Lee, R. Lau, G. Q. Yang, and L.-S. Fan. Maximum stable bubble size and gas holdup in high pressure slurry bubble columns. *AIChE J.*, in press, 1998a.

Luo, X., G. Q. Yang, D. J. Lee, and L.-S. Fan. Single bubble formation in high pressure liquid-solid suspensions. *Powder Technology*, 100, 103, 1998c.

Luo X., D.J. Lee, R. Lau, G.Yang and L.S. Fan, Maximum stable bubble size and gas hold up in high pressure slurry bubble columns, AICHE J., 45, 665-680, 1999.

Marano, J.J. and Holder, G.D., Prediction of bulk properties of Fischer-Tropsch derived liquid, *Ind. Eng. Chem. Res.*, 36(6), 2409-2420, 1997.

Maretto, C. and Krishna, R., 1999. Modeling of a bubble column slurry reactor for Fischer-Tropsch synthesis. *Catalysis Today*. 52, 279-289.

Mendelson, H. D. The motion of an air bubble rising in water. *AIChE J.*, 13, 250, 1967.

Mills, P.L., Turner, J.R., Ramachandran, P.A. and Dudukovic, M.P., The Fischer-Tropsch synthesis in slurry bubble column reactors: analysis of reactor performance using the axial dispersion model, *Topics Chem. Eng.*, 8(Three Phase Sparged Reactors), 339, 1996.

Moslemian, D., Devanathan, N. and Dudukovic, M.P., Radioactive particle tracking technique for investigation of phase recirculation and turbulence in multiphase systems, *Rev. Sci. Instrum.*, 63, 4361, 1992.

Murray, P and Fan, L.-S., Axial solid distribution in slurry bubble columns, *Ind. Eng. Chem. Res.*, 28, 1697, 1989.

Ong, B.-C., N. Rados, P. Gupta, Y. Wu, M.H. Al-Dahhan, M.P. Dudukovic, R. Lau, L.S. Fan. Hydrodynamic of slurry bubble column. Internal report, Chemical Reaction Engineering Laboratory (CREL), Washington University, St. Louis, 2000.

Oukachi R., Singelton, A.H. and Goodwin, J.G., Comparison of patented Co F-T catalysts using fixed-bed and slurry bubble column recators, *Appl. Catal.*, 186(1-2), 129, 1999.

Ozturk, S.S., A. schumpe and W.D. Deckwer, Organic liquids in a bubble column: Hold up and mass transfer coefficients, AICHE J., 33, 1473-1480, 1987.

Patel, S.A., Daly, J.G. and Bukur, D.B., Bubble-Size Distribution in Fischer-Tropsch-Derived Waxes in a Bubble Column, *AIChE J.*, 36(1), 93, 1990.

Prakash, A., On the effect of syngas composition and water-gas-shift reaction rate on FT synthesis over iron based catalyst in a slurry reactor, *Chem. Eng. Commun.*, 128, 143, 1993.

Qicker, G., W.D. Deckwer. A further note on mass transfer limitations in the Fischer-Tropsch slurry process. *Chem. Eng. Sci.*, 36, 1577-1579, 1981.

Rados, N. Slurry bubble column hydrodynamics, D.Sc. Proposal, Washington University, St. Louis, 1999.

Rao, V.U.S., Stiegel, G.J., Cinquegrane, G.J. and Srivastava, R.D., Iron-based catalyst for slurry-phase Fischer-Tropsch process: Technology review, *Fuel Process. Technol.*, 30 (1), 83, 1992.

Rice, R.G., N.W. Geary. Prediction of liquid circulation in viscous bubble columns. *AIChE J.*, 36, 1339-1348, 1990.

Sannaes, B.H., Solids movement and concentration profiles in column slurry reactors, *Dr. Ing. Thesis*, Norweign University of Science and Technology, Trondheim, Norway, 1997.

Sannaes, B.H., M.P. Dudukovic, and H. Svendsen. Experimental and numerical investigation of solids dynamics in slurry bubble columns, in Hamid Amstoopour, Editor, *Fluidization and Fluid-Particle Systems*, preprints, 159-163, Particle Forum of AIChE, 1995.

Shah, Y. T., B. G. Kelkar, S. P. Godbole, and W.-D. Deckwer. Design parameters estimations for bubble column reactors. *AIChE J.*, 28, 353, 1982.

Soong, Y., Harke, F.W., Gamwo, I.K., Schehl, R.R. and Zarochak, M.F., Hydrodynamic study in a slurry-bubble column reactor, *Catalysis Today*, 35, 427-434, 1997.

Srivastava, R.D., Rao, V.U.S. Cinquegrane, G. and Stiegel, G.J., Catalysts for Fischer-Tropsch, *Hydrocarbon Porcess., Int. Ed.*, 69(2), 59, 1990.

Stern, D., Bell, A.T. and Heinemann, H., A theoretical model for the performance of bubble-column recators used for Fischer-Tropsch synthesis, *Chem. Eng. Sci.*, 40(9), 1665, 1985.

Storch, H.H., Golumbic, N. and Anderson, R.B., The Fischer-Tropsch and related synthesis, *John Wiley & Sons, Inc.*, New York, 1951.

Tomiyama, A., I. Kataoka, and T. Sakaguchi. Drag coefficients of bubbles (1st report, drag coefficients of a single bubble in a stagnant liquid). *Nippon Kikai Gakkai Ronbunshu B Hen,* 61(587), 2357, 1995.

Turner, J.R. and Mills, P.L., Comparison of axial dispersion and mixing cell models for design and simulation of Fischer-Tropsch slurry bubble column reactors, *Chem. Eng. Sci.*, 45(8), 2317, 1990.

van der Laan, G.P., Beenackers, A.A.C.M. and Krishna, R., Multicomponent reaction engineering model for Fe-catalyzed Fischer-Tropsch synthesis in commercial scale slurry bubble column reactors, *Chem. Eng. Sci.*, 54, 5013, 1999.

Wasan, D. T. and M. S. Ahluwalia. Consecutive film and surface renewal mechanism for heat and mass transfer from a wall. *Chem. Eng. Sci.*, 24, 1535, 1969.

Wilkinson, P.M., A.P. Apek, and L.L. van Dierendonck, Design parameters estimation for scale-up of high-pressure bubble columns, AICHE J.,38(4), 544-554, 1992.

Wilkinson, P.M., H. Haringa, L. Laurent and Van Dierendonck, Mass transfer and bubble size in a bubble column under pressure, Chem.Eng. Sci., 49(9), 1417-1427, 1994.

Wilkinson, P.M. Physical aspects and scale-up of high-pressure bubble columns", PhD thesis, University of Groningen, The Netherlands, 1991.

Wu, Y.X. and Al-Dahhan, Prediction of gas hold up profiles in bubble column reactors, Accepted in *Chem. Eng. Sci.*, 2000.

Zhang, J., L.-S. Fan, C. Zhu, R. Pfeffer, and D. Qi. Dynamic behavior of collinear collision of elastic spheres in viscous fluids, *Advanced Technologies for Particle Processing,* Vol. II, 44, Particle Technology Forum, AIChE; *Proceedings* of *PTF Topical Conference at AIChE Annual Meeting*, Nov. 15-20, Miami Beach, FL; *Powder Technology*, in press, 1998a.

Zhang, J., Y. Li, and L.-S. Fan. Numerical simulation of gas-liquid-solid fluidization systems using a combined CFD-DPM-VOF method: single bubble rise behavior, *Advanced Technologies for Particle Processing,* Vol. II, 509, Particle Technology Forum, AIChE; *Proceedings* of *PTF Topical Conference at AIChE Annual Meeting*, Nov. 15-20, Miami Beach, FL, 1998b.

APPENDIX A

SOME ASPECTS OF HIGH-PRESSURE PHENOMENA OF BUBBLES IN LIQUIDS AND LIQUID-SOLID SUSPENSIONS

Some aspects of high-pressure phenomena of bubbles in liquids and liquid-solid suspensions

L.-S. Fan, G. Q. Yang, D. J. Lee, K. Tsuchiya, and X. Luo
Department of Chemical Engineering
The Ohio State University
Columbus, Ohio 43210
U.S.A.

ABSTRACT

Some aspects of bubble dynamics and macroscopic hydrodynamic properties in high-pressure bubble columns and three-phase fluidization systems are discussed. Experimental results along with discrete-phase simulations of a single bubble rising in liquids and liquid-solid suspensions at high pressures are presented. A mechanistic model is described, which accounts for the initial size of bubble from a single orifice in liquid-solid suspensions. The mechanism for bubble breakup at high pressures is illustrated by considering bubble instability induced by internal gas circulation inside a bubble, and an analytical expression is obtained to quantify the maximum stable bubble size. Experimental examinations on the roles of bubbles of different sizes indicate the importance of large bubbles in dictating the macroscopic hydrodynamics of slurry bubble columns. Further, extensive studies are made of the key macroscopic hydrodynamic properties, including moving packed bed phenomena, flow regime transition, overall gas holdup, mean bubble size, and bubble size distribution. An empirical correlation is introduced which predicts the gas holdup in slurry bubble columns of different scales. A similarity rule is revealed for the overall hydrodynamics of high-pressure slurry bubble columns, which takes into account the operating conditions, the maximum stable bubble size, and the physical properties of the gas, liquid, and solids. The heat transfer characteristics under high pressures are also investigated. A consecutive film and surface renewal model is used to characterize the heat transfer mechanism.

Keywords — bubble breakup, bubble dynamics, bubble formation, bubble rise velocity, high-pressure three-phase fluidized bed, maximum stable bubble size, slurry bubble column

1. INTRODUCTION

Gas-liquid bubble columns and three-phase fluidization systems are widely used in industry, particularly chemical and petrochemical industries. Three-phase fluidization describes a gas-liquid-solid flow system in which particles are in motion induced by gas and/or liquid phases. Fundamental studies of transport phenomena in bubble columns or three-phase fluidization systems have been extensive over the past decades, and comprehensive reviews are available (Shah *et al.*, 1982; Fan 1989; Deckwer, 1992; Saxena and Chen, 1994). Most studies were conducted under ambient conditions, and relatively little is known regarding high-pressure systems with relevance to industrial processes. Many industrial processes of considerable commercial interest are conducted under high pressures. Examples are: methanol synthesis (at P = 5.5 MPa and T = 0°C), resid hydrotreating (at P = 5.5 to 21 MPa and T = 300 to 425°C), Fischer-Tropsch synthesis (at P = 1.5 to 5.0 MPa and T = 250°C), and benzene hydrogenation (at P = 5.0 MPa and T = 180°C) (Fox, 1990; Jager and Espinoza, 1995; Saxena, 1995; Mill *et al.*, 1996; Peng *et al.*, 1998).

This paper is intended to address the recent advances in transport phenomena of high-pressure bubble columns and three-phase fluidization systems. Selected areas of research centered around the work recently completed by the research group of the senior author at the Ohio State University are discussed together with some relevant works reported in the literature. Experimental results obtained at the Ohio State University are from a high-pressure/high-temperature system of 2- and 4-inch ID columns. The system can be operated at pressures up to 21 MPa and temperatures up to 180°C. Three pairs of windows installed on the column wall allow direct flow visualization to be carried out. Various types of intrusive high-pressure and high-temperature probes, such as the optical fiber probe, and microfoil heat transfer probe, are developed and used to obtain the bubble characteristics and transport properties of the phases. Furthermore, various techniques *via* visualization yield *in-situ* physical properties of the fluids, *e.g.*, the emerging-bubble technique for the surface tension measurement, the hydrostatic weighing method for the density measurement, and the falling-ball technique for the viscosity measurement (Lin and Fan, 1997; Lin *et al.*, 1998).

The selected high-pressure areas discussed in this paper include the bubble

dynamics, covering single bubble rise velocity, bubble formation, and bubble breakup, and the macroscopic hydrodynamic properties, covering moving packed bed phenomena, flow regime transition, overall gas holdup, bubble size, and bubble size distribution, in bubble columns and three-phase fluidized beds. Bubbles rising in liquids and liquid-solid suspensions are examined experimentally as well as numerically. A mechanistic model is described on the bubble formation process from a single orifice in liquid-solid suspensions. The bubble breakup at high pressures is illustrated by considering bubble instability induced by the internal gas circulation inside a bubble, and further, an analytical expression is obtained to quantify the maximum stable bubble size. A correlation is provided to obtain the gas holdup in bubble and slurry bubble columns over a wide range of flow conditions. A similarity rule is revealed for the overall hydrodynamics of high-pressure slurry bubble columns, which takes into account the operating conditions, the maximum stable bubble size, and the physical properties of the gas, liquid, and solids. The heat transfer characteristics are also discussed.

2. BUBBLE DYNAMICS

2.1. Single bubble rise velocity

The characteristics of a rising bubble can be described in terms of the rise velocity, shape and motion of the bubble. These rise characteristics are closely associated with the flow and physical properties (mainly viscosity and presence/absence of solid particles) of the surrounding medium as well as the interfacial properties (*i.e.* presence/absence of surfactant) of the bubble surface. The bubble rise velocity, u_b, is the single most critical parameter in characterizing the hydrodynamics and transport phenomena of bubbles in liquids and liquid-solid suspensions (Fan and Tsuchiya, 1990). The rise velocity of a single gas bubble inherently depends on its size: for small bubbles, the rise velocity strongly depends on liquid properties such as surface tension and viscosity; for large bubbles, the rise velocity is insensitive to liquid properties (Fan, 1989). Under limited conditions, the rise velocities of single bubbles in liquid-solid suspensions were found to be similar to those in highly viscous liquids (Massimilla *et al.*, 1961; Darton and Harrison, 1974). Liquid-solid suspensions can thus be characterized as Newtonian homogeneous media, but they often exhibit non-Newtonian or heterogeneous

behavior (Tsuchiya *et al.*, 1997). Studies in the literature on the bubble rise velocity in liquid-solid suspensions were mainly conducted in water-suspended/fluidized systems and mostly under ambient conditions. Differences in fluidizing media, pressure, and temperature may lead to different bubble rise characteristics.

This section focuses on the bubble rise characteristics in liquids and liquid-solid fluidized beds under frequently encountered industrial conditions, *i.e.* elevated pressure and temperature, and with a non-water based liquid medium. In liquid-solid suspensions under these conditions, the bubble rise velocity is discussed in light of both the apparent homogeneous (or effective) properties of the suspension and the recently evolved numerical prediction based on a computational model for gas-liquid-solid fluidization systems.

2.1.1. In liquids

Krishna *et al.* (1994) studied the pressure effect on the bubble rise velocity and found that the single bubble rise velocity does not depend on the gas density over the range of 0.1 to 30 kg/m^3. The conclusion is limited to a narrow range of pressures. Lin *et al.* (1998) measured the rise velocity of single bubbles of known sizes in Paratherm NF heat transfer fluid at various pressures ranging from 0.1 to 19.4 MPa for three temperatures: 27, 47, and 78°C. The bubble size is represented by the equivalent spherical diameter, d_b. Figure 1 shows their results for (a) 27°C and (b) 78°C. As shown in the figure, for a given bubble size, u_b tends to decrease with increasing pressure at both temperatures. They found that the effects of pressure and temperature, or more directly, the effects of physical properties of the gas and liquid phases on the variation of u_b with d_b could be represented or predicted most generally by the Fan-Tsuchiya equation (Fan and Tsuchiya, 1990) among three predictive equations. The other two are the modified Mendelson's wave-analogy equation (Mendelson, 1967) by Maneri (1995) and a correlation proposed by Tomiyama *et al.* (1995).

The Fan-Tsuchiya equation, generalized for high-pressure systems, can be written in a dimensionless form:

$$u_b' = u_b\left(\frac{\rho_l}{\sigma g}\right)^{1/4} = \left\{\left[\frac{Mo^{-1/4}}{K_b}\left(\frac{\Delta\rho}{\rho_l}\right)^{5/4} d_b'^2\right]^{-n} + \left[\frac{2c}{d_b'} + \left(\frac{\Delta\rho}{\rho_l}\right)\frac{d_b'}{2}\right]^{-n/2}\right\}^{-1/n} \quad (1)$$

where the dimensionless bubble diameter is given by

$$d_b' = d_b(\rho_l g/\sigma)^{1/2}. \quad (2)$$

Three empirical parameters, n, c, and K_b, in Eq. (1) reflect three specific factors governing the rate of bubble rise. They relate to the contamination level of the liquid phase, to the varying dynamic effects of the surface tension, and to the viscous nature of the surrounding medium. The suggested values of these parameters are:

$$n = \begin{cases} 0.8 & \text{for contaminated liquids} \\ 1.6 & \text{for purified liquids} \end{cases}, \quad (3a)$$

$$c = \begin{cases} 1.2 & \text{for monocomponent liquids} \\ 1.4 & \text{for multicomponent liquids} \end{cases}, \text{ and} \quad (3b)$$

$$K_b = \max\left(K_{b0} Mo^{-0.038}, 12\right) \quad (3c)$$

where

$$K_{b0} = \begin{cases} 14.7 & \text{for aqueous solutions} \\ 10.2 & \text{for organic solvents/mixtures} \end{cases}. \quad (3d)$$

The modified Mendelson's equation is a special form of the Fan-Tsuchiya equation where the viscous term, *i.e.* the first term on the right side of Eq. (1), is omitted. Equally general as the Fan-Tsuchiya equation for bubbles in liquids, the correlation by Tomiyama *et al.* (1995), which is given in terms of drag coefficient,

$$C_D = \frac{4}{3}\frac{g\,\Delta\rho\,d_b}{\rho_l u_b^2}, \quad (4)$$

consists of three equations under different system purity:

$$C_D = \max\left\{\min\left[\frac{16}{Re}(1+0.15Re^{0.687}), \frac{48}{Re}\right], \frac{8}{3}\frac{Eo}{Eo+4}\right\} \quad (5a)$$

for purified systems;

$$C_D = \max\left\{\min\left[\frac{24}{Re}(1+0.15Re^{0.687}), \frac{72}{Re}\right], \frac{8}{3}\frac{Eo}{Eo+4}\right\} \quad (5b)$$

for partially contaminated systems; and

$$C_D = \max\left[\frac{24}{Re}(1+0.15Re^{0.687}),\ \frac{8}{3}\frac{Eo}{Eo+4}\right] \tag{5c}$$

for sufficiently contaminated systems. In Eqs (1) and (5), the dimensionless groups are defined as

$$Mo = \frac{g\,\Delta\rho\,\mu_l^4}{\rho_l^2\,\sigma^3}, \tag{6a}$$

$$Re = \frac{d_b u_b \rho_l}{\mu_l}, \text{ and} \tag{6b}$$

$$Eo = \frac{g\,\Delta\rho\,d_b^2}{\sigma} \tag{6c}$$

where $\Delta\rho = \rho_l - \rho_g$. It is noted that u_b can be obtained explicitly from Eq. (1) for a given d_b as well as gas and liquid physical properties, while it can only be obtained implicitly from Eq. (5).

For predictions included in Fig. 1, measured values of physical properties under various operating pressures and temperatures (Lin and Fan, 1997; Lin *et al.*, 1998) are used. As shown in the figure, the modified Mendelson equation, which is valid only under the inviscid condition, provides limited agreement between the measured and calculated results at the low temperature [Fig. 1(a)], suggesting that viscous forces predominate in the bubble rise process. On the other hand, at the high temperature [Fig. 1(b)], there is a strong agreement over the bubble size range of $d_b > 2$ mm including the sharp breakpoint/peak. This indicates that the liquid used tends to behave as a pure inviscid liquid. Note that over the pressure range from 0.1 to 19.4 MPa, the liquid viscosity varies from 29 to 48 mPa·s at 27°C, whereas it is almost constant within a range from 4.7 to 5.2 mPa·s at 78°C (Lin *et al.*, 1998).

The Fan-Tsuchiya equation, Eq. (1), applied for the given liquid, a pure (n = 1.6), multicomponent (c = 1.4) organic solvent (K_{b0} = 10.2), demonstrates good overall predictive capability except for the sharp peak existing for the high-temperature data [Fig. 1(b)]. The equation by Tomiyama *et al.* (1995) also has good general applicability, especially around the peak behavior occurring near d_b = 2 mm at 78°C; however, it tends to underestimate the u_b values over the rest of the d_b range.

The consistent difference in u_b prevailing between 0.1 and 19.4 MPa for $d_b > 2$ mm is due to the significant increase in gas density (as large as 200-fold increase with pressure from 0.1 to 19.4 MPa). The density effect is accounted for in Eq. (1) in terms of $\Delta\rho/\rho_l$ or in Eq. (5) in terms of both $\Delta\rho/\rho_l$ and *Eo*. As can be seen from the equations and figure, the density difference between the continuous liquid phase and the dispersed gas phase plays an important role in determining u_b, especially for large bubbles.

Figure 2 shows the *Re–Eo* relationship often utilized in representing the general rise characteristics of single bubbles in liquids (Clift *et al.*, 1978; Bhaga and Weber, 1981). The thin, background lines signify the general, quantitative trend for the rise velocity of single bubbles in purified Newtonian liquids under ambient conditions, plotted with constant intervals of log *Mo*. The figure shows the general agreement in correlation predictions. The experimental results under four conditions (Lin *et al.*, 1998) are plotted in the figure. By employing accurate values for physical properties of the liquid phase and the gas density at given pressures and temperatures, the experimental results can be successfully represented over the entire *Eo* range, *i.e.* bubble size range, by Eq. (1). The prediction is proven to represent experimental data for various liquids under ambient conditions within some deviations (Tsuchiya *et al.*, 1997). Furthermore, the single bubble rise velocity at high pressures can be reasonably estimated by incorporating the physical properties of the gas and liquid under the operating conditions.

2.1.2. In liquid-solid suspensions

Figure 3 shows the effect of pressure on the bubble rise velocity in a fluidized bed with Paratherm NF heat transfer fluid and 0.88-mm glass beads at (a) 26.5°C and (b) 87.5°C (Luo *et al.*, 1997b). At both temperatures, the bubble rise velocity decreases with an increase in pressure for a given solids holdup. The extent of the reduction is as high as by 50% from 0.1 to 17.3 MPa. A more drastic reduction in u_b, however, arises from the addition of solid particles. While the particle effect is small at low solids holdup ($\varepsilon_s <$ 0.4), the effect is appreciable at high solids holdup (ε_s = 0.545), especially for high liquid viscosity [Fig. 3(a)]. A comparison of the data at 26.5°C and 87.5°C, for the same ε_s of 0.545, indicates that the viscosity effect appears to be significant. The reduction of

the bubble rise velocity with an increase in pressure can lead to a significant increase in the gas holdup of three-phase fluidized beds. The extent of the increase in gas holdup was reported to be around 100% at all gas velocities when the pressure is increased from 0.1 to 15.6 MPa (Luo *et al.*, 1997a). By comparing the pressure effect on the gas holdup with that on the bubble rise velocity, the increase in gas holdup with pressure is a consequence of the decreases in both the bubble size and the bubble rise velocity.

Similar plots are shown in Fig. 4 for the fluidized bed containing 0.21-mm glass beads (Luo *et al.*, 1997b). While the extent of decrease in bubble rise velocity with an increase in pressure is comparable between 0.88- and 0.21-mm glass beads, the extent of decrease in bubble rise velocity with an increase in solids holdup is much smaller for the smaller particles. By comparing the corresponding data in Figs 3 and 4, this difference in the sensitivity of u_b reduction to solids holdup variation is clearly shown for the high solids holdup cases.

The decrease in bubble rise velocity occurs due to corresponding variations of gas and liquid properties with pressure. In the presence of solid particles, it can be assumed, as a first approximation, that the particles modify only homogeneous properties of the surrounding medium. Luo *et al.* (1997b) examined the applicability of this homogeneous approach. The calculated results based on the Fan-Tsuchiya equation, Eq. (1), for u_b are also plotted in Figs 3 and 4, where Eq. (1) is extended to liquid-solid suspensions by replacing the liquid properties, ρ_l and μ_l, by the effective properties of the liquid-solid suspension, ρ_m and μ_m (Tsuchiya *et al.*, 1997), respectively. The effective density can be estimated by

$$\rho_m = \rho_l(1-\varepsilon_s) + \rho_s\varepsilon_s . \tag{7}$$

The calculated results with constant values of μ_m given in Figs 3 and 4 are obtained by coupling Eq. (1) with the following relationship proposed by Tsuchiya *et al.* (1997) for the effective viscosity of liquid-solid suspensions:

$$\frac{\mu_m}{\mu_l} = \exp\left[\frac{K\varepsilon_s}{1-(\varepsilon_s/\varepsilon_{sc})}\right] \tag{8}$$

with two parameters correlated by Luo *et al.* (1997b):

$$K = \frac{3.1 - 1.4 \tanh\left[0.3(10 - 10^2 u_t)\right]}{\phi} \quad \text{and} \tag{9a}$$

$$\varepsilon_{sc} = \left\{1.3 - 0.1 \tanh\left[0.5(10 - 10^2 u_t)\right]\right\} \varepsilon_{s0} \tag{9b}$$

where u_t is in m/s. The ranges of applicability of Eqs (8) and (9) are: $840 < \rho_l < 1000$ kg/m^3; $1 < \mu_l < 47$ mPa·s; $19 < \sigma < 73$ mN/m; $0 < \varepsilon_s < 0.95\,\varepsilon_{s0}$; $7.9\times10^{-4} < u_t < 0.26$ m/s; $0.88 < \phi \leq 1$; and $0.56 < \varepsilon_{s0} < 0.61$.

Equation (1) with parametric values of μ_m, estimated from Eq. (8) under given conditions, predicts reasonably well the general trend exhibited by the reported data. However, a detailed match between the calculated and experimental results appears to be difficult to attain by assigning a constant value of μ_m under each condition. A more elaborate analysis is required to account for the effect of bubble size on interactions of the bubble with the surrounding medium (non-Newtonian approach) or with individual particles (heterogeneous approach).

2.2. Heterogeneous approach: Discrete-phase computation

Jean and Fan (1990) developed a mechanistic model that accounts for impact forces on a rising bubble due to particles. The model can predict the bubble rise velocity for small particles ($d_p < 500$ μm), low-to-intermediate solids holdups ($\varepsilon_s < 0.45$) and large spherical-cap bubbles ($d_b > 15$ mm). It is desired to extend their model to cover the range of smaller bubble sizes as well. This was conducted by Luo *et al.* (1997b) with partial success based on a force balance on a rising bubble involving the net gravity, liquid drag, and particle-bubble collision forces.

A much more thorough scheme of prediction of a single bubble rising in a liquid-solid fluidized bed has recently been developed by Zhang *et al.* (1998b) using a two-dimensional discrete-phase simulation model for gas-liquid-solid fluidization systems. In this model, the volume-averaged method, the dispersed particle method (DPM) and the volume-of-fluid (VOF) method are used to account for the flow of liquid, solid, and gas phases, respectively. A bubble induced force (BIF) model, a continuum surface force (CSF) model, and Newton's third law are applied to account for the couplings of particle-bubble (gas), gas-liquid, and particle-liquid interactions, respectively. A close distance

interaction (CDI) model (Zhang *et al.*, 1998a) is included in the particle-particle collision analysis, which considers the liquid interstitial effects between colliding particles.

2.2.1. Liquid-phase model

The governing equations for the continuous phase of multiphase flows can be derived based on the Navier-Stokes equations for single-phase flows. Considering the existence of dispersed particles, a volume-averaging technique is used to develop a set of partial differential equations to describe the mass and momentum conservation of the liquid phase. The continuity equation for the liquid phase can be given as

$$\frac{\partial \varepsilon_l}{\partial t} + \nabla \cdot (\varepsilon_l v) = 0 . \tag{10}$$

The momentum equation for the liquid phase is

$$\rho_l \frac{\partial (\varepsilon_l v)}{\partial t} + \rho_l \nabla \cdot (\varepsilon_l v v) = -\nabla p + \varepsilon_l \nabla \cdot \tau + \varepsilon_l \rho_l g + f_b \tag{11}$$

where v is the liquid velocity vector, ε_l is the liquid holdup, ρ_l is the liquid density, p is the scalar pressure, τ is the viscous stress tensor, g is the gravitational acceleration, and f_b is the total volumetric body force acting on the liquid phase other than the gravity force.

The Newtonian viscous stress tensor is used which is given as

$$\tau = 2\mu S = \mu \left[(\nabla v) + (\nabla v)^T \right] \tag{12}$$

where S is the rate-of-strain tensor and μ is the coefficient of dynamic viscosity.

2.2.2. Gas-phase model

Under high-pressure conditions, the effects of gas density and viscosity on the flow behavior would be significant. The simulation model for high pressures is conducted by including the simulation of the flow inside the gas bubble. The flow inside the gas bubble is governed by single-phase Navier-Stokes equations. Because of the difficulty of numerical calculation due to the discontinuous jump of properties across the interface between the gas bubble and the liquid-solid suspension, a continuous transition method (CTM) is employed. In this method, the discontinuous characteristics are replaced by a smooth variation of the properties (*e.g.*, density and viscosity) from one phase to another

within the finite interface thickness. The continuous transition method can overcome the problem of numerical divergence while simulating the flow field at both sides of the interface where the physical properties of the fluids strongly differ. By using the high-pressure fluid conditions, the resulting discrete phase simulation method can reveal the pressure effects on the variation of the flow characteristics in a gas-liquid-solid fluidization system.

The scalar fraction function, $\alpha(x, t)$, solved by the VOF method (Hirt and Nichols, 1981) is used to construct this continuous transition function, and the fluid property at the interface can be given by:

$$Q = Q_m^* \alpha(x,t) + Q_g^* [1 - \alpha(x,t)] \tag{13}$$

where Q represents a property of the fluid, Q_m^* and Q_g^* represent the properties of liquid-solid suspension and gas bubble, respectively. By definition, $\alpha(x, t) = 1$ in the liquid or liquid-solid mixture, $0 < \alpha(x, t) < 1$ at the free surface, and $\alpha(x, t) = 0$ in the gas bubble. Therefore, Q is replaced by Q_m^* or Q_g^* when $\alpha(x, t)$ equals 1 in the liquid-solid suspension or equals 0 in the gas bubble.

The advection equation for $\alpha(x, t)$ is

$$\frac{\partial \alpha}{\partial t} + (v \cdot \nabla)\alpha = 0. \tag{14}$$

On the gas-liquid free surfaces, the stress boundary condition follows the Laplace equation as

$$p_s = p - p_v = \sigma\kappa \tag{15}$$

where the surface pressure, p_s, is the surface tension-induced pressure jump across a fluid interface. The continuum surface force (CSF) model (Brackbill *et al.*, 1992) converts the surface force into a volume force within free surfaces. The volume force at the free surfaces is given by the CSF model as

$$f_{sv}(x,t) = \sigma\kappa(x,t)\nabla\alpha(x,t). \tag{16}$$

This volume force is added to the volumetric body force term, f_b, in the momentum equation at the free surfaces.

2.2.3. Dispersed particle method

The motion of a particle in a flow field can be described in Lagrangian coordinates with its origin attached to the center of the moving particle. The motion of a single particle can be described by its acceleration and rotation in a nonuniform flow field. The particle accelerating in the liquid is governed by Newton's second law of motion as

$$m_p \frac{dv_p}{dt} = F_{total} . \tag{17}$$

The forces acting on a particle include interface forces between the fluid and particle, and forces imposed by external fields. The total force acting on a particle is composed of all applicable forces, including drag, added mass, gravity/buoyancy, Magnus force, Basset force, and other forces:

$$F_{total} = F_D + F_{AM} + F_{G/B} + F_{Magnus} + F_{Basset} + \sum_i F_i . \tag{18}$$

The general scheme of a stepwise molecular dynamic (MD) simulation (Allen and Tildesley, 1987), based on a predictor-corrector algorithm, is used to compute the particle motion. The hard sphere approach is used for the collision dynamics. The normal velocity and momentum changes of colliding particles are determined by a collinear collision model developed by Zhang *et al.* (1998a). The model includes the detailed close-range particle-fluid and particle-particle interactions during the entire process of particle collision. The tangential velocity and momentum changes are formulated and calculated based on a sticking/sliding model.

2.2.4. Coupling among individual phases

When particles move into the gas-liquid interface, *i.e.* into the domain where $0.5 < \alpha(x, t) < 1$, the surface tension force is also acting on the particle. This force equals the volumetric surface tension force, f_{sv}, of Eq. (16) multiplied by the particle volume. If the total force of the particle is larger than the surface tension force, the particle would penetrate the bubble surface. The penetrating particle breaks the bubble surface momentarily upon contact. If the penetrating particle is small, the bubble may recover its original shape upon particle penetration (Chen and Fan, 1989). However, if there are several particles colliding with the bubble surface simultaneously, the resulting force may

cause bubble breakage.

Based on Newton's third law of motion, the forces acting on particles from the liquid phase, which include F_D, F_{AM}, and F_{Basset}, yield a reaction force on the liquid. Therefore, the momentum transfer from particles to liquid is taken into account by adding the volumetric liquid-particle interaction force to the body force term, f_b, in Eq. (11).

The liquid properties on the particle surface are obtained by an area-weighted averaging based on the properties at the four grid points of the computational cell containing the particle. The liquid holdup, ε_l, is obtained by subtracting the volume fraction of the particles in the computational cell. However, this cell-averaged liquid holdup is only used for solving the volume-averaged equations of liquid phase. When accounting for the liquid holdup effect on the particle drag coefficient in the liquid-solid medium, a particle-centered area averaging method is used for the calculation.

2.3. Computational results: Single bubble rising

The simulations of representative cases, *i.e.* a single bubble rising and particle entrainment by a bubble in a liquid-solid fluidized bed under ambient conditions (Zhang *et al.*, 1998b), and a single bubble rising in a liquid under high-pressure conditions, are presented in this section.

2.3.1. Ambient conditions

Comparisons of the simulation and the experimental results of a single bubble rising in a liquid-solid suspension are shown in Fig. 5. The simulation domain is 30 × 80 mm^2 and a computational grid size is 0.15 × 0.16 mm^2. One thousand particles with a density of 2,500 kg/m^3 and a diameter of 1.0 mm are used as the solid phase. An aqueous glycerin solution (80 wt%) with ρ_l = 1,206 kg/m^3, μ_l = 52.9 mPa·s, and σ = 62.9 mN/m is used as the liquid phase. A circular bubble with a diameter of 10 mm is initially imposed in the computational domain with its center 15 mm above the bottom. Initially, the particles are randomly positioned in a 30 × 240 mm^2 area. Then, the simulation is performed for particles settling at a liquid velocity of 5 mm/s. At this stage, the bubble is treated as an obstacle and fixed in the original place. An equilibrium bed height is

reached at 80 mm, which gives a three-dimensional equivalent solids holdup of 0.44. After the bed reaches its equilibrium height, the simulation is restarted with bubble tracking and particle movement. The time step of simulation for liquid and solid phases is 5 μs. Experiments are performed in a two-dimensional column with a thickness of 7 mm. The solids holdup, liquid velocity, and the liquid and solids properties are the same as the simulation conditions. As shown in the figure, the simulation and experimental results of the bubble rise velocity and the bubble shape generally agree well.

By closely following the evolution of the particle flow around a single bubble, the mechanisms of particle entrainment in a liquid-solid suspension were studied by Miyahara *et al.* (1989), Fan and Tsuchiya (1990), and Tsuchiya *et al.* (1992). These studies indicated that particles are drawn from the upper surface of the suspension into the freeboard of liquid in the wake behind the bubble, and particle-containing vortices are shed from the wake in the freeboard. The simulation results of the bubble emerging from the bed surface are shown in Fig. 6. As seen in subsequent frames of Fig. 6, a group of particles are dragged by the bubble wake. An agreement in spatial and temporal variations of the solid particles in the entrainment process with the rising bubble is found between the simulation and the experimental results by Miyahara *et al.* (1989) and Tsuchiya *et al.* (1992).

2.3.2. High-pressure conditions

A single bubble rising in a liquid at elevated pressures (P = 19.4 MPa) is simulated. The properties of the liquid phase under ambient conditions are: ρ_l = 868 kg/m^3; μ_l = 29 mPa·s; and σ = 30 mN/m. The computational domain is 100 × 90 mm^2 with 90 × 90 grids. A circular nitrogen bubble with a diameter of 80 mm is initially imposed at 15 mm from the bottom, and its rising behavior is tracked by numerical simulation. The time step of simulation for the liquid and solid phases is 5 μs. Simulation results are shown in Fig. 7, in which the original point of the coordinate system is fixed on the mass center of the rising bubble. The numerical simulation indicates that the bubble rise velocity decreases with an increase in pressure, and is in good agreement with the experimental data and the prediction by the Fan-Tsuchiya equation, Eq. (1). It also can be seen in the figure that the elevated pressure causes the bubble shape to become

more flat due to the variation of properties inside the bubble. As shown in Fig. 7, the simulation cannot only capture the wake structure, but also predict the internal flow circulation structure in the bubble.

2.4. Bubble formation, initial bubble size, and jetting

Numerous experimental and modeling studies have been conducted over the past decades on bubble formation from a single orifice or nozzle submerged in liquids, mostly under ambient conditions (Kupferberg and Jameson, 1969; Kumar and Kuloor, 1970; Azbel, 1981; Lin *et al.*, 1994; Ruzicka *et al.*, 1997). Among various factors that affect the bubble formation, the wettability of the orifice surface is an important factor, which affects the initial size of the bubble formed on the orifice. Lin *et al.* (1994) found that initial bubble size increases significantly with the contact angle between the bubble and the orifice surface when the contact angle exceeds the threshold value of 45°. Various models were established to predict the initial bubble size from a single nozzle in liquids. However, only a few studies were conducted at elevated pressures (LaNauze and Harris, 1974; Idogawa *et al.*, 1987; Tsuge *et al.*, 1992; Wilkinson and Van Dierendonck, 1994). The high-pressure studies indicated that an increase in gas density reduces the size of bubbles formed from a single orifice. However, these results were limited to water systems only. The pressure effect on the initial bubble size in hydrocarbon liquids is not fully understood. Furthermore, studies of the bubble formation in liquids in the presence of particles, as in slurry bubble columns and three-phase fluidized bed systems, are very limited. The experimental data of Massimilla *et al.* (1961) in an air-water-glass beads three-phase fluidized bed revealed that the bubbles formed from a single nozzle in the fluidized bed are larger in size than those in water, and the initial bubble size increases with the solids concentration. Yoo *et al.* (1997) investigated bubble formation in pressurized liquid-solid suspensions. They used 18.6 wt% aqueous glycerol solution and 0.1-mm polystyrene beads as the liquid and solid phases, respectively. The densities of the liquid and the particles were identical, and thus, the particles were neutrally buoyant in the liquid. The results indicated that initial bubble size decreases inversely with pressure under otherwise constant conditions, *i.e.* gas flow rate, temperature, solids concentration, orifice diameter, and gas chamber volume. Their results also showed that

the particle effect on initial bubble size is insignificant. The difference in the finding regarding the particle effects on initial bubble size between Massimilla *et al.* (1961) and Yoo *et al.* (1997) may possibly be due to the difference in particle density.

A mechanistic model is described to predict the initial bubble size in liquid-solid suspensions at high-pressure conditions (Luo *et al.*, 1998c). The model considers various forces induced by the particles, and is an extension of a two-stage spherical bubble formation model developed by Ramakrishnan *et al.* (1969) for liquids. In the two-stage spherical bubble formation model, bubbles are assumed to be formed in two stages, namely, the expansion stage and the detachment stage. The bubble expands with its base attached to the nozzle during the first stage. In the detachment stage, the bubble base moves away from the nozzle, although the bubble remains connected with the nozzle through the neck. The shape of the bubble is assumed to remain spherical during the entire bubble formation process. It is also assumed in this model that a liquid film always exists around the bubble. During the expansion and detachment stages, particles collide with the bubble and stay on the liquid film. The particles and the liquid surrounding the bubble are set in motion as the bubble grows and rises.

The volume of the bubble at the end of the first stage and during the second stage can be described by considering a balance of all the forces acting on the bubble being formed if the instantaneous gas flow rate, Q_o, or the instantaneous gas velocity, u_o, through the orifice, is known. The forces induced by the liquid include the upward forces (effective buoyancy force, F_B, and gas momentum force, F_M), and the downward resistance (liquid drag, F_D, surface tension force, F_σ, bubble inertial force, $F_{I,g}$, and Basset force, F_{Basset}) as shown in Fig. 8. It is assumed that the particles affect the bubble formation process only through two additional downward forces on the bubble, *i.e.* the particle-bubble collision force, F_C, and the suspension inertial force, $F_{I,m}$, due to the acceleration of the liquid and particles surrounding the bubble. Therefore, the overall force balance on the bubble in this model can be written as

$$F_B + F_M = F_D + F_\sigma + F_{Basset} + F_{I,g} + F_C + F_{I,m}. \qquad (19)$$

The expansion stage and the detachment stage follow the same force balance equation, Eq. (19), although the expression for the same force in the two stages may be

different. The expressions for all the forces under two stages are listed in Table 1. The particle-bubble collision force is merely the rate of momentum change of the particles colliding with the bubble surface. The suspension inertial force is calculated from the suspension flow field around an accelerating bubble, obtained from a particle image velocimetry system.

The model is applied to simulate the bubble formation process under constant flow conditions, which are characterized by constant gas flow rate through the orifice. When the volume of the gas chamber is small, the bubble formation can normally be assumed under constant flow conditions. It can be seen from Fig. 9 that the model closely predicts experimental data on the initial bubble size in high-pressure slurry systems (Luo *et al.*, 1998c). Under constant flow conditions ($Nc < 1$), the pressure effect is insignificant. Note that Nc is the dimensionless capacitance number and is equal to $4V_c g\rho_l / \pi D_o^2 P_s$.

In most industrial gas distributors, the gas chamber volume is large and the bubble formation process is under other conditions, *e.g.*, constant pressure or intermediate conditions; in these cases, the orifice gas flow rate is not constant and depends on the pressure fluctuations in the chamber and in the bubble. The experimental study under such conditions is scarce. Yang *et al.* (1999) measured the initial bubble size in a slurry bubble column under intermediate conditions ($Nc > 1$) using an optical fiber probe. As shown in Fig. 10, the pressure has a significant effect on the initial bubble size under these conditions (Yang *et al.*, 1999). The initial bubble size decreases with an increase of pressure for the bubble formation with a large gas chamber. In order to model the bubble formation under such conditions, the pressure fluctuations in the gas chamber and in the bubble must be considered to account for the time-variant orifice gas flow rate as illustrated below.

The instantaneous gas flow rate through the orifice depends on the pressure difference in the gas chamber, P_c, and inside the bubble, P_b, as well as the flow resistance of the orifice, which can be described by the orifice equation as given in Eq. (20a). The pressure in the gas chamber can be evaluated by applying the first law of thermodynamics, considering an adiabatic compression process as given in Eq. (20b) (Wilkinson and Van Dierendonck, 1994). The pressure inside the bubble is governed by a

modified Rayleigh's equation (Pinczewski, 1981). In order to simulate the bubble formation in liquid-solid suspensions, the effect of particles on the pressure inside the bubble must be considered. Yang *et al.* (1999) replaced the liquid inertial term in the modified Rayleigh equation with the suspension inertia, quantified based on the suspension flow field around an accelerating bubble obtained by the PIV measurement, as given in Eq. (20c).

$$\Delta P = \left| P_c - P_b \right| = \left(\frac{Q_o}{k_o} \right)^2 . \tag{20a}$$

$$\frac{\mathrm{d}P_c}{\mathrm{d}t} = \frac{\gamma}{V_c} \left(P_c Q_g - P_c Q_o \right). \tag{20b}$$

$$P_b - P_o = \zeta \rho_m \left[\frac{r_b}{3} \frac{\mathrm{d}^2 r_b}{\mathrm{d}t^2} + \left(\frac{\mathrm{d}r_b}{\mathrm{d}t} \right)^2 \right] + \frac{2\sigma}{r_b} + \frac{4\mu_l}{r_b} \frac{\mathrm{d}r_b}{\mathrm{d}t} . \tag{20c}$$

where p_o is the hydrostatic pressure at the bubble surface. The three terms on the right-hand side of Eq. (20c) represent the contributions of inertial, surface tension, and viscous forces, respectively. The coefficient ζ in Eq. (20c) is equal to 3.86 for bubbles formed in liquid-solid suspensions (Luo *et al.*, 1998c) and to $11/16$ for bubbles formed in liquids, corresponding to the added mass in inviscid liquids (Milne-Thomson, 1955). Combining Eqs (19) and (20a, b, c), and solving these coupled ordinary differential equations simultaneously, the change of the initial bubble size with the time can be obtained. If a certain bubble detachment criterion is used, the initial bubble size can be estimated.

At a low gas velocity, discrete bubbles are formed. On the other hand, at a high gas velocity, jetting occurs and bubbles are formed from the top of the jet. The bubbles formed from a jet are of a wide size distribution. The empirical correlation provided by Idogowa *et al.* (1987) indicated that the bubbling-jetting transition velocity in a liquid is proportional to the gas density raised to the power of -0.8. Luo *et al.* (1998b) investigated the transition from bubbling to jetting under high pressures. They revealed a significant effect of the orifice Reynolds number, $Re_o = \rho_g D_o u_o / \mu_g$, on the bubbling and jetting

phenomena. Photographs of the gas flow through an orifice in Paratherm NF heat transfer fluid at a high pressure for various Re_o are shown in Fig. 11. At Re_o = 1,075, single bubbles are formed from the orifice. With increasing Re_o to 5,321, bubbles being formed at the orifice start to interact with the preceding ones. Bubble coalescence occurs between the two bubbles, sometimes involving more bubbles. At Re_o = 8,809, frequent coalescence of successive bubbles is observed, *i.e.* the beginning of the bubbling-jetting transition. As Re_o increases, the jetting regime becomes more apparent. Bubbles break away from the top of the jet. Moreover, the jet penetration depth increases with an increase in Re_o.

2.5. Bubble coalescence

For gas-liquid systems, the experimental results available in the literature indicate that an increase of pressure retards the bubble coalescence (Sagert and Quinn, 1977, 1978). There are three steps in the bubble coalescence process (Vrij, 1966; Chaudhari and Hoffmann, 1994): (1) approach of two bubbles to form a thin liquid film between them; (2) thinning of the film by the drainage of the liquid under the influence of gravity and suction due to capillary forces; and (3) rupture of the film at a critical thickness. The second step is the rate controlling step in the coalescence process and the bubble coalescence rate can be approximated by the film thinning rate (Vrij, 1966). The film thinning velocity can be expressed as (Sagert and Quinn, 1977, 1978)

$$-\frac{dl}{dt}=\frac{32l^3\sigma}{3\phi R_d^2 \mu_l d_b} \tag{21}$$

where the parameter ϕ is a measure of the surface drag or velocity gradient at the surface due to the adsorbed layer of the gas.

It is known that surface tension decreases and liquid viscosity increases with increasing pressure. In addition, ϕ increases with pressure. As seen from Eq. (21), all these variations contribute to the reduction of the film thinning velocity, and hence, the bubble coalescence rate, as pressure increases. As a result, the time required for two bubbles to coalesce is longer and hence the rate of overall bubble coalescence in the bed is reduced at high pressures. Moreover, the frequency of bubble collision decreases with

increasing pressure. An important mechanism for bubble collision is bubble wake effects (Fan and Tsuchiya, 1990). When the differences in bubble size and bubble rise velocity are small at high pressures, the likelihood of small bubbles being caught and trapped by the wakes of large bubbles decreases. Therefore, bubble coalescence is suppressed by the increase in pressure, due to the longer bubble coalescence time and the smaller bubble collision frequency.

2.6. Bubble breakup and maximum stable bubble size

It is known that the variation of bubble size with pressure is the key to understanding pressure effects on hydrodynamics. The upper limit of the bubble size is set by the maximum stable bubble size, D_{max}, above which the bubble is subjected to breakup and hence is unstable. Several mechanisms have been proposed for the bubble breakup phenomenon and based on these mechanisms, theories have been established to predict the maximum bubble size in gas-liquid systems.

Hinze *et al.* (1955) proposed that the bubble breakup is caused by the dynamic pressure and the shear stresses on the bubble surface induced by different liquid flow patterns, *e.g.*, shear flow and turbulence. When the maximum hydrodynamic force in the liquid is larger than the surface tension force, the bubble disintegrates into smaller bubbles. This mechanism can be quantified by the liquid Weber number. When the Weber number is larger than a critical value, the bubble is not stable and disintegrates. This theory was adopted to predict the breakup of bubbles in gas-liquid systems (Walter and Blanch, 1986). Calculations by Lin *et al.* (1998) showed that the theory underpredicts the maximum bubble size and cannot predict the effect of pressure on bubble size.

A maximum stable bubble size exists for bubbles rising freely in a stagnant liquid without external stresses, *e.g.*, rapid acceleration, shear stress, and/or turbulence fluctuations (Grace *et al.*, 1978). The Rayleigh-Taylor instability has been regarded as the mechanism for bubble breakup under such conditions. A horizontal interface between two stationary fluids is unstable to disturbances with wavelengths exceeding a critical value if the upper fluid has a higher density than the lower one (Bellman and Pennington, 1954):

$$\lambda_c = 2\pi\sqrt{\frac{\sigma}{g(\rho_l - \rho_g)}} \tag{22}$$

Chen and Fan (1988) obtained an equation for a curved surface as in the case of bubble. Grace *et al.* (1978) modified the Rayleigh-Taylor instability theory by considering the time available for the disturbance to grow and the time required for the disturbance to grow to an adequate amplitude. Batchelor (1987) pointed out that the observed size of air bubbles in water was considerably larger than that predicted by the model of Grace *et al.* (1978). Batchelor (1987) further took into account the stabilizing effects of the liquid acceleration along the bubble surface and the non-constant growth rate of the disturbance. In Batchelor's model, the information of the magnitude of the disturbances is required for the prediction of the maximum bubble size; however, the magnitude of the disturbances is not known. The models based on the Rayleigh-Taylor instability predict an almost negligible pressure effect on the maximum bubble size; in fact, Eq. (22) implies that the bubble is more stable when the gas density is higher.

The Kelvin-Helmholtz instability is similar to the Rayleigh-Taylor instability, except that the former allows a relative velocity between the fluids, u_r. Using the same concept of Grace *et al.* (1978), Kitscha and Kocamustafaogullari (1989) applied the Kelvin-Helmholtz instability theory to model the breakup of large bubbles in liquids. Wilkinson and Van Dierendonck (1990) applied the critical wavelength to explain the maximum stable bubble size in high-pressure bubble columns:

$$\lambda_c = \frac{2\pi\sqrt{\dfrac{\sigma}{g(\rho_l - \rho_g)}}}{\dfrac{\rho_l}{\rho_l + \rho_g}\dfrac{\rho_g u_r^2}{2\sqrt{\sigma g(\rho_l - \rho_g)}} + \sqrt{1 + \dfrac{\rho_l^2 \rho_g^2 u_r^4}{4(\rho_l + \rho_g)^2 \sigma g(\rho_l - \rho_g)}}}. \tag{23}$$

Disturbances in the liquid with a wavelength larger than the critical wavelength can break up a bubble. Equation (23) indicates that the critical wavelength decreases with an increase in pressure and therefore bubbles are easier to disintegrate by disturbances at higher pressures. However, the critical wavelength is not equivalent to the maximum stable bubble size, and Eq. (23) alone cannot quantify the effect of pressure on bubble size.

All of the models mentioned above do not account for the internal circulation of the gas. The internal circulation velocity is of the same order of magnitude as the bubble rise velocity. A centrifugal force is induced by this circulation, pointing outwards toward the bubble surface. This force can suppress the disturbances at the gas-liquid interface and thereby stabilizing the interface. The centrifugal force may be another reason to explain the underestimation of D_{max} by the model by Grace *et al.* (1978). On the other hand, the centrifugal force can also disintegrate the bubble, as it increases with an increase in bubble size. The bubble breaks up when the centrifugal force exceeds the surface tension force, especially at high pressures when gas density is high. Levich (1962) assumed the centrifugal force to be equal to the dynamic pressure induced by the gas moving at the bubble rise velocity, *i.e.* $k_f \rho_g u_b^2 / 2$ ($k_f \approx 0.5$), and proposed a simple equation to calculate the maximum stable bubble size:

$$D_{max} \approx \frac{3.63\sigma}{u_b^2 \sqrt[3]{\rho_l^2 \rho_g}}. \tag{24}$$

Equation (24) severely underpredicts the maximum bubble size in air-water systems, although it shows a significant effect of pressure on the maximum bubble size. Considering all the theories proposed in the literature, the mechanism for bubble breakup at high pressures is still unknown.

An analytical criterion for the bubble breakup is derived by considering a single large bubble rising in a stagnant liquid or slurry at a velocity of u_b, without any disturbances on the gas-liquid interface. The bubble is subjected to breakup when its size exceeds the maximum stable bubble size due to the circulation-induced centrifugal force (Luo *et al.*, 1998a). Large bubbles normally assume a spherical cap shape; in this work, the spherical-cap bubble is approximated by an ellipsoidal bubble with the same volume and the same aspect ratio (height to width). The circulation of gas inside the bubble can be described by Hill's vortex (Hill, 1894). To model the bubble breakup, it is necessary to evaluate the x-component of the centrifugal force, F_x, induced by the circulation on the entire bubble surface as shown in Fig. 12. A rigorous theoretical derivation from Hill's vortex yields the expression for F_x:

$$F_x = \frac{9\pi \rho_g u_b^2 a^2}{64\sqrt{2\alpha}}. \tag{25}$$

The surface tension force is the product of the surface tension and the circumference of the bubble,

$$F_\sigma = \sigma L = \sigma \int_{\text{ellipse}} \sqrt{(\delta r_c)^2 + (\delta z)^2} = 4\sigma a \mathrm{E}(\sqrt{1-\alpha^2}). \tag{26}$$

Also, the volume equivalent bubble diameter, d_b, is related to a and α by

$$a = \frac{d_b}{\sqrt[3]{8\alpha}}. \tag{27}$$

Note that the centrifugal force is affected significantly by the gas density, the aspect ratio of the bubble, the bubble size, and the bubble rise velocity. The bubble is not stable if F_x is larger than F_σ, *i.e.*

$$u_b^2 d_b \geq \frac{8\alpha^{4/3} \mathrm{E}(\sqrt{1-\alpha^2})}{0.312} \frac{\sigma}{\rho_g}. \tag{28}$$

When the centrifugal force is larger than the surface tension force, the bubble should be stretched in the x direction. During the stretching, the aspect ratio, α, becomes smaller while d_b and u_b can be assumed to remain constant. As a result, the centrifugal force increases, the surface tension force decreases, and the bubble stretching becomes an irreversible process. The sequence of bubble images shown in Fig. 13 confirms the proposed mechanism of bubble breakup. The bubble images in the figure are obtained at a pressure of 3.5 MPa. Using the Davies-Taylor equation (Davies and Taylor, 1950) for the bubble rise velocity, the maximum stable bubble size is

$$D_{max} \approx 7.16\alpha^{2/3} \mathrm{E}(\sqrt{1-\alpha^2})^{1/2} \sqrt{\frac{\sigma}{g\rho_g}}. \tag{29}$$

The simplified forms of Eq. (29) are (Luo *et al.*, 1998a):

$$D_{max} \approx 2.53 \sqrt{\frac{\sigma}{g\rho_g}} \quad (\text{for } \alpha = 0.21) \tag{30a}$$

in liquids, and

$$D_{max} \approx 3.27\sqrt{\frac{\sigma}{g\rho_g}} \quad (\text{for } \alpha = 0.3) \tag{30b}$$

in liquid-solid suspensions. Further, based on the Davies-Taylor equation, the rise velocity of the maximum stable bubble is

$$u_{max} = C\left(\frac{\sigma g}{\rho_g}\right)^{1/4} \tag{31}$$

where C is a constant. The comparison between experimental data and the predictions of Eq. (30) and by other instability theories is shown in Fig. 14(a). The figure indicates that the proposed model can explain the observed effect of pressure on the bubble size. It is clear that the internal circulation model captures the intrinsic physics of bubble breakup at high pressures. The comparison of the predictions by different models indicates that the bubble breakup is governed by the internal circulation mechanism at high pressures over 10 atm, whereas the Rayleigh-Taylor instability or Kelvin-Helmholtz instability is the dominant mechanism at low pressures. Based on the experimental results at elevated pressures, in which the bubble rise velocity is noted to be proportional to $\rho_g^{-0.5}$, Letzel *et al.* (1998) concluded that the Kelvin-Helmholtz theory governs the bubble instability. However, this proportional relationship between the bubble rise velocity and the gas density should be perceived to be only as a sufficient condition, but not as a necessary condition. This proportional relationship is not necessarily required to be held for a constant square of the growth factor of the disturbance in the Kelvin-Helmholtz theory as the critical wave number may vary with flow conditions under different gas densities. Figure 14(b) presents experimental data and correlation or model predictions of bubble velocity or bubble swarm velocity by various investigators (Davenport *et al.*, 1967; El-Temtamy and Epstein, 1980; Schumpe and Grund, 1986; Wilkinson and Van Dierendonck, 1990; Yu and Kim, 1991; Grund *et al.*, 1992; Wilkinson *et al.*, 1992; Liu and Bankoff, 1993; Hyndman *et al.*, 1997; Letzel *et al.*, 1997, 1998; Luo *et al.*, 1998a) under various operating conditions for air (or nitrogen)-water systems. Relevant information on bubble or bubble swarm velocities in air-water systems regarding these investigations is given in Table 2. It is seen in the figure that bubble or bubble swarm

velocities decrease with an increase in gas density or gas pressure at low gas densities, and this effect is substantially less pronounced at high gas densities. It is found that there is an appreciable variation of the bubble or bubble swarm velocities at low gas densities under various conditions. However at high gas densities, the variation of these velocities appears to be small and these velocities are within the range of prediction of the mechanistic model for high pressures developed by Luo *et al.* (1998a).

3. Macroscopic Hydrodynamics

3.1. Moving packed bed phenomenon

For three-phase fluidization systems involving large particles, two striking phenomena pertaining to macroscopic hydrodynamic behavior are bed contraction and moving packed bed flow. Bed contraction is characterized by a decrease in the bed height of a liquid-solid fluidized bed when a low velocity of gas is introduced to the bed. The bed contraction is caused by the behavior of bubble wake, which entraps liquid and particles and therefore is associated with large bubble systems. The entrainment of the liquid and particles by the bubble wake reduces the effective amount of liquid in the bed used to fluidize the remaining particles. The bed contraction phenomenon has been extensively studied under ambient fluidization conditions (Massimilla *et al.*, 1959; Ostergaard, 1964; El-Temtamy and Epstein, 1979). At high pressures, such a phenomenon has also been observed to occur (Jiang *et al.*, 1997).

The moving packed bed flow is characterized by the motion of solids in piston flow in a three-phase fluidized bed. The moving packed bed flow, which usually occurs during the start-up of the bed, depends not only on the gas and liquid velocities, but also on how they are introduced to the bed. It is caused by the surface phenomena involving fine bubbles attached onto particles and subsequent formation of a fine bubble blanket under the packed solids; a liquid flow would move the entire bed upward. This phenomenon is thus associated with the small bubble system. The moving packed bed flow in a three-phase fluidized bed is a known, anomalous event in the resid hydrotreating industry. It was observed in the 1960s in the bench and pilot units during the development and commercialization of the resid hydrotreating process (Fan, 1999). The reactor was typically operated at pressures between 5.5 and 21 MPa and at

temperatures between 300°C and 425°C. In the early 1970s, the moving packed bed flow was observed in a commercial three-phase fluidized bed reactor. The occurrence of the moving packed bed in a three-phase fluidized bed could simply be circumvented by utilizing a start-up procedure that involves degassing the bed first and then introducing liquid flow to expand the bed prior to commencing the gas flow. Commercial operators of three-phase fluidized bed reactors have long recognized and undertaken a proper start-up procedure of this nature since observing this anomalous event. As the small bubbles can also be generated under the ambient conditions using surfactants in an air-water system, the moving packed bed flow was reported in open literature first by Saberian-Broudjenni *et al.* (1984) and later by Bavarian and Fan (1991a, b) in small columns with small bubbles generated in such manner.

3.2. Flow regime transition

Three flow regimes can be identified based on the bubble flow behavior in bubble columns and slurry bubble columns: the dispersed bubble (or homogeneous bubble flow), the coalesced bubble (or churn-turbulent flow), and the slugging regimes. In the homogeneous bubble flow regime, no bubble coalescence occurs and the bubbles are of uniform, small size. The homogeneous bubble flow regime predominates at high liquid velocities and at low and intermediate gas velocities. At low liquid and high gas velocities, either the churn-turbulent flow or slugging regime occurs depending on the column diameter. In columns of large diameter, the churn-turbulent flow regime always occurs at high gas velocities. In this regime, bubbles tend to coalesce and both bubble size and bubble rise velocity become large and show a wide distribution.

The knowledge of the transition between the homogeneous bubble flow and the churn-turbulent flow regimes is important for the design and operation of industrial reactors. The transition velocity depends on gas distributor design, physical properties of the phases, operating conditions, and column size. The flow regimes and the regime transition have been studied extensively under ambient conditions over the last three decades (Wallis, 1969; Joshi and Lali, 1984; Shnip *et al.*, 1992; Tsuchiya and Nakanishi, 1992; Zahradnik *et al.*, 1997). Most of these studies pointed out a critical role played by the liquid-phase turbulence during the regime transition, and employed

phenomenological models to predict the flow transition from the homogeneous regime to the heterogeneous regime. The effect of the operating pressure on the regime transition has been examined by many researchers in bubble columns (Tarmy *et al.*, 1984; Clark, 1990; Krishna *et al.*, 1991, 1994; Wilkinson *et al.*, 1992; Hoefsloot and Krishna, 1993; Reilly *et al.*, 1994; Letzel *et al.*, 1997; Lin *et al.*, 1999b), in three-phase fluidized beds (Luo *et al.*, 1997a), and in slurry bubble columns (Clark, 1990).

Letzel *et al.* (1997) studied the influence of pressure on the stability of bubbly flows in a bubble column with the nitrogen-water system by using the stability theory of Batchelor (1988) and Lammers and Biesheuvel (1996). They found that a higher gas density has a stabilizing effect on the flow and that the gas fraction at the instability point increases with gas density, while the gas velocity at the instability point only slightly increases with gas density. However, the conclusion is limited to a narrow range of operating pressures (0.1 to 1.3 MPa). Lin *et al.* (1999b) used the standard deviation of the pressure fluctuation and the drift flux model to identify the flow transition from the homogeneous regime to the heterogeneous regime in a bubble column using nitrogen and Paratherm NF heat transfer fluid at pressures up to 15.2 MPa and temperatures up to 78°C. It was found that increasing pressure or temperature delays the regime transition as shown in Fig. 15(a).

Wilkinson *et al.* (1992) proposed a correlation to estimate the gas holdup and gas velocity at the transition point under high-pressure conditions. This predictive scheme incorporates the concept of bimodal bubble size distribution presented by Krishna *et al.* (1991), *i.e.* the churn-turbulent regime is characterized by a bimodal bubble size distribution, consisting of fast rising large bubbles (> 5 cm in diameter) and small bubbles (typically, < 5 mm in diameter). Wilkinson *et al.* (1992) found that the transition velocity depends on the liquid properties and can be estimated by the following correlations:

$$\varepsilon_{g,tran} = \frac{U_{g,tran}}{u_{small}} = 0.5\exp(-193\rho_g^{-0.61}\mu_l^{0.5}\sigma^{0.11}), \text{ and} \tag{32}$$

$$u_{small} = 2.25\left(\frac{\sigma}{\mu_l}\right)\left(\frac{\sigma^3\rho_l}{g\mu_l^4}\right)^{-0.273}\left(\frac{\rho_l}{\rho_g}\right)^{0.03} \tag{33}$$

where u_{small} is the rise velocity of small bubbles. As shown in Fig. 15(a), a reasonable agreement for the regime transition velocity can be obtained between the experimental data obtained by Lin *et al.* (1999b) and the correlation of Wilkinson *et al.* (1992) when the *in-situ* physical properties of the fluids at a given temperature and pressure are used in the correlation.

The studies of the regime transition in three-phase fluidized beds and slurry bubble columns are scarce. Luo *et al.* (1997a) studied the transition velocity in a three-phase fluidized bed over a pressure range of 0.1 to 15.6 MPa by analyzing the drift flux of gas. Two types of glass beads of 2.1 and 3 mm in diameter are used as the solid phase. The drift flux of gas increases with the gas holdup in the dispersed regime; in the coalesced bubble regime, the rate of increase is much larger. As the pressure increases, the transition gas velocity and the gas holdup at the transition point increase, under all the particle size and liquid velocity conditions. The pressure effect on the regime transition is significant, but the effect levels off at a pressure around 6 MPa as shown in Fig. 15(b). The experimental study also shows that the transition velocity increases with liquid velocity and slightly increases with particle size, similar to the regime transition behavior at ambient conditions. Clark (1990) studied the regime transition in a hydrogen-methanol-catalyst system at pressures between 2.5 and 10 MPa and temperatures from 20°C to 180°C. Glass beads with a particle size range of 45 to 63 μm were used as the solid catalyst. It was found that the addition of fine particles to the liquid phase promotes bubble coalescence, which accelerates the transition to the churn-turbulent regime. However, the regime transition at high-pressure conditions in slurry bubble columns is still not fully understood, and further studies are needed to examine the effect of solids concentration on the transition velocity, to develop an accurate correlation, and to explore the transition mechanism.

In general, the pressure effect on the flow regime transition is a result of the variation in bubble characteristics, such as bubble size and bubble size distribution. The bubble size and distribution are closely associated with factors such as initial bubble size, bubble coalescence rates and bubble breakup rates. Under high-pressure conditions, bubble coalescence is suppressed and bubble breakup is enhanced. Also, the distributor tends to generate smaller bubbles. All these factors contribute to small bubble sizes and

narrow bubble size distributions and, consequently, delay the flow regime transition in high-pressure bubble columns and slurry bubble columns.

3.3. Overall gas holdup and hydrodynamic similarity

Gas holdup is a key parameter to characterize the macroscopic hydrodynamics of slurry bubble column systems. The gas holdup depends on gas and liquid velocities, gas distributor design, column geometry (diameter and height), physical properties of the gas and liquid, particle concentration, and physical properties of the particles. The gas holdup generally increases with gas velocity, with a larger rate of increase in the dispersed bubble regime than in the churn-turbulent regime. Such distributors as perforated plate, nozzle injector, and sparger affect the gas holdup significantly only at low gas velocities (Lin *et al.*, 1999a). Lin *et al.* (1999a) also showed that the fluid dynamic behavior of gas and liquid in the plenum region is complex. They observed that the liquid flow in the bottom plenum to the bulk phase of the column through a perforated plate occurs *via* the liquid entrainment mechanism, *i.e.* turbulent gas bubbles and gas circulation in the gas layer entrain liquid from the liquid layer to the distributor as shown in Fig. 16. The gas and liquid flow patterns given in Fig. 16 may characterize, for example, an ebullated bed reactor for resid hydrotreating. In bubble columns, the effect of column size on gas holdup is negligible when the column diameter is larger than 0.1 to 0.15 m (Shah *et al.*, 1982). The influence of the column height is insignificant if the height is above 1 to 3 meters and the ratio of the column height to the diameter is larger than 5 (Kastaneck *et al.*, 1984). Gas holdup decreases as liquid viscosity and/or gas-liquid surface tension increase; however, the effect of liquid density is not clear. The addition of particles into a bubble column leads to a larger bubble size and thus a decreased gas holdup, especially when the particle concentration is low. The particle size effect on the gas holdup can be ignored in the particle size range of 44 to 254 μm.

Numerous studies have been conducted to investigate the effect of pressure on the gas holdup of bubble columns (Deckwer *et al.*, 1980; Tarmy *et al.*, 1984; Idogawa *et al.*, 1986; Kojima *et al.*, 1991; Wilkinson *et al.*, 1992; Reilly *et al.*, 1994; Jiang *et al.*, 1995; Inga, 1997; Letzel *et al.*, 1997; Lin *et al.*, 1998) and three-phase fluidized beds (Luo *et al.*, 1997a). Further, empirical correlations have been proposed for gas holdup in bubble

columns operated at elevated pressure and temperature (Wilkinson *et al.*, 1992; Reilly *et al.*, 1994). It is commonly accepted that elevated pressures lead to a higher gas holdup in both bubble columns and three-phase fluidized beds except in those systems which are operated with porous plate distributors and at low gas velocities. The increased gas holdup is directly related to the smaller bubble size and, to a lesser extent, to the slower bubble rise velocity at higher pressures (Luo *et al.*, 1997b). Figure 17 shows bubbles emerging from the three-phase fluidized bed of Paratherm NF heat transfer fluid and 2.1-mm glass beads over a wide range of operating conditions. As shown in the figure, bubble size is drastically reduced as pressure increases. The most fundamental reason for the bubble size reduction can be attributed to the variation in physical properties of the gas and liquid with pressure.

A significant pressure effect on the gas holdup should exist in slurry bubble columns; however, little is reported concerning such an effect. Deckwer *et al.* (1980) found little effect of pressure on gas holdup in a Fischer-Tropsch slurry bubble column with a porous plate distributor (P = 0.4 to 1.1 MPa; T = 143 to 260°C; U_g = 0 to 3.5 cm/s). The experimental data of Kojima *et al.* (1991) indicated that the gas holdup increases with pressure; but no pressure effect was observed at the 30 wt% solids concentration (P = 0.1 to 1.1 MPa; U_g = 1.7 to 9 cm/s; single orifice distributor). Inga (1997) measured the gas holdup in slurry bubble columns at pressures up to 0.72 MPa and a significant pressure effect was observed. In general, no viable model is available to predict the gas holdup in high-pressure slurry bubble columns. The gas holdup behavior in high-pressure slurry bubble columns is not well understood, especially at high gas velocities.

The dynamic gas disengagement technique, first applied in bubble columns by Sriram and Mann (1977), is utilized to measure the gas holdup in a slurry bubble column under wide operating conditions (Lee *et al.*, 1998). The results obtained with this technique for high-pressure systems are given in Luo *et al.* (1998a). Elevated pressures lead to higher gas holdups in a slurry bubble column. The presence of particles reduces the gas holdup at both ambient and elevated pressures as shown in Fig. 18. An empirical correlation is obtained to estimate the gas holdup in high-pressure slurry bubble columns as

$$\frac{\varepsilon_g}{1-\varepsilon_g} = \frac{2.9\left(\frac{U_g^4 \rho_g}{\sigma g}\right)^{\alpha}\left(\frac{\rho_g}{\rho_m}\right)^{\beta}}{\left[\cosh\left(Mo_m^{0.054}\right)\right]^{4.1}} \tag{34}$$

where Mo_m is the modified Morton number for the slurry phase, $g(\rho_m - \rho_g)(\xi \mu_l)^4 / \rho_m^2 \sigma^3$, and

$$\alpha = 0.21 Mo_m^{0.0079} \tag{35a}$$

$$\beta = 0.096 Mo_m^{-0.011}. \tag{35b}$$

A correction factor ξ accounts for the effect of particles on the slurry viscosity:

$$\ln \xi = 4.6\varepsilon_s \left\{5.7\varepsilon_s^{0.58} \sinh\left[-0.71\exp(-5.8\varepsilon_s)\ln(Mo)^{0.22}\right] + 1\right\} . \tag{36}$$

Table 3 lists the various experimental systems and their corresponding references used to obtain the correlation. The average error of the predictions is 13% for both the slurry and gas-liquid systems and the maximum error is 53%. The applicable ranges of the correlation are summarized in Table 4.

The physical meaning of the dimensionless group of $U_g^4 \rho_g / \sigma g$ in Eq. (34) can be shown by substituting Eq. (31) into the group:

$$\frac{U_g^4 \rho_g}{\sigma g} \propto \left(\frac{U_g}{u_{max}}\right)^4 \tag{37}$$

Clearly, the dimensionless group represents the contribution of large bubbles to the overall gas holdup, which is the major reason why the correlation can cover such wide ranges of experimental conditions.

For high-pressure bubble columns and slurry bubble columns operated under the wide range of conditions outlined in Table 3, hydrodynamic similarity requires the following dimensionless groups to be the same: U_g / u_{max}, Mo_m, and ρ_g / ρ_m. To simulate the hydrodynamics of industrial reactors, cold models can be used and milder pressure and temperature conditions can be chosen, as long as the three groups are similar to those in the industrial reactor. The similarity rule needs to be tested in industrial reactors.

3.4. Bubble size distribution and dominance of large bubbles

The bubble size can be measured by photographic or probe techniques. In multi-bubble systems, a mean bubble size is usually used to describe the system. The mean bubble size is commonly expressed through the Sauter, or volume-surface, mean. For a group of bubbles with measured diameters, the Sauter mean is

$$d_{vs} = \frac{\sum n_i d_{bi}^3}{\sum n_i d_{bi}^2} \tag{38}$$

where n_i is the number of bubbles in the class i with its volume equivalent size d_{bi}.

Some studies have been conducted to investigate pressure or gas density effects on mean bubble size and bubble size distribution in bubble columns (Idogawa *et al.*, 1986, 1987; Jiang *et al.*, 1995; Soong *et al.*, 1997; Lin *et al.*, 1998) as well as in three-phase fluidized beds (Jiang *et al.*, 1992, 1997). According to these experimental studies, pressure has a significant effect on mean bubble diameter. The mean bubble diameter decreases with increasing pressure; however, above a certain pressure, the bubble size reduction is not significant. The effect of pressure on the mean bubble size is due to the change of bubble size distribution with pressure. At atmospheric pressure, the bubble size distribution is broad, while under high pressure, the bubble size distribution becomes narrower and is in smaller size ranges as shown in Fig. 19 (Luo *et al.*, 1998a). At ambient conditions and U_g = 38.5 cm/s, the slurry bubble column is in the slugging regime with the maximum bubble size of 7.2 cm, approximately. At P = 5.6 MPa, bubble size is much smaller and slugs are not observed even at U_g = 37.4 cm/s. According to the literature, bubble size is affected by bubble formation at gas distributor, bubble coalescence and bubble breakup. When the pressure is increased, the bubble size at the distributor is reduced (Luo *et al.*, 1998c), bubble coalescence is suppressed (Jiang *et al.*, 1995), and large bubbles tend to breakup, *i.e.* the maximum stable bubble size is reduced (Luo *et al.*, 1998a). The combination of these three factors causes the decrease of mean bubble size with increasing pressure.

The bubble size distribution can normally be approximated by a log-normal distribution with its upper limit at the maximum stable bubble size. The contribution of bubbles of different sizes can be examined by analyzing the relationship between overall

gas holdup and bubble size distribution. In slurry bubble columns, the gas holdup can be related to the superficial gas velocity, U_g, and the average bubble rise velocity, $\overline{u}_b$, (based on bubble volume) by a simple equation:

$$U_g = \varepsilon_g \overline{u}_b . \tag{39}$$

When the distributions of bubble size and bubble rise velocity are taken into account, $\overline{u}_b$ can be expressed as

$$\overline{u}_b = \frac{\int_{d_{b,min}}^{d_{b,max}} V_b(d_b) f(d_b) u_b(d_b) \mathrm{d}d_b}{\int_{d_{b,min}}^{d_{b,max}} V_b(d_b) f(d_b) \mathrm{d}d_b} . \tag{40}$$

The outcome of Eq. (40) and the gas holdup strongly depend on the existence of large bubbles, because of the large volume and high rise velocity of such large bubbles. An experimental study by Lee *et al.* (1998) revealed that, in the coalesced bubble regime, more than 70% of the small bubbles are entrained by the wakes of large bubbles and consequently have a velocity close to that of large bubbles. It is clear that the large bubbles have a dominant effect on the overall hydrodynamics of slurry bubble columns due to their large volume, their high rise velocity, and the wakes associated with the large bubbles.

3.5. Heat transfer characteristics

Studies reported in the literature for heat transfer characteristics in slurry bubble columns (Saxena *et al.*, 1990; Li and Prakash, 1997) have been limited to ambient conditions. Little has been reported for high-pressure conditions. Since heat transfer behavior is closely associated with macroscopic flow structures and microscopic flow characteristics, a variation in pressure, which alters the physical properties of the gas and liquid, and also affects the hydrodynamics, would yield a complex effect on heat transfer behavior in the system. Previous studies on heat transfer in three-phase fluidized beds with liquids of different viscosity indicates that liquid viscosity has a negative effect on heat transfer (Kato *et al.*, 1981; Kang *et al.*, 1985). Since liquid viscosity increases with pressure, pressure would have a negative effect on heat transfer. Other physical properties

of liquid, which are less affected by pressure, include liquid density, ρ_l, liquid thermal conductivity, k_l, and liquid heat capacity, C_{pl} (Reid *et al.*, 1977).

Studies on instantaneous heat transfer in liquids and liquid-solid systems which involve the injection of single bubbles revealed the importance of bubble wakes to heat transfer behavior (Kumar *et al.*, 1992). The heat transfer enhancement by bubbles increases with bubble size due to the increased wake size and wake vortical intensity. When the pressure increases, the bubble size decreases, and hence the wake contribution to the heat transfer by single bubbles is reduced. In chain bubbling systems, Kumar and Fan (1994) reported that the time-averaged heat transfer coefficient increases with bubbling frequency due to the intense bubble-wake, bubble-bubble, and bubble-surface interactions. The effect of pressure on heat transfer due to the variations in liquid properties and hydrodynamic parameters is summarized in Table 5. The overall effect of pressure on heat transfer behavior depends on the outcome of the counteracting effects of each individual factor.

Deckwer *et al.* (1980) measured the heat transfer coefficient from an immersed heat source to the surrounding gas-liquid or gas-liquid-solid systems under conditions which prevail the Fischer-Tropsch slurry process (P = 0.1 to 1.0 MPa; T = 250 to 300°C; 16 wt% of 5 μm particles). Based on the surface renewal model and Kolmogoroff's theory of isotropic turbulence, a correlation was obtained to predict the heat transfer coefficient in slurry bubble columns:

$$St = 0.1\left(Re\ Fr\ Pr^2\right)^{-0.25}. \tag{41}$$

In the model, the liquid-solid suspension was considered as a homogeneous phase, and consequently, the estimation scheme of the physical properties of the suspension from the individual phase was required.

Luo *et al.* (1997a) studied the heat transfer behavior in a three-phase fluidized bed over a pressure range of 0.1 to 15.6 MPa. Two types of glass beads, 2.1 and 3 mm in diameter, were used as the solid phase. The effects of gas velocity and pressure on the heat transfer coefficient are shown in Fig. 20. With an increase in pressure, the heat transfer coefficient increases, reaches a maximum at pressures of 6 to 8 MPa, and then decreases. An empirical equation is proposed to correlate the experimental data in their

study:

$$h = h'\varepsilon_g^{0.45}\left(\frac{0.396}{U_g^{0.45}} + \frac{0.6768}{u_{pt,0}}\right) \tag{42}$$

where h' is the heat transfer coefficient of a liquid-solid fluidized bed with the same solids holdup, and $u_{pt,0}$ is the particle terminal velocity in the fluidizing liquid at ambient pressure. In Eq. (42), the units for U_g and $u_{pt,0}$ are in m/s. The heat transfer coefficient, h', can be calculated by the correlation given below (Richardson *et al.*, 1976):

$$Nu' = 0.67 Re^{0.62} Pr^{0.33} \frac{\varepsilon_s^{0.38}}{1-\varepsilon_s}. \tag{43}$$

The average deviation of the prediction from the experimental data is within ±10%.

Yang *et al.* (1998) studied heat transfer between an immersed solid surface and bulk fluids in a slurry bubble column at pressures of 0.1 to 6.3 MPa and temperatures of 35 to 81°C. Glass beads of 50 μm in diameter are used as the solid phase. The solids concentrations are varied up to 35 vol%, while the superficial gas velocities are varied up to 20 cm/s. The pressure effect on the heat transfer coefficient is shown in Fig. 21. It is found that pressure has a significant effect on the heat transfer characteristics in a slurry bubble column. The heat transfer coefficient decreases appreciably with increasing pressure except under very high pressures. The variation of the heat transfer coefficient with pressure is attributed to the counteracting effects of the variations of liquid viscosity, bubble size and bubbling frequency with pressure. When pressure increases, bubble size decreases; however, the bubbling frequency increases, which augments the rate of heat transfer (Kumar and Fan, 1994). The counteracting effects of the above two factors give rise to the overall effect of pressure on the heat transfer rate. In a slurry bubble column, pressure reduces bubble size significantly at pressures lower than 4 MPa, which results in the decrease of heat transfer coefficient. When the pressure is further increased, the bubble size reduction is relatively smaller, and the increase in bubbling frequency contributes to an increase in the heat transfer coefficient. However, in a three-phase fluidized bed, due to the large particle size, the bubble size reduction becomes a less important factor in affecting the heat transfer coefficient, and the heat transfer coefficient increases with the increase of bubbling frequency.

A consecutive film and surface renewal model originally developed by Wasan and Ahluwalia (1969) may be used to analyze the heat transfer behavior. The model assumes that a thin liquid film with a thickness of δ exists surrounding the heating surface; and liquid elements are forced to contact the outer surface of the film, due to the passage of bubbles. The liquid elements contact the film for a short time, t_c, and then, are replaced by fresh liquid elements. The heat is transferred to the bulk liquid through conduction by the liquid film and unsteady state conduction by the liquid elements. The heat transfer coefficient is expressed in terms of the physical properties of the liquid, the film thickness, and the contact time of the liquid elements (Wasan and Ahluwalia, 1969):

$$h = \frac{2k_l}{\sqrt{\pi\alpha t_c}} + \frac{k_l\delta}{\alpha t_c}\left[e^{\alpha t_c/\delta^2}\left(1-\operatorname{erf}\frac{\sqrt{\alpha t_c}}{\delta}\right)-1\right] \tag{44}$$

Based on Eq. (44), the heat transfer coefficient is a function of film thickness and contact time between the liquid element and film. The order of magnitude of the film thickness may be estimated by (Kumar and Fan, 1994)

$$\delta = \frac{6.14L}{Re_m^{3/4}} Pr^{-1/3} \tag{45}$$

where Re_m is equal to $\rho_m L u_b/\mu_m$. Assuming that the element contact time is equal to the bubble contact time with the film, the contact time can be estimated from (Kumar and Fan, 1994)

$$t_c = \frac{L}{u_b} \tag{46}$$

where u_b is the actual bubble rise velocity in a stream of bubbles. By considering the pressure effects on the physical properties of liquid and bubble characteristics, such as bubble size and bubble rise velocity, this model may be used to analyze the heat transfer behavior in a high-pressure system.

4. CONCLUDING REMARKS

Experimental results show the rise velocity of single bubbles in liquids and liquid-solid suspensions decreases with an increase in pressure and with a decrease in temperature. This decrease, combined with the pressure effect of reducing the bubble size, contributes to high gas holdups observed at high pressures. The bubble rise velocity

in liquids and liquid-solid suspensions with low solids holdups can be reasonably estimated by use of the predictive equation available for ambient conditions, if the *in-situ* physical properties of the gas and liquid are used. Significant reduction in the rise velocity occurs at high solids holdups, especially for high liquid viscosity. The extent of reduction can be examined in terms of an increase in the apparent suspension viscosity by applying the homogeneous, Newtonian analogy. Along with the experimental results, discrete-phase simulations of a single bubble rising in liquid-solid suspensions at ambient conditions and in liquids at an elevated pressure are presented. A mechanistic model is described which accounts for the initial bubble size from a single orifice in liquid-solid suspensions. The mechanistic analysis indicates that the heterogeneous characteristics of liquid-solid suspensions can be satisfactorily accounted for by considering the particle-bubble collision behavior. The proposed mechanistic model successfully predicts the initial bubble size from a single orifice in high-pressure liquid-solid suspensions. The mechanism for bubble breakup at high pressures is illustrated by considering the bubble instability induced by internal gas circulation inside a bubble, and an analytical expression is obtained to quantify the maximum stable bubble size. Theoretical and experimental examinations on the roles of bubbles of different sizes indicate the important role that large bubbles play in dictating the macroscopic hydrodynamics of slurry bubble columns. An empirical correlation is provided to predict the gas holdup in slurry bubble columns over a wide range of conditions. A similarity rule is revealed for the overall hydrodynamics of high-pressure slurry bubble columns, which takes into account the operating conditions, the maximum stable bubble size, and the physical properties of the gas, liquid, and solids. A consecutive film and surface renewal model is used to explore the heat transfer characteristics in high-pressure three-phase fluidized beds and slurry bubble columns.

5. acknowledgement

This work was supported by the National Science Foundation Grant CTS-9528380, the U.S. Department of Energy Grant DEFC22-95 PC 95051 with Cooperative Agreement with Air Products and Chemicals, Inc., and the Ohio State University / Industry Consortium Program on Fluidization and Multiphase Flow.

6. NOTATION

a	half x-axis length in Fig. 12
C	constant in Eq. (31)
C_D	drag coefficient
C_{pl}	liquid heat capacity
c	parameter in Eq. (1) reflecting surface tension effect
D_c	column diameter
D_{max}	maximum stable bubble size
D_o	orifice diameter
d_b	volume equivalent bubble diameter
d_b'	dimensionless bubble diameter
d_p	particle diameter
d_{vs}	Sauter mean bubble diameter
$\mathrm{E}\left(\sqrt{1-\alpha^2}\right)$	complete second kind Elliptic integral
Eo	Eötvös number
e	restitution coefficient
F_{AM}	added mass force
F_B	buoyancy force
F_{Basset}	Basset force
F_c	particle-bubble collision force
F_D	liquid drag force
$F_{G/B}$	gravity/buoyancy force
$F_{I,g}$	bubble inertial force
$F_{I,m}$	liquid-solid suspension inertial force
F_M	gas momentum force
F_{Magnus}	Magnus force
F_{total}	total force

F_x	x-component of centrifugal force induced by internal circulation
F_σ	surface tension force
Fr	Froude number
f_b	volumetric body force
f_{sv}	volume force within free surface
$f(d_b)$	probability density function of bubble size
g	gravitational acceleration
H	column height
h	time-averaged heat transfer coefficient
h'	heat transfer coefficient in liquid-solid fluidized beds
K	proportionality constant defined by Eq. (9a)
K_b	parameter in Eq. (1) reflecting viscous nature of surrounding medium
K_{b0}	proportionality constant defined by Eq. (3d)
k_l	liquid thermal conductivity
k_o	orifice constant
L	circumference of the ellipse
	length of the heat transfer probe
l	thickness of the liquid film between two coalescing bubbles
Mo	Morton number
Mo_m	modified Morton number based on slurry properties
m_p	particle mass
Nc	dimensionless capacitance number
Nu'	Nusselt number in liquid-solid fluidized beds
n	parameter in Eq. (1) reflecting system purity
n_i	number of bubbles
P	pressure
P_b	pressure in the bubble
P_c	pressure in the gas chamber
P_e	pressure at the gas inlet to the chamber

P_o	hydrostatic pressure at the bubble surface
P_s	system pressure
Pr	Prandtl number
p_s	surface pressure
Q	property of fluid in Eq. (13)
Q_g^*	property of gas
Q_m^*	property of liquid-solid suspension
Q_o	volumetric gas flow-rate through the orifice
Q_g	volumetric gas flow-rate into the gas chamber
R_d	radius of a contacting circle between two bubbles
Re	bubble Reynolds number based on liquid properties
Re_m	bubble Reynolds number based on slurry properties
Re_o	orifice Reynolds number
r_b	radius of bubble
r_c	radius in a cylindrical coordinate system
r_o	radius of orifice
S	rate-of-strain stress
St	Stanton number
T	temperature
t	time
t_c	contact time between liquid element and film
U_g	superficial gas velocity
$U_{g,tran}$	transition gas velocity
U_l	superficial liquid velocity
u	rise velocity of bubble base
u_b	bubble rise velocity relative to the liquid phase
	absolute bubble rise velocity in a stream of bubble in Eq. (46)
u_b'	dimensionless bubble rise velocity defined by Eq. (1)

$\overline{u}_b$	average bubble rise velocity
u_e	bubble expansion velocity
u_{large}	large bubble rise velocity
u_m	suspension velocity
u_{max}	rise velocity of maximum stable bubble
u_o	superficial gas velocity through the orifice
$u_{pt,0}$	particle terminal velocity in the fluidizing liquid at the ambient pressure
u_r	relative velocity between liquid and gas inside a bubble
u_{small}	small bubble rise velocity
u_{swarm}	bubble swarm velocity
u_t	particle terminal velocity in liquid
V_c	volume of gas chamber
$\boldsymbol{v}$	liquid velocity vector
$\boldsymbol{v}_p$	particle velocity vector
z	z-axis in a cylindrical coordinate system

Greek letters

α	aspect ratio of bubble
	scalar field function in Eq. (13)
	thermal diffusivity
δ	thickness of liquid film
ε_g	gas holdup
$\varepsilon_{g,tran}$	gas holdup at the transition point
ε_l	liquid holdup
ε_s	solids holdup
ε_{sc}	critical solids holdup
ε_{s0}	solids holdup at incipient fluidization
ϕ	particle sphericity

	parameter in Eq. (21) reflecting the surface drag
γ	heat capacity ratio
	contact angle
κ	free surface curvature
λ_c	critical wavelength
μ	coefficient of dynamic viscosity
μ_g	gas viscosity
μ_l	liquid viscosity
μ_m	(effective) viscosity of liquid-solid suspension
ρ_g	gas density
ρ_l	liquid density
ρ_m	density of liquid-solid suspension
ρ_s	solids density
σ	surface tension
τ	viscous stress tensor
ξ	correction factor defined by Eq. (36)
ζ	coefficient in Eq. (20c)

7. REFERENCES

Akita, K. and F. Yoshida, 1973. Gas holdup and volumetric mass transfer coefficient in bubble columns. *Ind. Eng. Chem. Process Des. Develop.*, **12**, 76.

Allen, M. P. and D. J. Tildesley, 1987. *Computer Simulation of Liquids*, Clarendon Press, Oxford.

Azbel, D., 1981. *Two-Phase Flows in Chemical Engineering*, Cambridge Univ. Press, Cambridge, UK.

Bach, H. F. and T. Pilhofer, 1978. Variation of gas hold-up in bubble columns with physical properties of liquids and operating parameters of columns. *Ger. Chem. Eng.*, **1**, 270.

Batchelor, G. K., 1987. The stability of a large gas bubble rising through liquid. *J. Fluid Mech.*, **184**, 399.

Batchelor, G. K., 1988. A new theory of the instability of a uniform fluidized bed. *J. Fluid Mech.*, **193**, 75.

Bavarian, F., and L.-S. Fan, 1991a. Mechanisms of hydraulic transport of a packed bed at the start-up of a three-phase fluidized bed. *Chem. Eng. Sci.*, **46**, 3081.

Bavarian, F., and L.-S. Fan, 1991b. Hydraulic transport of a packed bed during the start-up of a three-phase fluidized bed with large gas holdups. *Ind. Eng. Chem. Res.*, **30**, 408.

Bellman, R. and R. H. Pennington, 1954. Effect of surface tension and viscosity on Taylor instability. *Q. Appl. Math.*, **51**, 151.

Bhaga, D. and M. E. Weber, 1981. Bubbles in viscous liquids: shapes, wakes, and velocities. *J. Fluid Mech.*, **105**, 61.

Brackbill, J. U., D. B. Kothe, and C. Zemach, 1992. A continuum method for modeling surface tension. *J. Comp. Phys.*, **100**, 335.

Chaudhari, R. V. and H. Hoffmann, 1994. Coalescence of gas bubbles in liquids. *Rev. Chem. Eng.*, **10**, 131.

Chen, Y.-M. and L.-S. Fan, 1988. On the criteria of Rayleigh-Taylor instability at a curved interface by a local force balance. Unpublished work.

Chen, Y.-M. and L.-S. Fan, 1989. Bubble breakage due to particle collision in a liquid medium. *Chem. Eng. Sci.*, **44**, 2762.

Clark, K. N., 1990. The effect of high pressure and temperature on phase distributions in a bubble column. *Chem. Eng. Sci.*, **45**, 2301.

Clift, R., J. R. Grace, and M. E. Weber, 1978. *Bubbles, Drops, and Particles*. Academic Press, New York.

Darton, R. C. and D. Harrison, 1974. The rise of single gas bubbles in liquid fluidized beds. *Trans. Instn Chem. Engrs*, **52**, 301.

Davenport, W. G., F. D. Richardson, and A. V. Bradshaw, 1967. Spherical cap bubbles in low density liquids. *Chem. Eng. Sci.*, **22**, 1221.

Davies, R. M. and G. I. Taylor, 1950. The mechanics of large bubbles rising through extended liquids and through liquids in tubes. *Proc. Roy. Soc. London*, **A200**, 375.

Deckwer, W.-D., 1992. *Bubble Column Reactors*, John Wiley and Sons, Chichester, England.

Deckwer, W.-D., Y. Louisi, A. Zaidi, and M. Ralek, 1980. Hydrodynamic properties of the Fischer-Tropsch slurry process. *Ind. Eng. Chem. Process Des. Dev.*, **19**, 699.

El-Temtamy, S. A. and N. Epstein, 1979. Contraction of expansion of three-phase fluidized beds containing fine/light solids. *Can. J. Chem. Eng.*, **57**, 520.

El-Temtamy, S. A. and N. Epstein, 1980. Rise velocities of large single two-dimensional and three-dimensional gas bubbles in liquids and in liquid fluidized beds. *Chem. Eng. J.*, **19**, 153.

Fan, L.-S., 1989. *Gas-Liquid-Solid Fluidization Engineering*, Butterworths, Stoneham, MA.

Fan, L.-S., 1999. Moving packed bed phenomena in three-phase fluidization. *Powder Technology*, in press.

Fan, L.-S. and K. Tsuchiya, 1990. *Bubble Wake Dynamics in Liquids and Liquid-Solid Suspensions*. Butterworth-Heinemann, Stoneham, MA.

Fox, J. M., 1990. Fischer-Tropsch reactor selection. *Catal. Lett.*, **7**, 281.

Grace, J. R., T. Wairegi, and J. Brophy, 1978. Break-up of drops and bubbles in stagnant media. *Can. J. Chem. Eng.*, **56**, 3.

Grund, G., A. Schumpe, and W.-D. Deckwer, 1992. Gas-liquid mass transfer in a bubble column with organic liquids. *Chem. Eng. Sci.*, **47**, 3509.

Hill, M. J. M., 1894. On a spherical vortex. *Phil. Trans. Roy. Soc. London*, **185**, 213.

Hinze, J. O., 1955. Fundamentals of the hydrodynamic mechanism of splitting in dispersion processes. *AIChE J.*, **1**, 289.

Hirt, C. W. and B. D. Nichols, 1981. Volume of fluid (VOF) method for the dynamics of free boundaries, *J. Comp. Phys.*, **39**, 201.

Hoefsloot, H. C. J. and R. Krishna, 1993. Influence of gas density on the stability of homogeneous flow in bubble columns. *Ind. Eng. Chem. Res.*, **32**, 747.

Hyndman, C. L., F. Larachi, and C. Guy, 1997. Understanding gas-phase hydrodynamics in bubble columns: A convective model based on kinetic theory. *Chem. Eng. Sci.*, **52**, 63.

Idogawa, K., K. Ikeda, T. Fukuda, and S. Morooka, 1986. Behavior of bubbles of the air-water system in a column under high pressure. *Int. Chem. Eng.*, **26**, 468.

Idogawa, K., K. Ikeda, T. Fukuda, and S. Morooka, 1987. Formation and flow of gas bubbles in a single orifice or nozzle gas distributor. *Chem. Eng. Comm.*, **59**, 201.

Inga, J. R., 1997. Scaleup and scaledown of slurry reactors: a new methodology. *Ph.D. thesis*, University of Pittsburgh, PA.

Jager, B. and R. Espinoza, 1995. Advances in low temperature Fischer-Tropsch synthesis. *Catal. Today*, **23**, 17.

Jean, R.-H. and L.-S. Fan, 1990. Rise velocity and gas-liquid mass transfer of a single large bubble in liquids and liquid-solid fluidized beds. *Chem. Eng. Sci.*, **45**, 1057.

Jiang, P., D. Arters, and L.-S. Fan, 1992. Pressure effects on the hydrodynamic behavior of gas-liquid-solid fluidized beds. *Ind. Eng. Chem. Res.*, **31**, 2322.

Jiang, P., T.-J. Lin, X. Luo, and L.-S. Fan, 1995. Visualization of high pressure (21 MPa) bubble column: bubble characteristics. *Chem. Eng. Res. & Des.*, **73**, 269.

Jiang, P., X. Luo, T.-J. Lin, and L.-S. Fan, 1997. High temperature and high pressure three-phase fluidization—bed expansion phenomena. *Powder Technology*, **90**, 103.

Joshi, J. B. and A. M. Lali, 1984. Velocity-hold up relationship in multiphase contactors-a unified approach. *Frontiers in Chem. Reaction Eng.*, **1**, 314, Wiley Eastern, New York.

Kang, Y., I. S. Suh, and S. D. Kim, 1985. Heat transfer characteristics of three-phase fluidized beds. *Chem. Eng. Comm.*, **34**, 1.

Kastaneck, F., J. Zahradnik, J. Kratochvil, and J. Cermak, 1984. Modelling of large-scale bubble column reactors for non-ideal gas-liquid systems in *Frontiers in Chemical Reaction Engineering*, edited by L. K. Doraiswamy and R. A. Mashelkar, **1**, 330, Whiley, Bombay, India.

Kato, Y., K. Uchida, and S. Morooka, 1981. Liquid holdup and heat transfer coefficient between bed and wall in liquid-solid and gas-liquid-solid fluidized beds. *Powder Technology*, **28**, 173.

Kitscha, J. and G. Kocamustafaogullari, 1989. Breakup criteria for fluid particles. *Int. J. Multiphase Flow*, **15**, 573.

Koide, K., A. Takazawa, and M. Komura, 1984. Gas Holdup and Volumetric Liquid-Phase Mass Transfer Coefficient in Solid-Suspended Bubble Columns. *J. Chem. Engng. Japan*, **17**, 459.

Kojima, H., B. Okumura, and A. Nakamura, 1991. Effect of pressure on gas holdup in a bubble column and a slurry bubble column. *J. Chem. Engng. Japan*, **24**, 115.

Krishna, R., J. W. A. De Swart, D. E. Hennephof, J. Ellenberger, and C. J. Hoefsloot, 1994. Influence of increased gas density on hydrodynamics of bubble-column reactors. *AIChE J.*, **40**, 112.

Krishna, R., P. M. Wilkinson, and L. L. Van Dierendonck, 1991. A model for gas holdup in bubble columns incorporating the influence of gas density on flow regime transitions. *Chem. Eng. Sci.*, **46**, 2491.

Kumar, R. and N. R. Kuloor, 1970. The formation of bubbles and drops. *Advances in Chemical Engineering*, **8**, 255.

Kumar, S., K. Kusakabe, K. Raghunathan, and L.-S. Fan, 1992. Mechanism of heat transfer in bubbly liquid and liquid-solid systems: single bubble injection. *AIChE J.*, **38**, 733.

Kumar, S. and L.-S. Fan, 1994. Heat-transfer characteristics in viscous gas-liquid and gas-liquid-solid systems. *AIChE J.*, **40**, 745.

Kupferberg, A. and G. J. Jameson, 1969. Bubble formation at a submerged orifice above a gas chamber of finite volume. *Trans. Instn Chem. Engrs*, **47**, T241.

Lammers, J. H. and A. Biesheuvel, 1996. Concentration waves and the instability of bubbly flows. *J. Fluid Mech.*, **328**, 67.

LaNauze, R. D. and I. J. Harris, 1974. Gas bubble formation at elevated system pressures. *Trans. Instn Chem. Engrs.*, **52**, 337.

Letzel, H. M., J. C. Schouten, C. M. Van den Bleek, and R. Krishna, 1997. Influence of elevated pressure on the stability of bubbly flows. *Chem. Eng. Sci.*, **52**, 3733.

Letzel, M. H., J. C. Schouten, C. M. Van den Bleek, and R. Krishna, 1998. Effect of gas density on large-bubble holdup in bubble column reactors. *AIChE J.*, **44**, 2333.

Lee, D. J., X. Luo, and L.-S. Fan, 1998. Gas disengagement technique in a slurry bubble column operated in the coalesced bubble regime. *Chem. Eng. Sci.*, in press.

Levich, V. G., 1962. *Physiochemical Hydrodynamics*, Prentice Hall, Englewood Cliffs, NJ.

Li, H., and A. Prakash, 1997. Heat transfer and hydrodynamics in a three-phase slurry bubble column. *Ind. Eng. Chem. Res.*, **36**, 4688.

Lin, J. N., S. K. Banerji, and H. Yasuda, 1994. Role of interfacial tension in the formation and the detachment of air bubbles. 1. A single hold on a horizontal plane immersed in water. *Langmuir*, **10**, 936.

Lin, T.-J. and L.-S. Fan, 1997. Characteristics of high-pressure liquid-solid fluidization. *AIChE J.*, **43**, 45.

Lin, T.-J., K. Tsuchiya, and L.-S. Fan, 1998. Bubble flow characteristics in bubble columns at elevated pressure and temperature. *AIChE J.*, **44**, 545.

Lin, T.-J., G. B. Bass, K. Tsuchiya, and L.-S. Fan, 1999a. Distributor effects on hydrodynamics of high pressure bubble columns. *Chem. Eng. Sci.*, in review.

Lin, T.-J., K. Tsuchiya, and L.-S. Fan, 1999b. On the measurements of regime transition in high pressure bubble columns. *Can. J. Chem. Eng.*, in press.

Liu, T.-J. and S. G. Bankoff, 1993. Structure of air-water bubbly flow in a vertical pipe – II. Void fraction, bubble velocity, and bubble size distribution. *Int. J. Heat Mass Transfer*, **36**, 1061.

Luo, X., P. Jiang, and L.-S. Fan, 1997a. High pressure three-phase fluidization: hydrodynamics and heat transfer. *AIChE J.*, **43**, 2432.

Luo, X., J. Zhang, J., K. Tsuchiya, and L.-S. Fan, 1997b. On the rise velocity of bubbles in liquid-solid suspensions at elevated pressure and temperature. *Chem. Eng. Sci.*, **52**, 3693.

Luo, X., D. J. Lee, R. Lau, G. Q. Yang, and L.-S. Fan, 1998a. Maximum stable bubble size and gas holdup in high pressure slurry bubble columns. *AIChE J.*, in press.

Luo, X., K. Tsuchiya, and L.-S. Fan, 1998b. Gas jetting and bubble formation in high pressure liquid-solid suspensions. In *Fluidization IX*, edited by L.-S. Fan and T. M. Knowlton, Engineering Foundation, NY, 637.

Luo, X., G. Q. Yang, D. J. Lee, and L.-S. Fan, 1998c. Single bubble formation in high pressure liquid-solid suspensions. *Powder Technology*, **100**, 103.

Maneri, C. C., 1995. New look at wave analogy for prediction of bubble terminal velocities. *AIChE J.*, **41**, 481.

Massimilla, L., N. Majuri, and P. Signorini, 1959. Sull'assorbimento di gas in sistema: solido-liquido, fluidizzato. *La Ricerca Scientifica*, **29**, 1934.

Massimilla, L., A. Solimando, and E. Squillace, 1961. Gas dispersion in solid-liquid fluidized beds. *Brit. Chem. Eng.*, **6**, 232.

Mendelson, H. D., 1967. The motion of an air bubble rising in water. *AIChE J.*, **13**, 250.

Mill, P. L., J. R. Turner, P. A. Ramachandran, and M. P. Dudukovic, 1996. The Fischer-Tropsch synthesis in slurry bubble column reactors: Analysis of reactor performance using the axial dispersion model. *Three-phase sparged reactors*, Edited by K.D.P. Nigam and A. Schumpe, Gordon and Breach Publishers, 339.

Milne-Thomson, L. M., 1955. *Theoretical Hydrodynamics*, 3rd ed., Macmillan and Co., London.

Miyahara, T. K., K. Tsuchiya, and L.-S. Fan, 1989. Mechanism of particle entrainment in a gas-liquid-solid fluidized bed. *AIChE J.*, **35**, 1195.

O'Dowd, W., D. N. Smith, J. A. Ruether, and S. C. Saxena, 1987. Gas and solids behavior in a baffled and unbaffled slurry bubble column. *AIChE J.*, **33**, 1959.

Ostergaard, K., 1964. *Fluidization*, Soc. Chem. Ind., London.

Oyevaar, M. H., 1989. Gas-liquid contacting at elevated pressures. *Ph.D. thesis*, Twente Univ., The Netherlands.

Peng, X. D., B. A. Toseland, and P. J. A. Tijm, 1998. Kinetic understanding of chemical synergy in LPDME^{TM} process. Presented at *the 1998 AIChE Annual Meeting*, Nov. 15-20, Miami Beach, FL.

Petukhov, V. I. and V. A. Kolokol'tsev, 1965. Effect of liquid viscosity on droplet entrainment and volumetric air content. *Therm. Eng.*, **12**, 41.

Pinczewski, W. V., 1981. The formation and growth of bubbles at a submerged orifice. *Chem. Eng. Sci.*, **36**, 405.

Rados, N., 1999. Slurry bubble column hydrodynamics. D.Sc. proposal, Washington University, St. Louis.

Ramakrishnan, S., R. Kumar, and N. R. Kuloor, 1969. Studies in bubble formation – I: bubble formation under constant flow conditions. *Chem. Eng. Sci.*, **24**, 731.

Reid, R. C., J. M. Prausnitz, and T. K. Sherwood, 1977. *The Properties of Gases and Liquids*. McGraw-Hill, New York.

Reilly, I. G., D. S. Scott, T. J. W. de Bruijn, and D. MacIntyre, 1994. The role of gas phase momentum in determining gas holdup and hydrodynamic flow regimes in bubble column operations. *Can. J. Chem. Eng.*, **72**, 3.

Richardson, J. F., M. N. Roman, and K. J. Shakiri, 1976. Heat transfer from immersed surfaces in liquid fluidized beds. *Chem. Eng. Sci.*, **31**, 619.

Ruzicka, M. C., J. Drahos, J. Zahradnik, and N. H. Thomas, 1997. Intermittent transition from bubbling to jetting regime in gas-liquid two phase flows. *Int. J. Multiphase Flow*, **23**, 671.

Saberian-Broudjenni, M., G. Wild, J. C. Charpentier, Y. Fortin, J. P. Euzen, and R. Patoux, 1984. Contribution à l'ètude hydrodynamique des rèacteurs à lit fludisè gaz-liquide-solide, *Entropie*, No. 120, 30.

Sagert, N. H. and M. J. Quinn, 1977. Influence of high-pressure gases on the stability of thin aqueous films. *J. Colloid Int. Sci.*, **61**, 279.

Sagert, N. H. and M. J. Quinn, 1978. Surface viscosities at high pressure gas-liquid interfaces. *J. Colloid Int. Sci.*, **65**, 415.

Saxena, S. C., 1995. Bubble column reactors and Fischer-Tropsch synthesis. *Catal. Rev.-Sci. Eng.*, **37**, 227.

Saxena, S. C. and Z. D. Chen, 1994. Hydrodynamics and heat transfer of baffled and unbaffled slurry bubble columns. *Reviews in Chem. Eng.*, **10**, 193.

Saxena, S. C., N. S. Rao, and A. C. Saxena, 1990. Heat Transfer from a cylindrical probe immersed in a three-phase slurry bubble column. *Chem. Eng. J.*, **44**, 141.

Saxena, S. C., R. Vadivel, and A. C. Saxena, 1989. Gas holdup and heat transfer from immersed surfaces in two- and three-phase systems in bubble columns. *Chem. Eng. Comm.*, **85**, 63.

Schumpe, A. and G. Grund, 1986. The gas disengagement technique for studying gas holdup structure in bubble columns. *Can. J. Chem. Eng.*, **64**, 891.

Shnip, A. I., R. V. Kolhatkar, D. Swamy, and J. B. Joshi, 1992. Criteria for the transition from the homogeneous to the heterogeneous regime in two-dimensional bubble column reactors. *Int. J. Multiphase Flow*, **18**, 705.

Shah, Y. T., B. G. Kelkar, S. P. Godbole, and W.-D. Deckwer, 1982. Design parameters estimations for bubble column reactors. *AIChE J.*, **28**, 353.

Shollenberger, K. A. and T. J. O'Hern, 1997. Characterization of slurry-phase flow in the Laporte alternative fuels development unit (AFDU) using differential pressure measurements. *U.S. DOE Report*, DE-FC22-95 PC 95051.

Soong, Y., F. W. Harke, I. K. Gamwo, R. R. Schehl, and M. F. Zarochak, 1997. Hydrodynamic study in a slurry-bubble-column reactor. *Catalysis Today*, **35**, 427.

Sriram, K. and R. Mann, 1977. Dynamic gas disengagement: A new technique for assessing the behaviour of bubble columns. *Chem. Eng. Sci.*, **32**, 571.

Tarmy, B., M. Chang, C. Coulaloglou, and P. Ponzi, 1984. Hydrodynamic characteristics of three phase reactors. *The Chemical Engineer*, Oct., No. 407, 18.

Tomiyama, A., I. Kataoka, and T. Sakaguchi, 1995. Drag coefficients of bubbles (1st report, drag coefficients of a single bubble in a stagnant liquid). *Nippon Kikai Gakkai Ronbunshu B Hen*, **61**(587), 2357.

Tsuchiya, K., A. Furumoto, L.-S. Fan, and J. Zhang, 1997. Suspension viscosity and bubble velocity in liquid-solid fluidized beds. *Chem. Eng. Sci.*, **52**, 3053.

Tsuchiya, K. and O. Nakanishi, 1992. Gas holdup behavior in a tall bubble column with perforated plate distributors. *Chem. Eng. Sci.*, **47**, 3347.

Tsuchiya, K., G.-H. Song, W.-T. Tang, and L.-S. Fan, 1992. Particle drift induced by a bubble in a liquid-solid fluidized bed with low-density particles, *AIChE J.*, **38**, 1847.

Tsuge, H., Y. Nakajima, and K. Terasaka, 1992. Behavior of bubbles formed from a submerged orifice under high system pressure. *Chem. Eng. Sci.*, **47**, 3273.

Vrij, A., 1966. Possible mechanism for the spontaneous rupture of thin, free liquid films. *Disc. Faraday Soc.*, **42**, 23.

Wallis, G. B., 1969. *One-Dimensional Two-Phase Flow*, McGraw-Hill, New York.

Walter, J. F. and H. W. Blanch, 1986. Bubble break-Up in gas-liquid bioreactors: break-up in turbulent flows. *Chem. Eng. J.*, **32**, B7.

Wasan, D. T. and M. S. Ahluwalia, 1969. Consecutive film and surface renewal mechanism for heat and mass transfer from a wall. *Chem. Eng. Sci.*, **24**, 1535.

Wilkinson, P. M., A. P. Sper, and L. L. Van Dierendonck, 1992. Design parameters estimation for scale-up of high-pressure bubble columns. *AIChE J.*, **38**, 544.

Wilkinson, P. M. and L. L. Van Dierendonck, 1990. Pressure and gas density effects on bubble break-up and gas hold-up in bubble columns. *Chem. Eng. Sci.*, **45**, 2309.

Wilkinson, P. M. and L. L. Van Dierendonck , 1994. A theoretical model for the influence of gas properties and pressure on single-bubble formation at an orifice. *Chem. Eng. Sci.*, **49**, 1429.

Yang, G. Q., X. Luo, R. Lau, and L.-S. Fan, 1998. Heat transfer characteristics in a high pressure slurry bubble column. Presented at *the 1998 AIChE Annual Meeting*, paper 191b, Nov. 15-20, Miami Beach, FL.

Yang, G. Q., X. Luo, R. Lau, and L.-S. Fan, 1999. Single bubble formation in high pressure liquid-solid suspensions with pressure fluctuations in the gas chamber. *Chem. Eng. Sci.*, in review.

Yoo, D.-H., H. Tsuge, K. Terasaka, and K. Mizutani, 1997. Behavior of bubble formation in suspended solution for an elevated pressure system. *Chem. Eng. Sci.*, **52**, 3701.

Yu, Y. H. and S. D. Kim, 1991. Bubble properties and local liquid velocity in the radial direction of cocurrent gas-liquid flow. *Chem. Eng. Sci.*, **46**, 313.

Zahradnik, J., M. Fialova, M. Ruzicka, J. Drahos, F. Kastanek, and N. H. Thomas, 1997. Duality of the gas-liquid flow regimes in bubble column reactors, *Chem. Eng. Sci.*, **52**, 3811.

Zhang, J., L.-S. Fan, C. Zhu, R. Pfeffer, and D. Qi, 1998a. Dynamic behavior of collinear collision of elastic spheres in viscous fluids, *Advanced Technologies for Particle Processing*, Vol. II, 44, Particle Technology Forum, AIChE; *Proceedings* of *PTF*

Topical Conference at AIChE Annual Meeting, Nov. 15-20, Miami Beach, FL; *Powder Technology*, in press.

Zhang, J., Y. Li, and L.-S. Fan, 1998b. Numerical simulation of gas-liquid-solid fluidization systems using a combined CFD-DPM-VOF method: single bubble rise behavior, *Advanced Technologies for Particle Processing*, Vol. II, 509, Particle Technology Forum, AIChE; *Proceedings* of *PTF Topical Conference at AIChE Annual Meeting*, Nov. 15-20, Miami Beach, FL.

FIGURES

Figure 1 Effect of pressure on terminal rise velocity of single bubbles and predicted values at (a) 27°C and (b) 78°C.

Figure 2 Comparisons of measured and calculated *Re* of single bubbles in Paratherm NF heat transfer fluid under varied pressure and temperature conditions. The Fan-Tsuchiya (1990) and Tomiyama *et al.* (1995) correlations are plotted (—— and — – —, respectively) at regular intervals of *Mo* values. The Fan-Tsuchiya correlation at measured *Mo* values for comparison with measured *Re-Eo* data (—).

Figure 3 Effect of pressure on bubble rise velocity in a fluidized bed at (a) 26.5°C and (b) 87.5°C. Solids holdups for +, open, and filled symbols are 0, 0.384, and 0.545, respectively.

Figure 4 Effect of pressure on bubble rise velocity in a fluidized bed at (a) 26.5°C and (b) 87.5°C. Solids holdups for +, open, and filled symbols are 0, 0.381, and 0.555, respectively.

Figure 5 Simulation and experimental results of a bubble rising in a liquid-solid fluidized bed.

Figure 6 Simulation of a bubble emerging from a liquid-solid fluidized bed.

Figure 7 Simulation results of a single bubble rising at $P = 19.4$ MPa.

Figure 8 The balance of all the forces acting on a growing bubble.

Figure 9 Comparison between the experimental data and model predictions of initial bubble size in high-pressure liquid-solid suspensions. Lines and symbols represent the model predictions and experimental data, respectively.

Figure 10 Initial bubble size in liquid-solid suspensions as a function of pressure and gas velocity for bubble formation with pressure fluctuation in the gas chamber.

Figure 11 A series of photographs showing the bubbling-jetting transition at $P = 4.24$ MPa and $T = 28$°C for (a) $u_o = 0.27$ m/s and $Re_o = 1{,}075$; (b) $u_o = 1.35$ m/s and $Re_o = 5{,}321$; (c) $u_o = 2.23$ m/s and $Re_o = 8{,}809$; (d) $u_o = 2.60$ m/s and $Re_o = 10{,}243$; (e) $u_o = 3.99$ m/s and $Re_o = 15{,}759$; (f) $u_o = 6.42$ m/s and $Re_o = 25{,}355$.

Figure 12 Schematic of the internal circulation model for bubble breakup.

Figure 13 A sequence of bubble images showing the process of bubble breakup at $P = 3.5$ MPa.

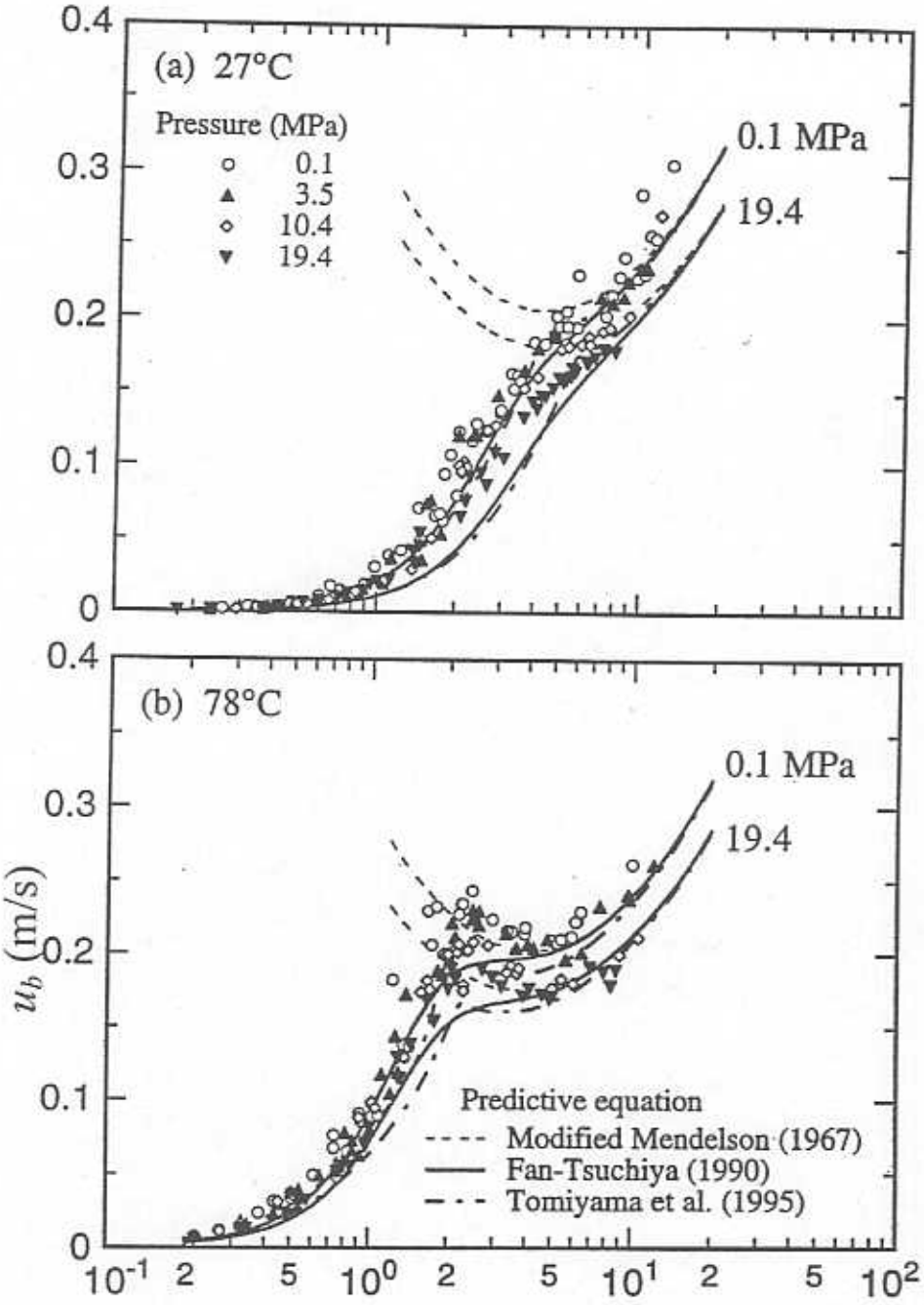
(a) 27°C
Pressure (MPa)
0.1
3.5
10.4
19.4
0.1 MPa
19.4
(b) 78°C
0.1 MPa
19.4
u_b (m/s)
Predictive equation
Modified Mendelson (1967)
Fan-Tsuchiya (1990)
Tomiyama et al. (1995)
0.4
0.3
0.2
0.1
0
10^{-1} 2 5 10^{0} 2 5 10^{1} 2 5 10^{2}

Figure 1

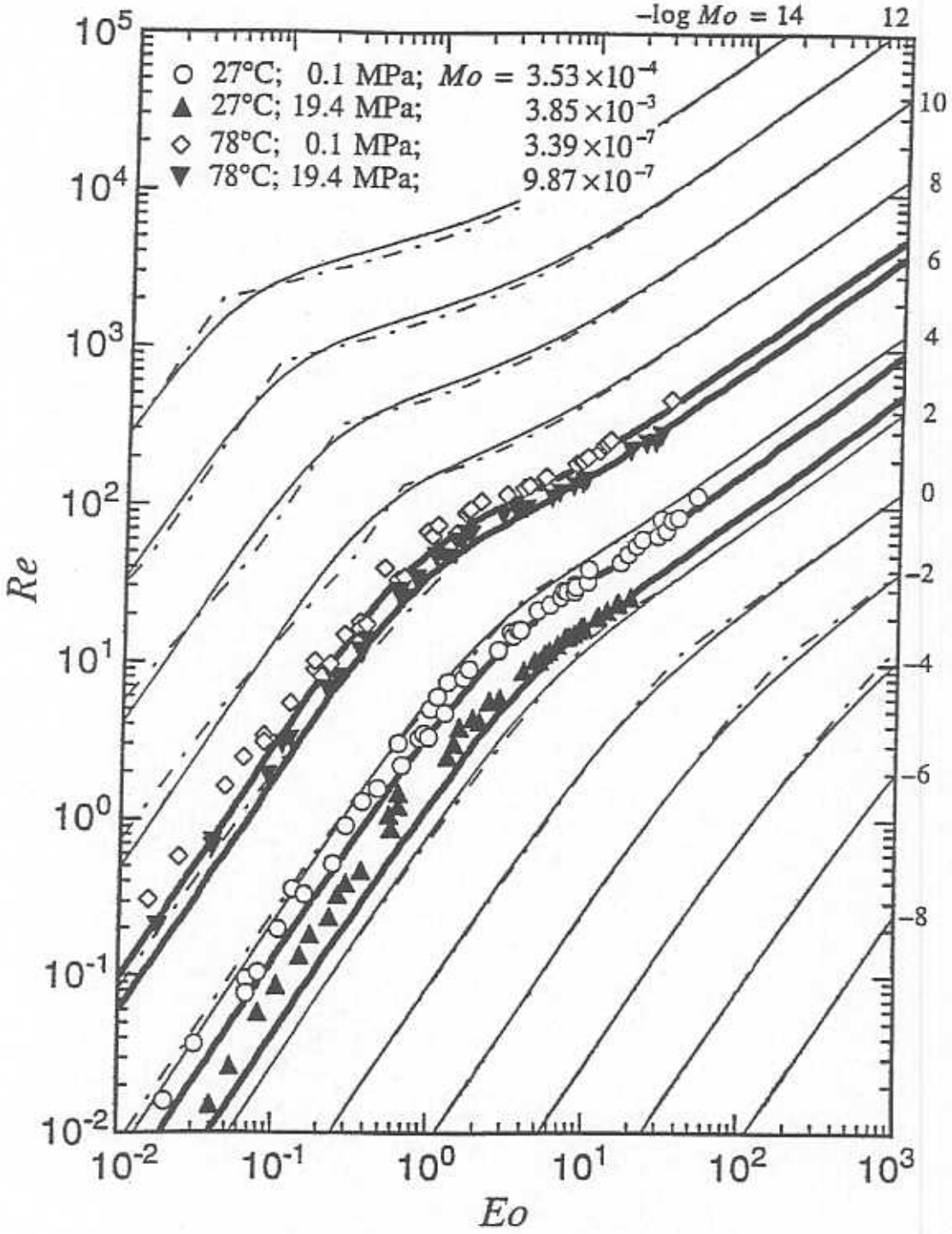
−log Mo = 14
12
10
8
6
4
2
0
−2
−4
−6
−8
○ 27°C; 0.1 MPa; Mo = 3.53×10⁻⁴
▲ 27°C; 19.4 MPa; 3.85×10⁻³
◇ 78°C; 0.1 MPa; 3.39×10⁻⁷
▼ 78°C; 19.4 MPa; 9.87×10⁻⁷
10⁵
10⁴
10³
10²
10¹
10⁰
10⁻¹
10⁻²
Re
10⁻²
10⁻¹
10⁰
10¹
10²
10³
Eo

Figure 2

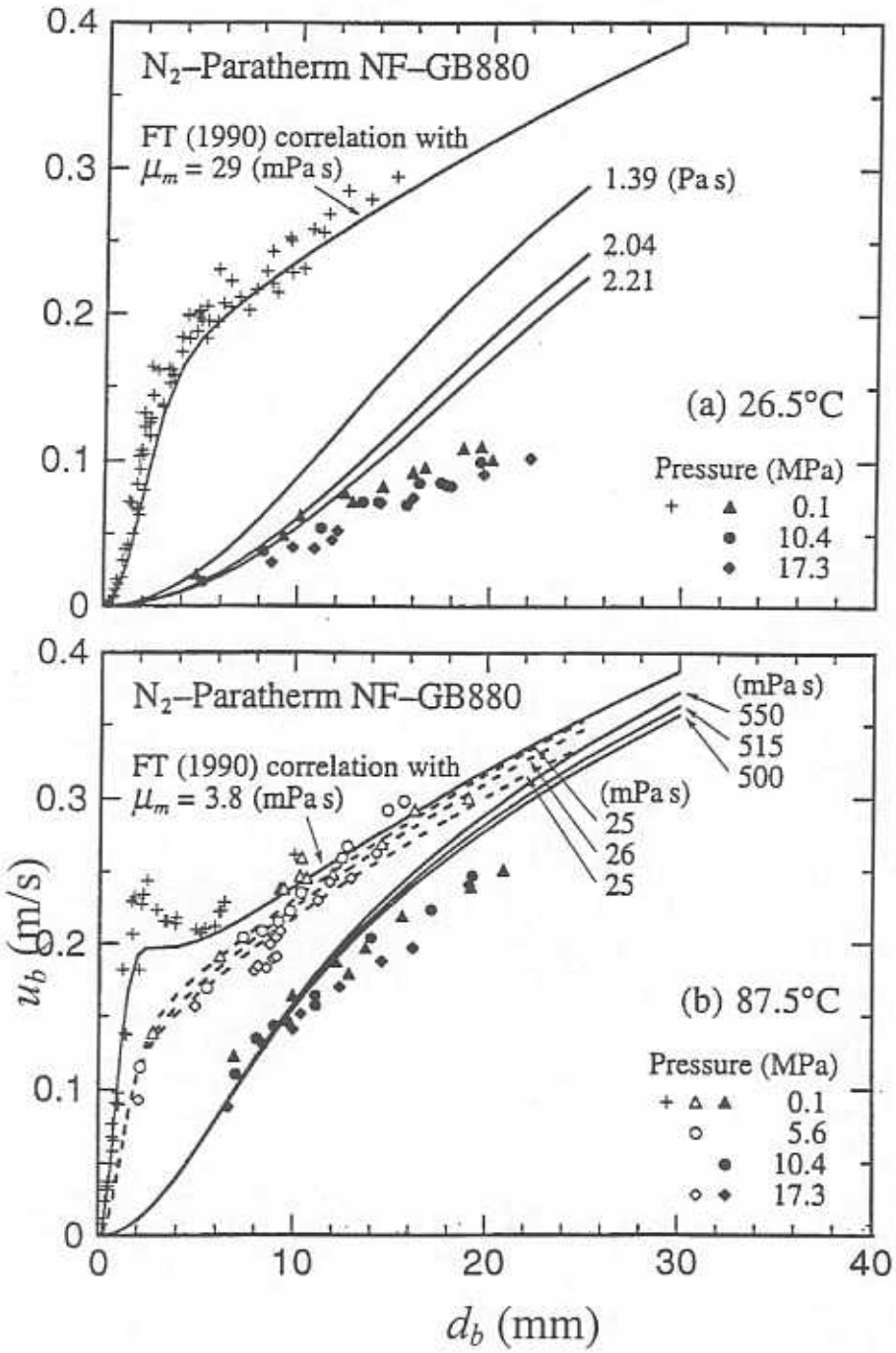
N2–Paratherm NF–GB880
FT (1990) correlation with
μm = 29 (mPa s)
1.39 (Pa s)
2.04
2.21
(a) 26.5°C
Pressure (MPa)
0.1
10.4
17.3
N2–Paratherm NF–GB880
FT (1990) correlation with
μm = 3.8 (mPa s)
(mPa s)
550
515
500
(mPa s)
25
26
25
(b) 87.5°C
Pressure (MPa)
0.1
5.6
10.4
17.3
ub (m/s)
db (mm)
0
0.1
0.2
0.3
0.4
10
20
30
40

Figure 3

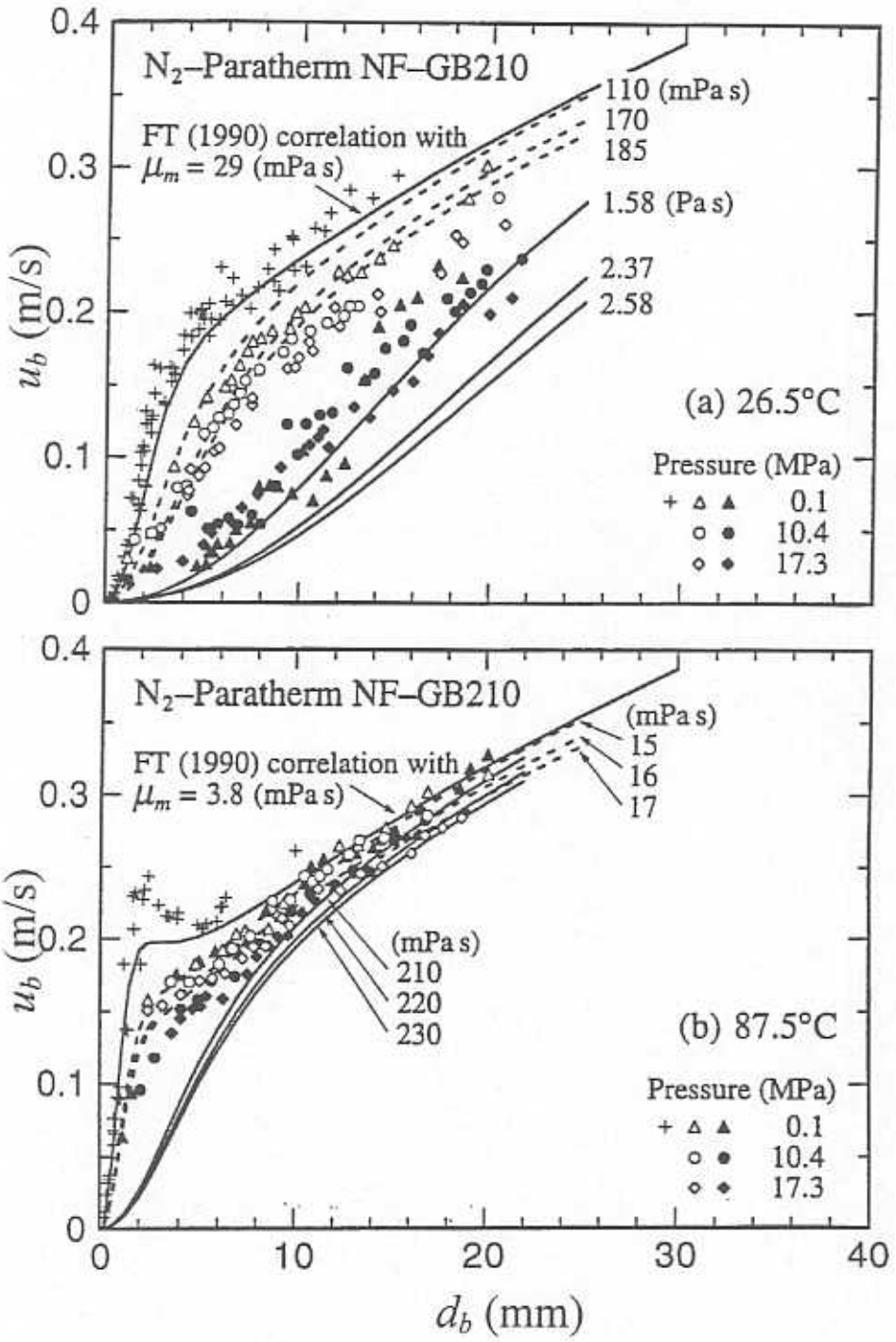
N2–Paratherm NF–GB210
FT (1990) correlation with
μm = 29 (mPa s)
110 (mPa s)
170
185
1.58 (Pa s)
2.37
2.58
(a) 26.5°C
Pressure (MPa)
0.1
10.4
17.3
N2–Paratherm NF–GB210
FT (1990) correlation with
μm = 3.8 (mPa s)
(mPa s)
15
16
17
(mPa s)
210
220
230
(b) 87.5°C
Pressure (MPa)
0.1
10.4
17.3
ub (m/s)
db (mm)
0
0.1
0.2
0.3
0.4
10
20
30
40

Figure 4

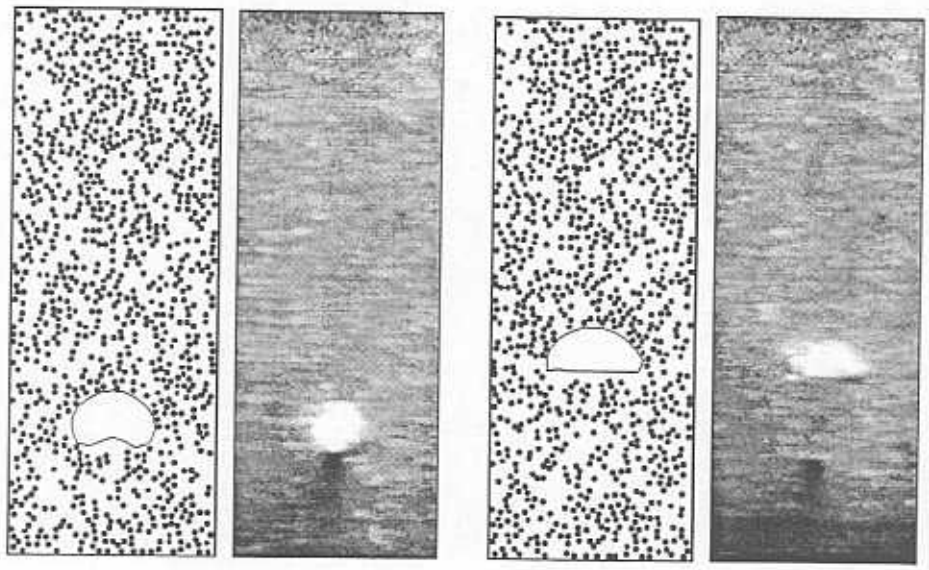

(a) $t = 0.06$ s (b) $t = 0.16$ s

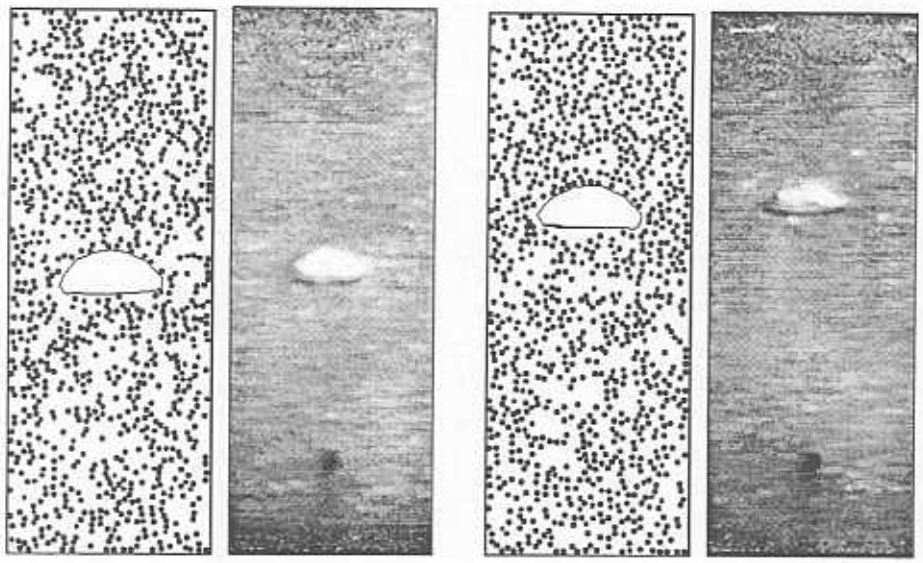

(c) $t = 0.26$ s (d) $t = 0.36$ s

Figure 5

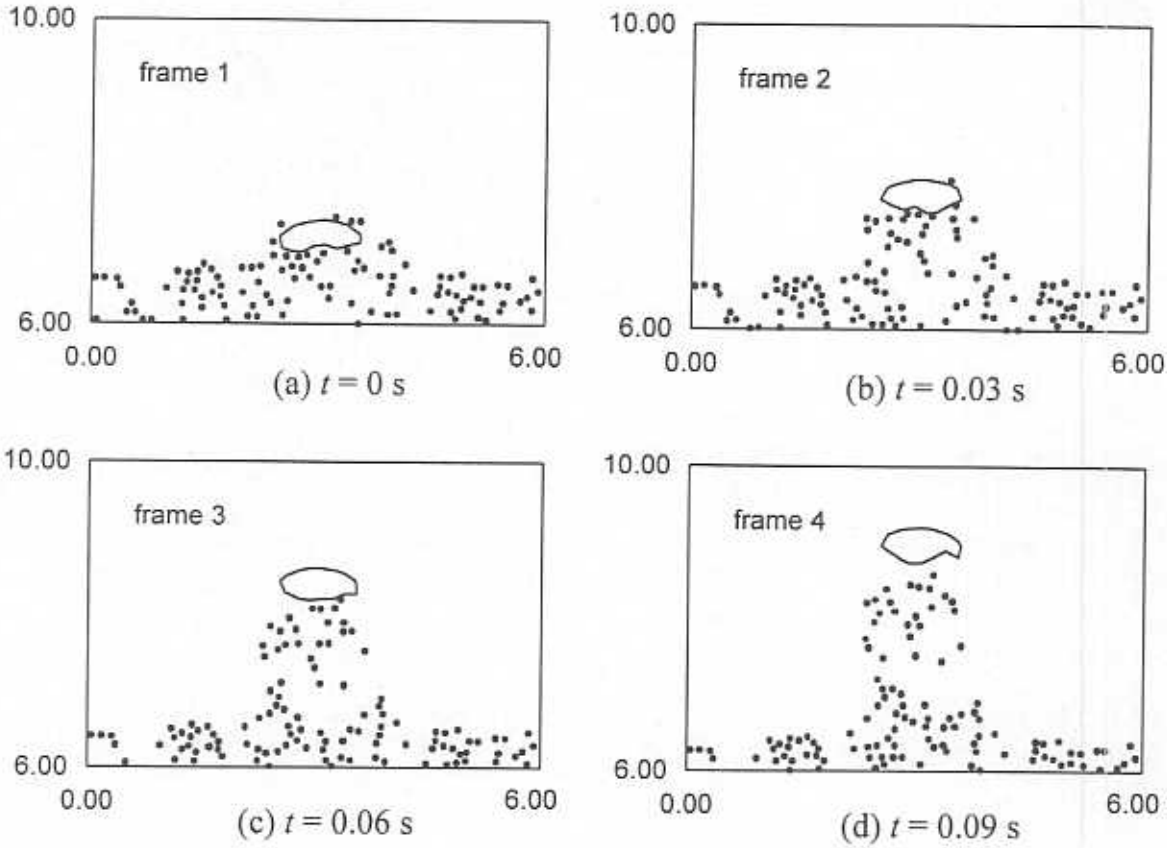
10.00
frame 1
6.00
0.00
6.00
(a) $t = 0$ s
10.00
frame 2
6.00
0.00
6.00
(b) $t = 0.03$ s
10.00
frame 3
6.00
0.00
6.00
(c) $t = 0.06$ s
10.00
frame 4
6.00
0.00
6.00
(d) $t = 0.09$ s

Figure 6

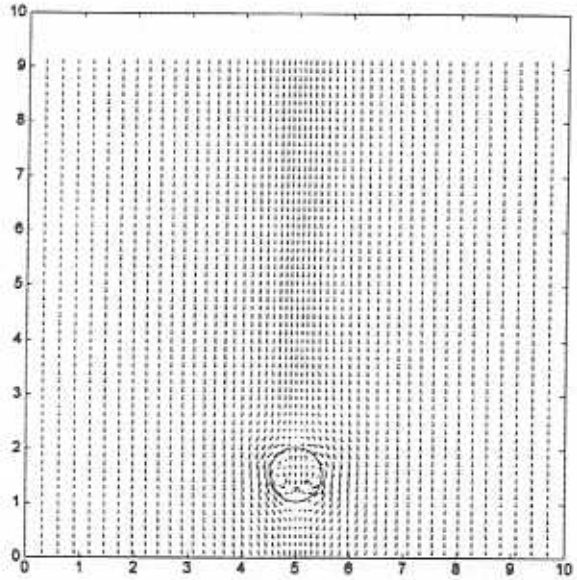

(a) $t = 0$ s

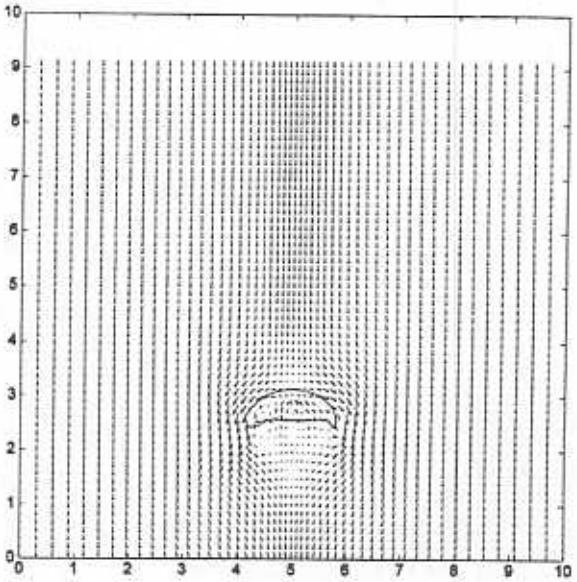

(b) $t = 0.06$ s

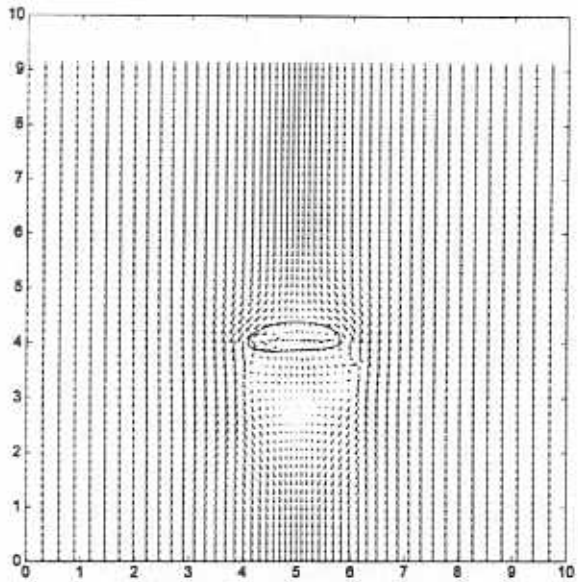

(c) $t = 0.12$ s

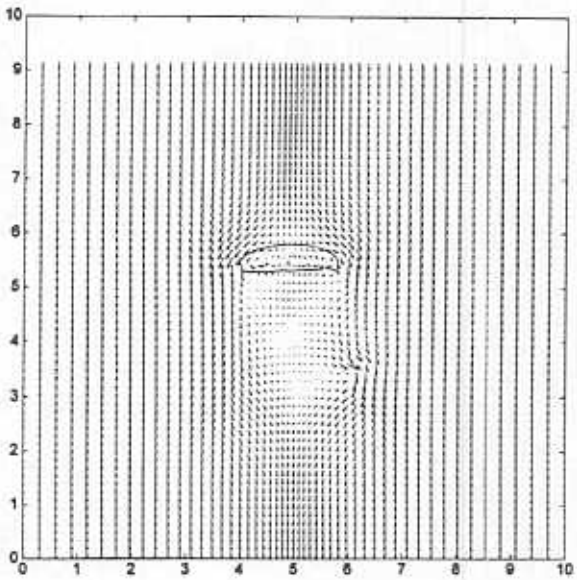

(d) $t = 0.18$ s

Figure 7

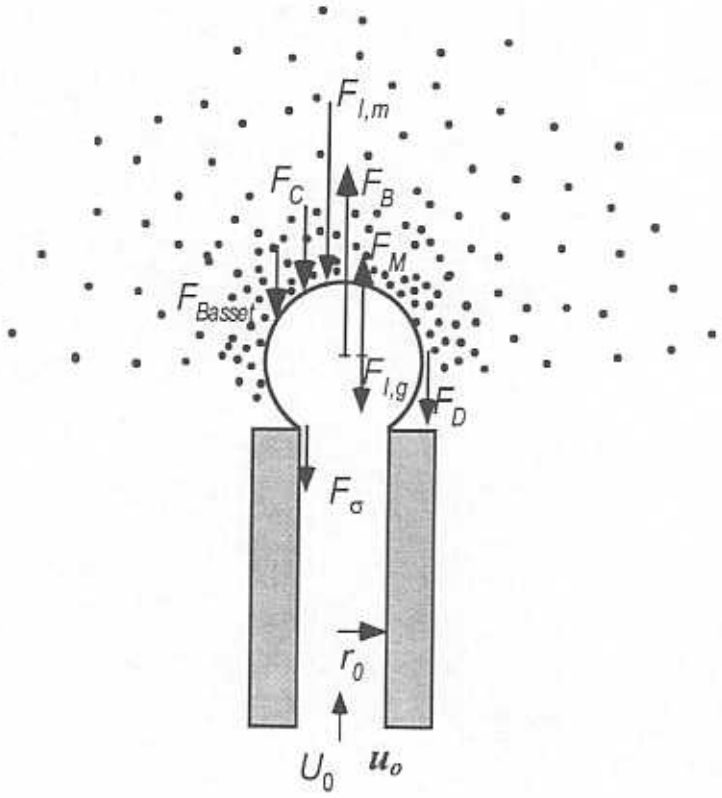

Figure 8

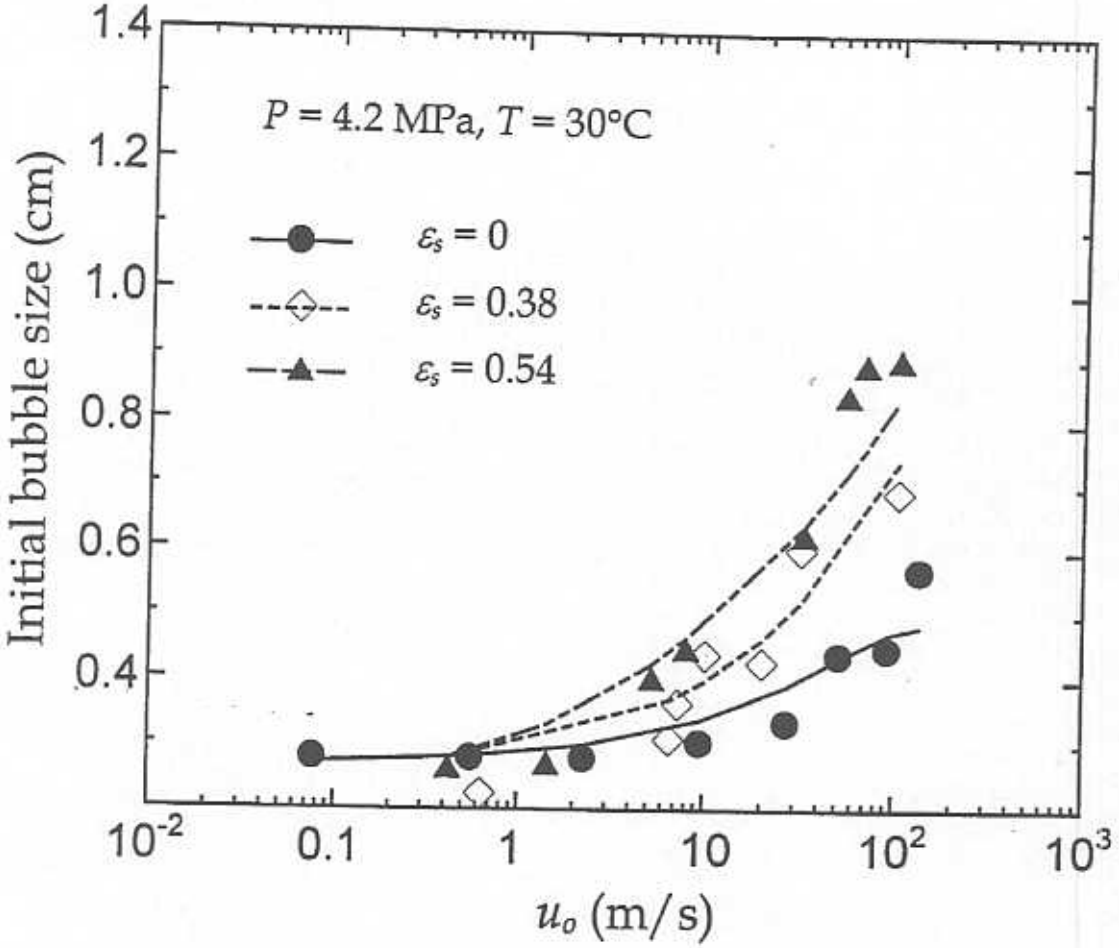
1.4
1.2
1.0
0.8
0.6
0.4
Initial bubble size (cm)
P = 4.2 MPa, T = 30°C
εs = 0
εs = 0.38
εs = 0.54
10-2
0.1
1
10
10²
10³
uo (m/s)

Figure 9

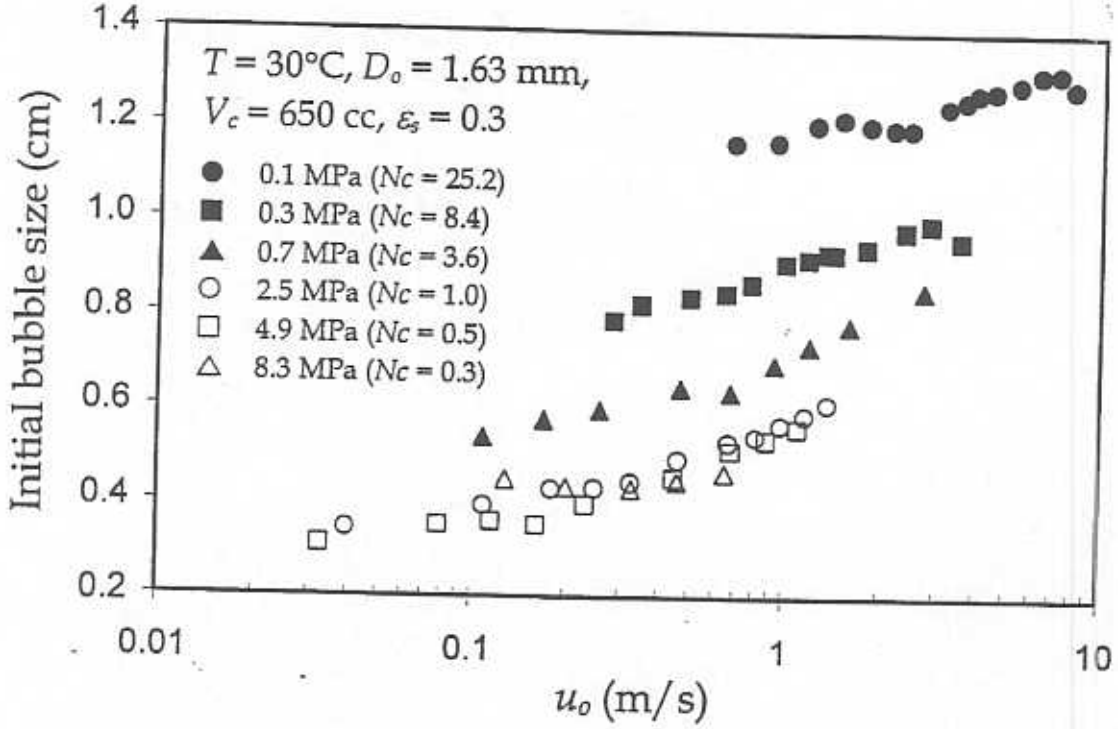
T = 30°C, D_o = 1.63 mm,
V_c = 650 cc, ε_s = 0.3
0.1 MPa (Nc = 25.2)
0.3 MPa (Nc = 8.4)
0.7 MPa (Nc = 3.6)
2.5 MPa (Nc = 1.0)
4.9 MPa (Nc = 0.5)
8.3 MPa (Nc = 0.3)
Initial bubble size (cm)
1.4
1.2
1.0
0.8
0.6
0.4
0.2
0.01
0.1
1
10
u_o (m/s)

Figure 10

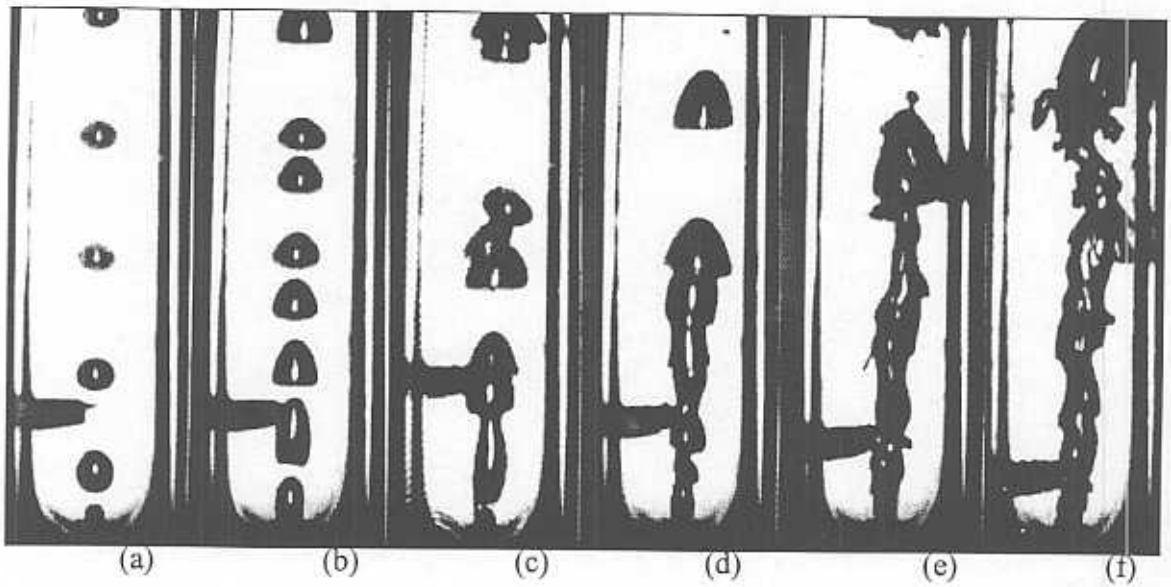

Figure 11

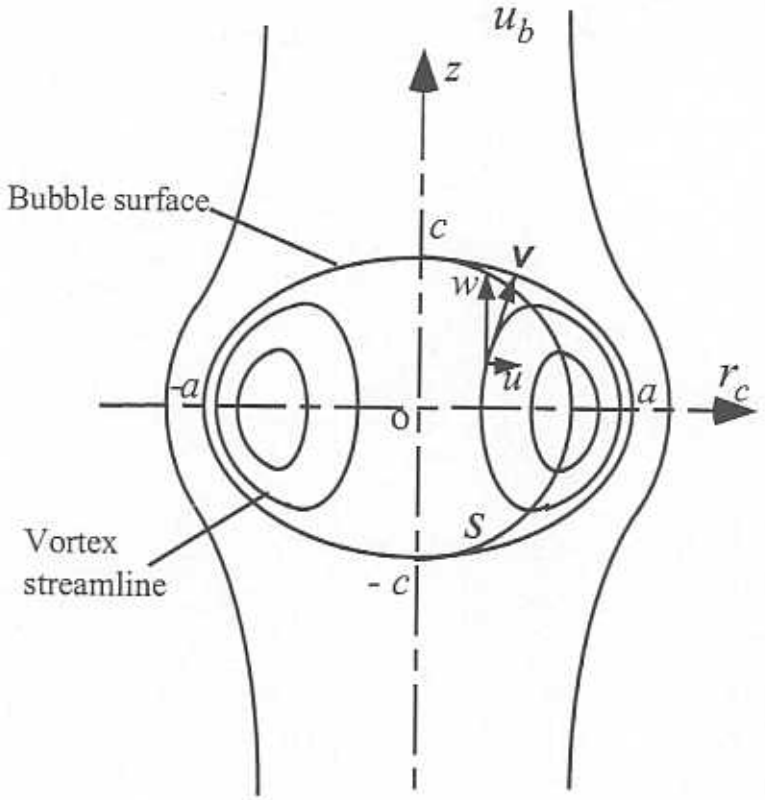

Figure 12

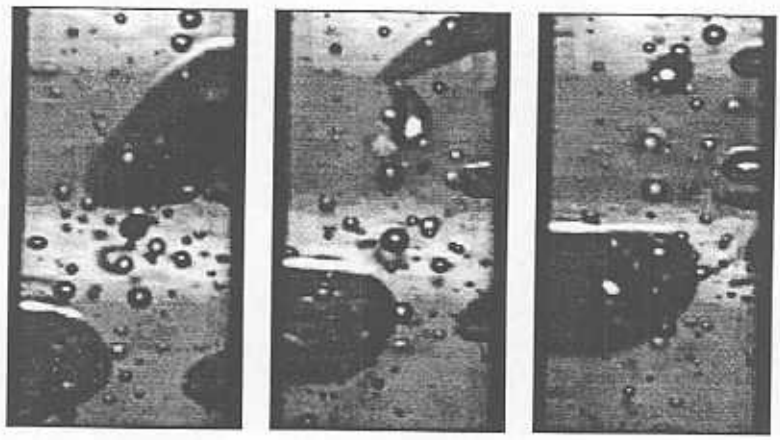

(a) $t = 0$ (b) $t = 0.017$ s (c) $t = 0.034$ s

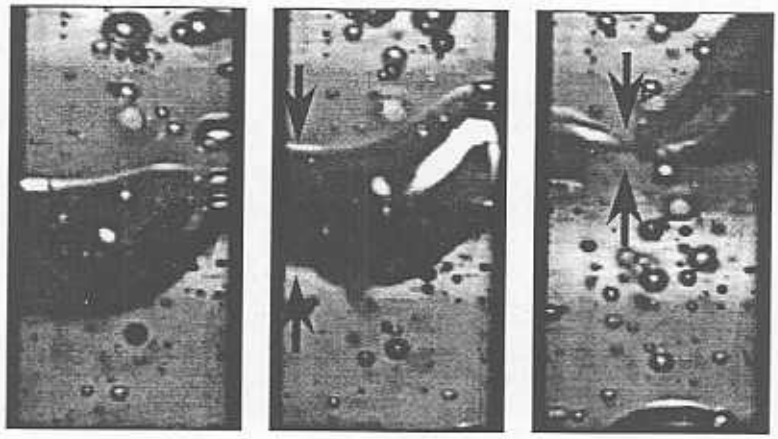

(d) $t = 0.052$ s (e) $t = 0.068$ s (f) $t = 0.085$ s

Figure 13

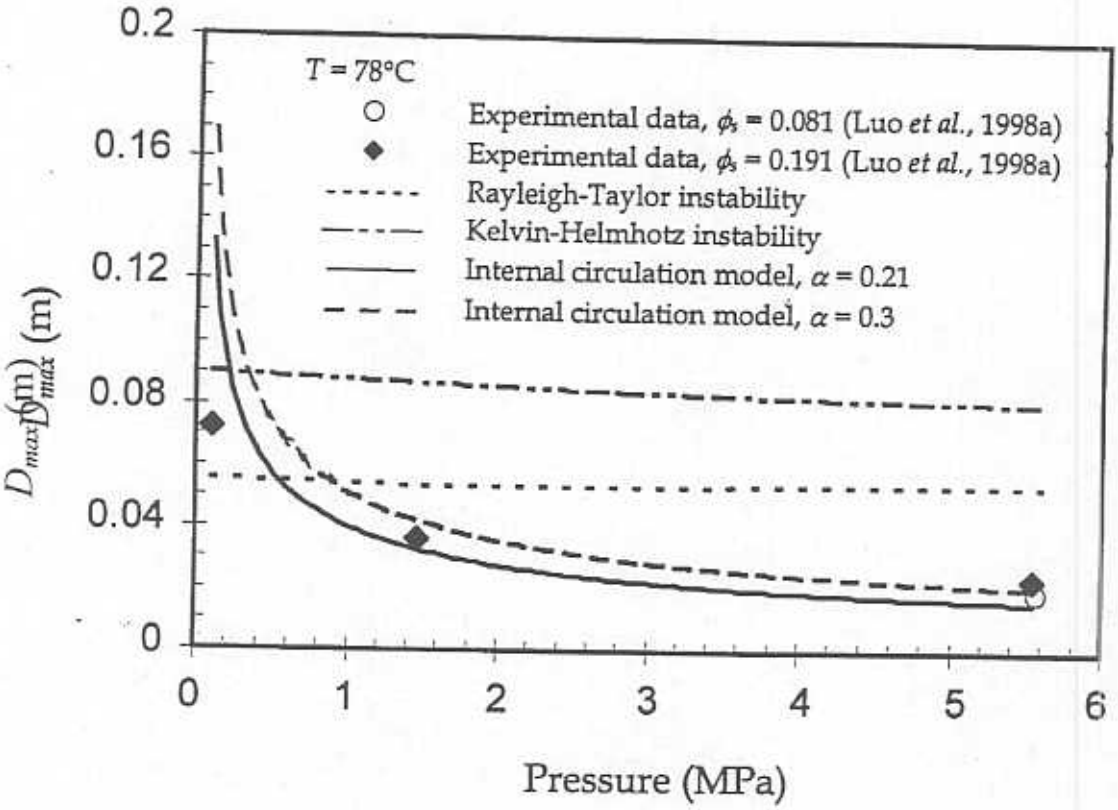
T = 78°C
Experimental data, ϕ_s = 0.081 (Luo et al., 1998a)
Experimental data, ϕ_s = 0.191 (Luo et al., 1998a)
Rayleigh-Taylor instability
Kelvin-Helmhotz instability
Internal circulation model, α = 0.21
Internal circulation model, α = 0.3
D_{max} (m)
0.2
0.16
0.12
0.08
0.04
0
0
1
2
3
4
5
6
Pressure (MPa)

Figure 14(a)

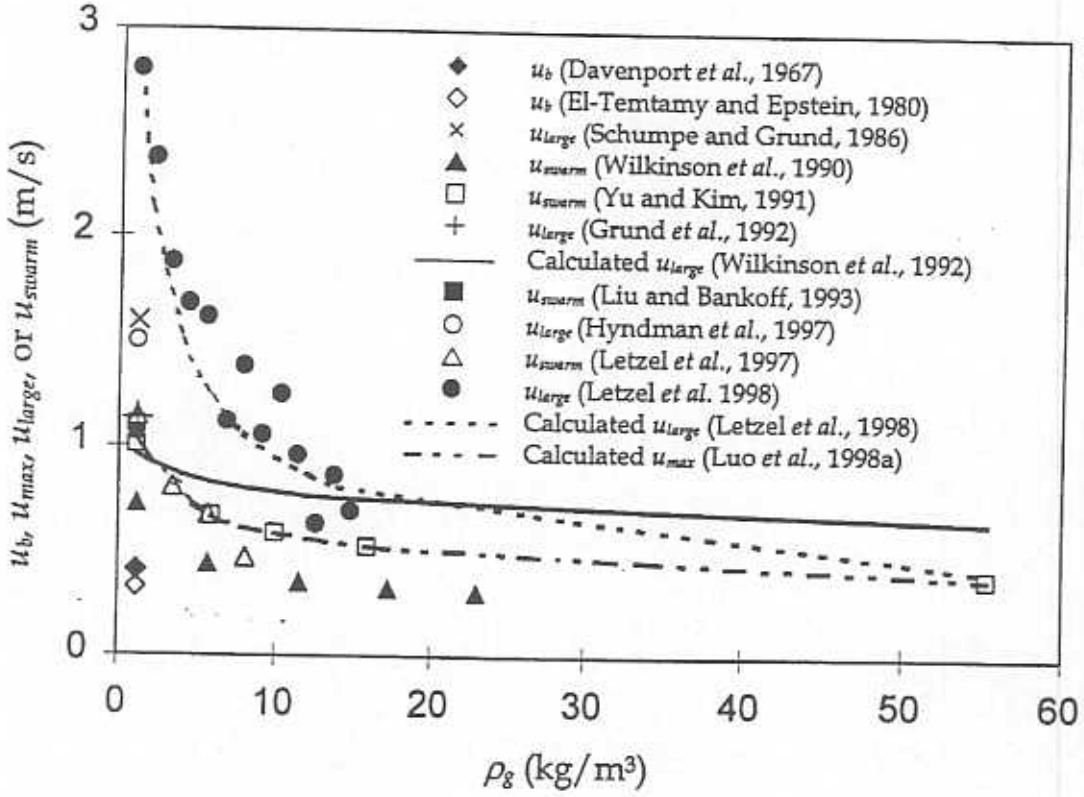
3
2
1
0
0
10
20
30
40
50
60
u_b, u_{max}, u_{large}, or u_{swarm} (m/s)
ρ_g (kg/m³)
u_b (Davenport *et al.*, 1967)
u_b (El-Temtamy and Epstein, 1980)
u_{large} (Schumpe and Grund, 1986)
u_{swarm} (Wilkinson *et al.*, 1990)
u_{swarm} (Yu and Kim, 1991)
u_{large} (Grund *et al.*, 1992)
Calculated u_{large} (Wilkinson *et al.*, 1992)
u_{swarm} (Liu and Bankoff, 1993)
u_{large} (Hyndman *et al.*, 1997)
u_{swarm} (Letzel *et al.*, 1997)
u_{large} (Letzel *et al.* 1998)
Calculated u_{large} (Letzel *et al.*, 1998)
Calculated u_{max} (Luo *et al.*, 1998a)

Figure 14(b)

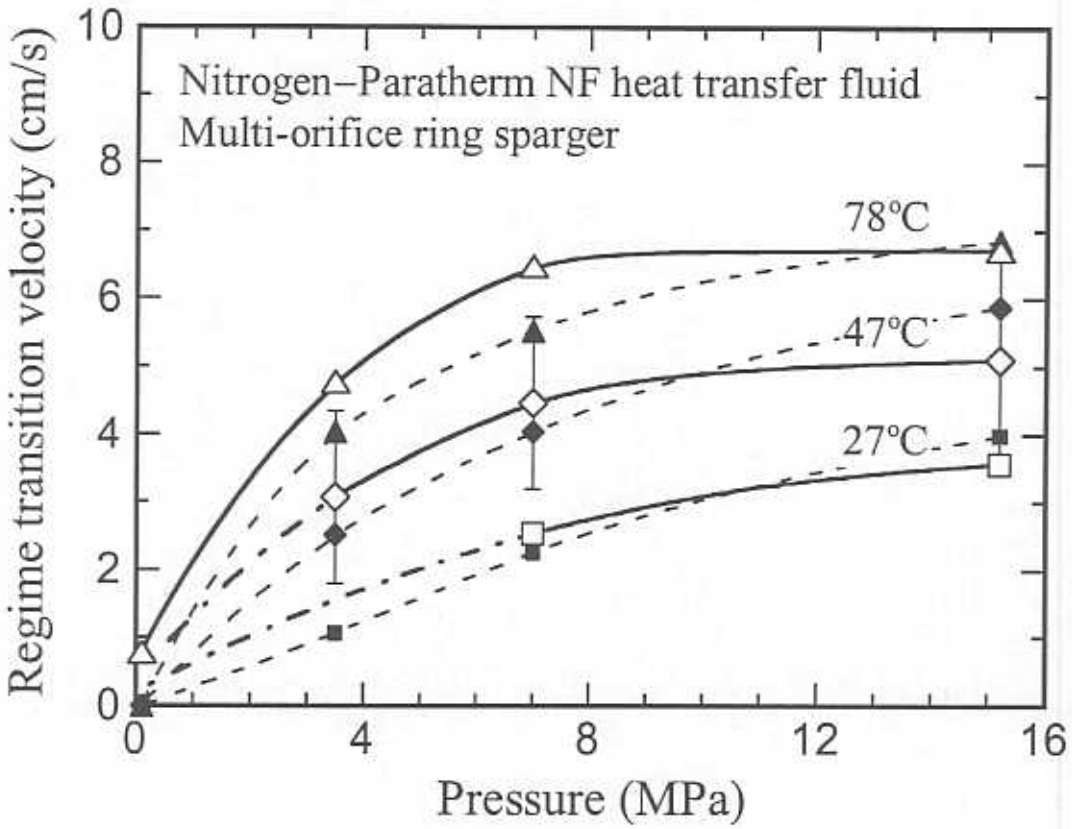
Nitrogen–Paratherm NF heat transfer fluid
Multi-orifice ring sparger
78°C
47°C
27°C
Regime transition velocity (cm/s)
Pressure (MPa)
0
2
4
6
8
10
0
4
8
12
16

Figure 15(a)

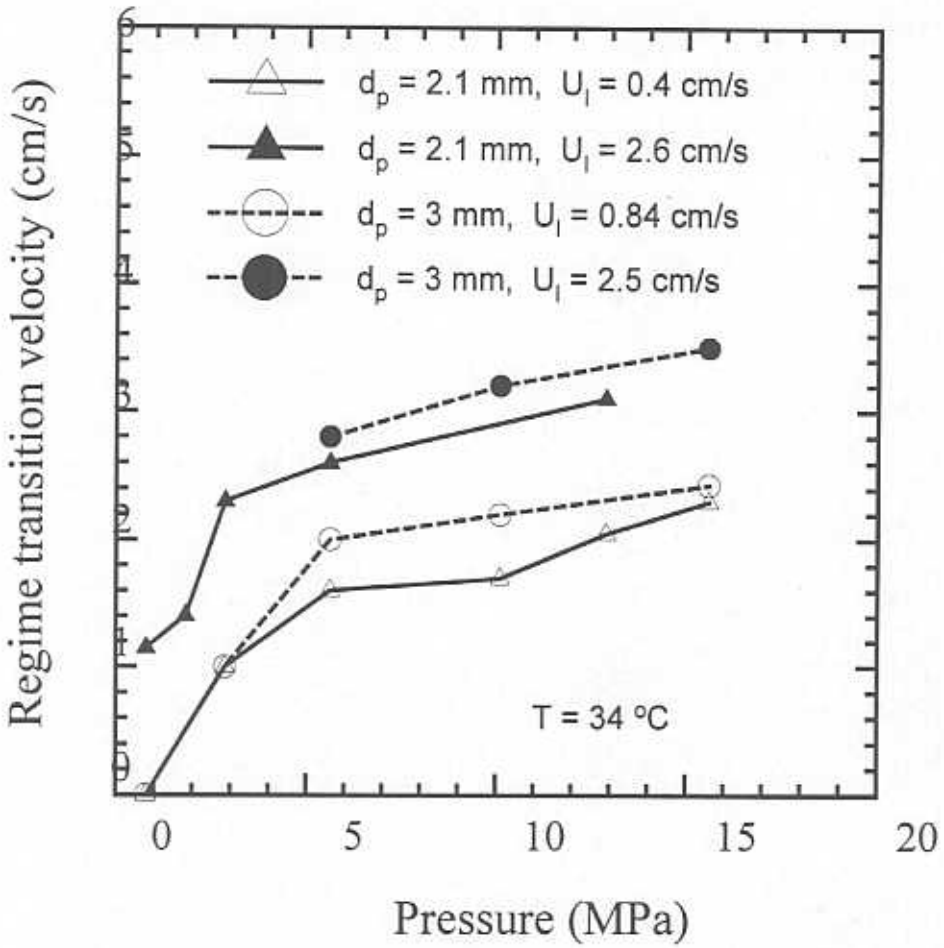
Regime transition velocity (cm/s)
d_p = 2.1 mm, U_l = 0.4 cm/s
d_p = 2.1 mm, U_l = 2.6 cm/s
d_p = 3 mm, U_l = 0.84 cm/s
d_p = 3 mm, U_l = 2.5 cm/s
T = 34 °C
0
5
10
15
20
Pressure (MPa)

Figure 15(b)

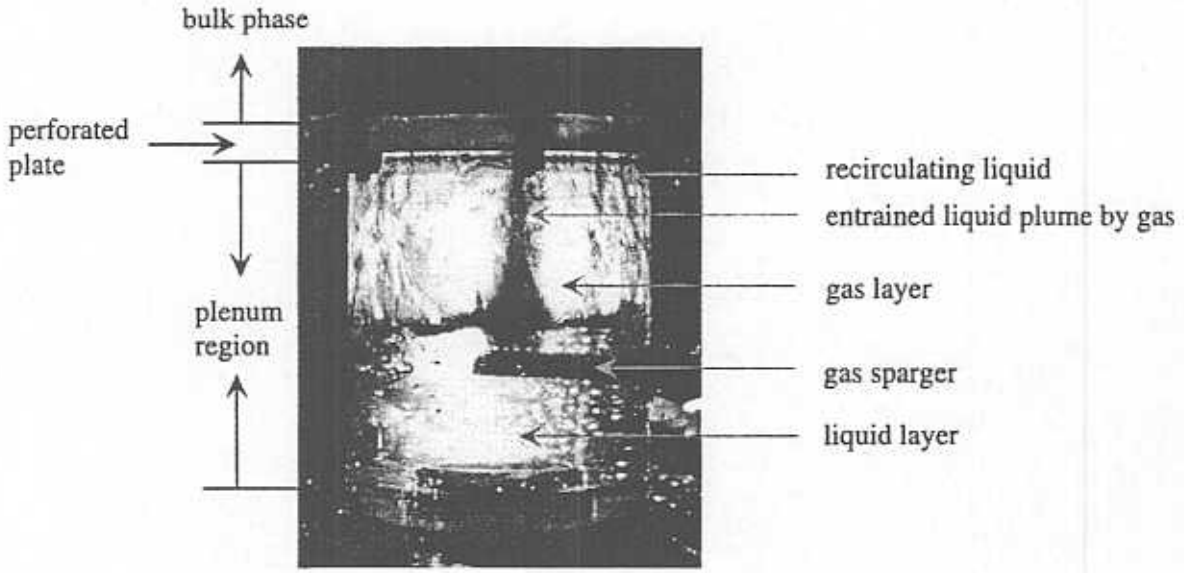
bulk phase
perforated plate
plenum region
recirculating liquid
entrained liquid plume by gas
gas layer
gas sparger
liquid layer

Figure 16

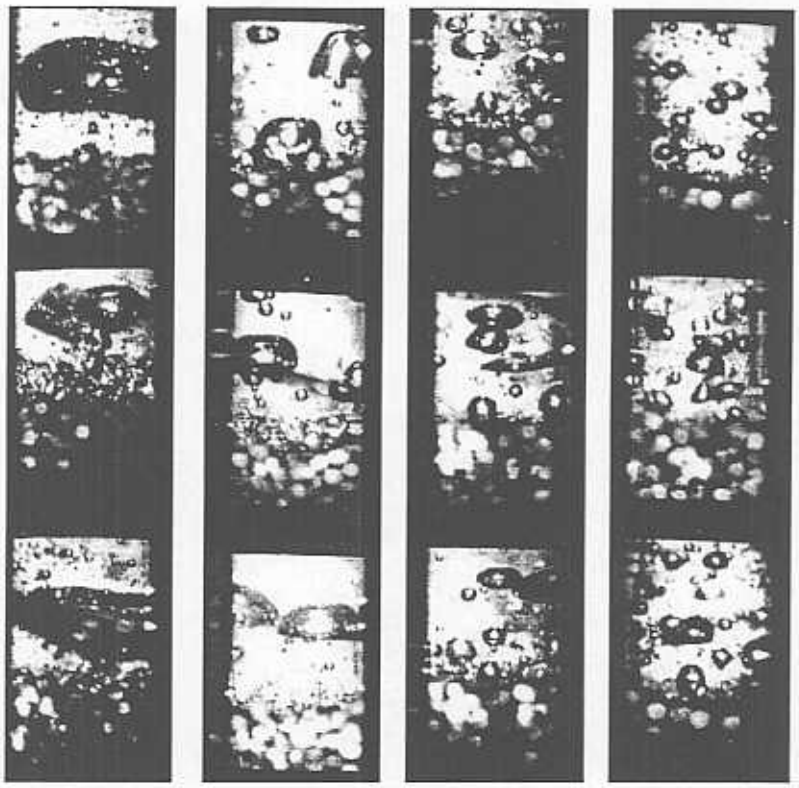

(a) (b) (c) (d)

Figure 17

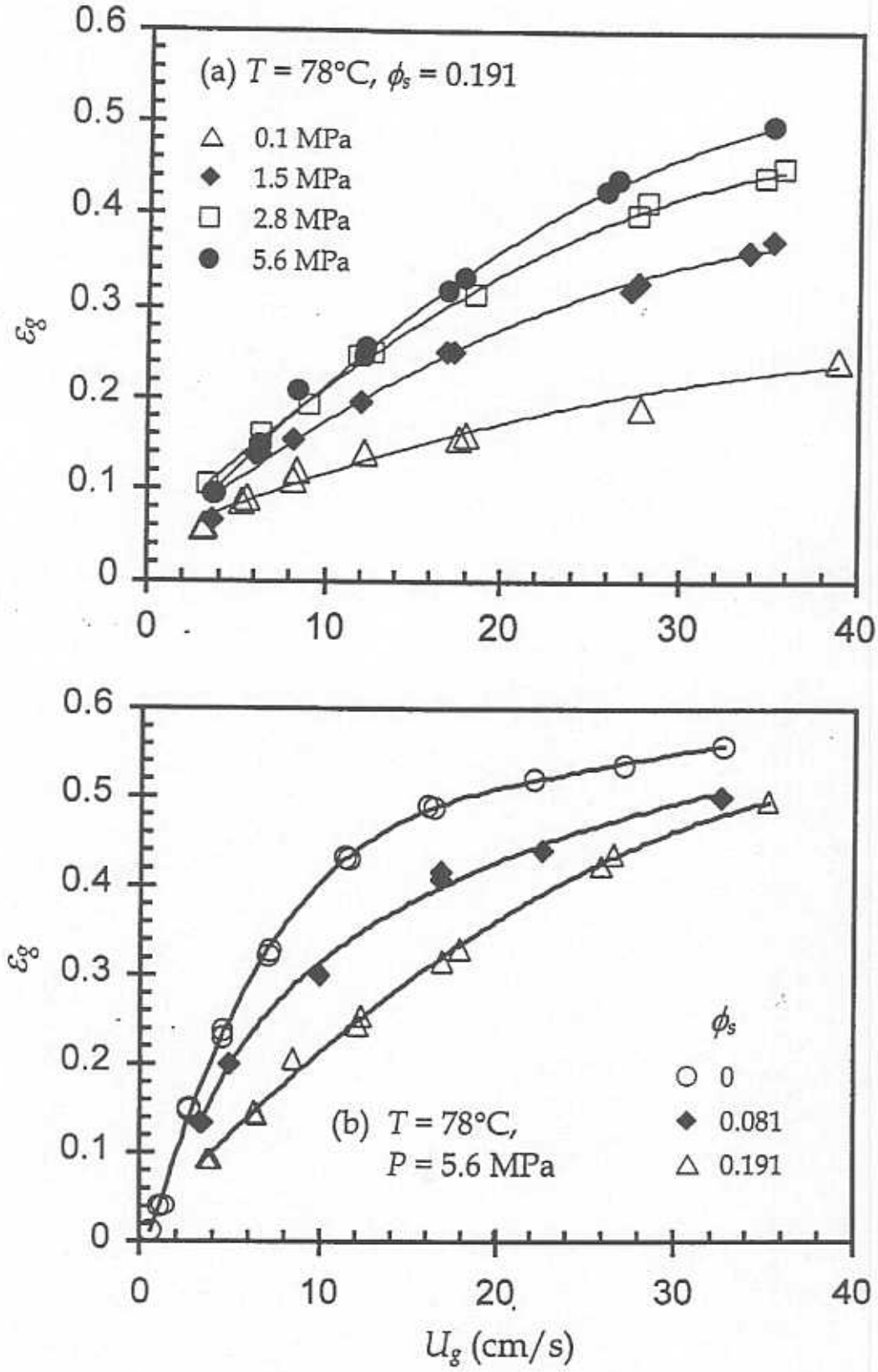
(a) T = 78°C, ϕ_s = 0.191
0.1 MPa
1.5 MPa
2.8 MPa
5.6 MPa
ε_g
0.6
0.5
0.4
0.3
0.2
0.1
0
0
10
20
30
40
(b) T = 78°C,
P = 5.6 MPa
ϕ_s
0
0.081
0.191
U_g (cm/s)

Figure 18

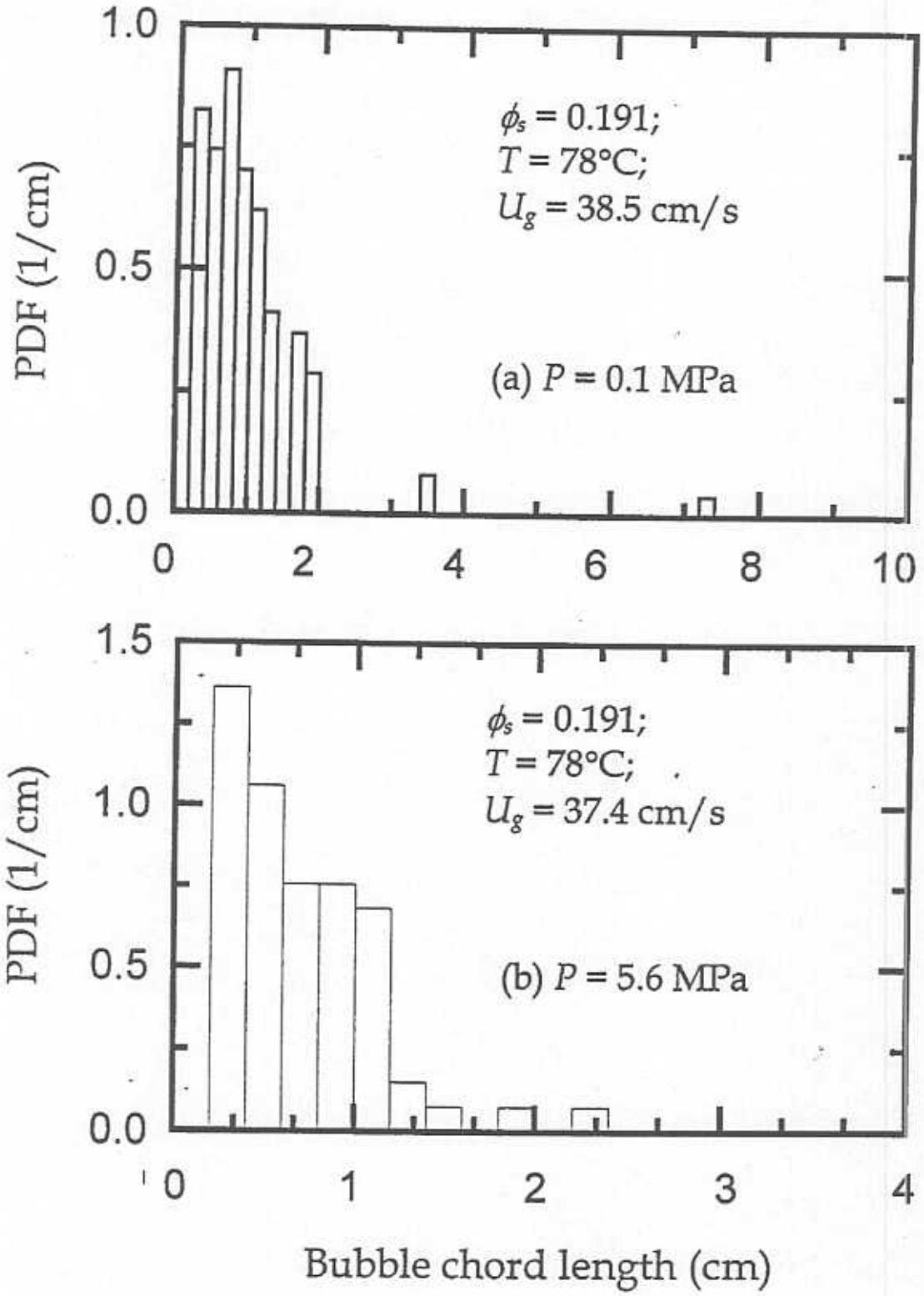
1.0
0.5
0.0
PDF (1/cm)
ϕ_s = 0.191;
T = 78°C;
U_g = 38.5 cm/s
(a) P = 0.1 MPa
0
2
4
6
8
10
1.5
1.0
0.5
0.0
PDF (1/cm)
ϕ_s = 0.191;
T = 78°C;
U_g = 37.4 cm/s
(b) P = 5.6 MPa
0
1
2
3
4
Bubble chord length (cm)

Figure 19

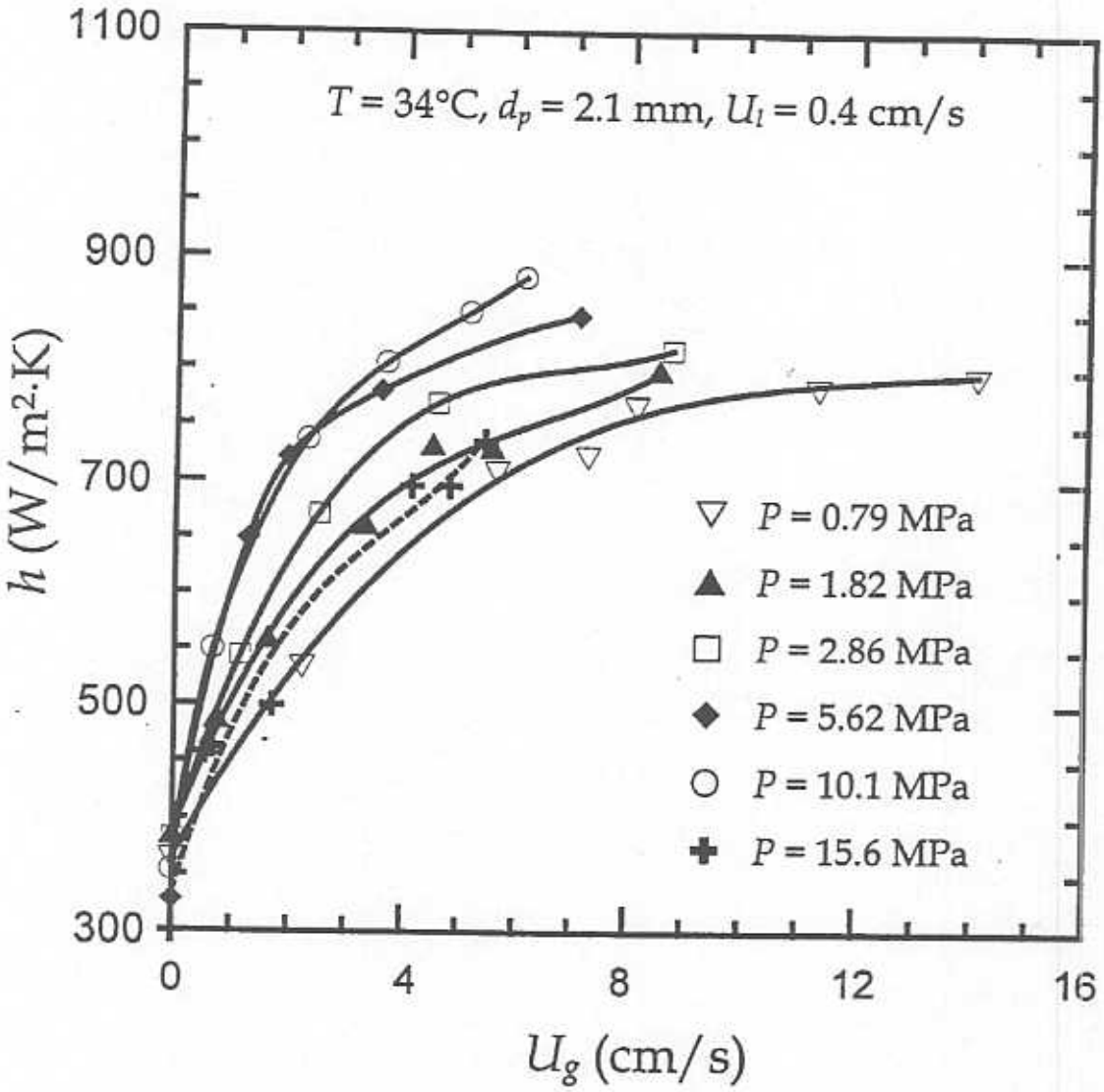
T = 34°C, d_p = 2.1 mm, U_l = 0.4 cm/s
h (W/m²·K)
1100
900
700
500
300
0
4
8
12
16
U_g (cm/s)
P = 0.79 MPa
P = 1.82 MPa
P = 2.86 MPa
P = 5.62 MPa
P = 10.1 MPa
P = 15.6 MPa

Figure 20

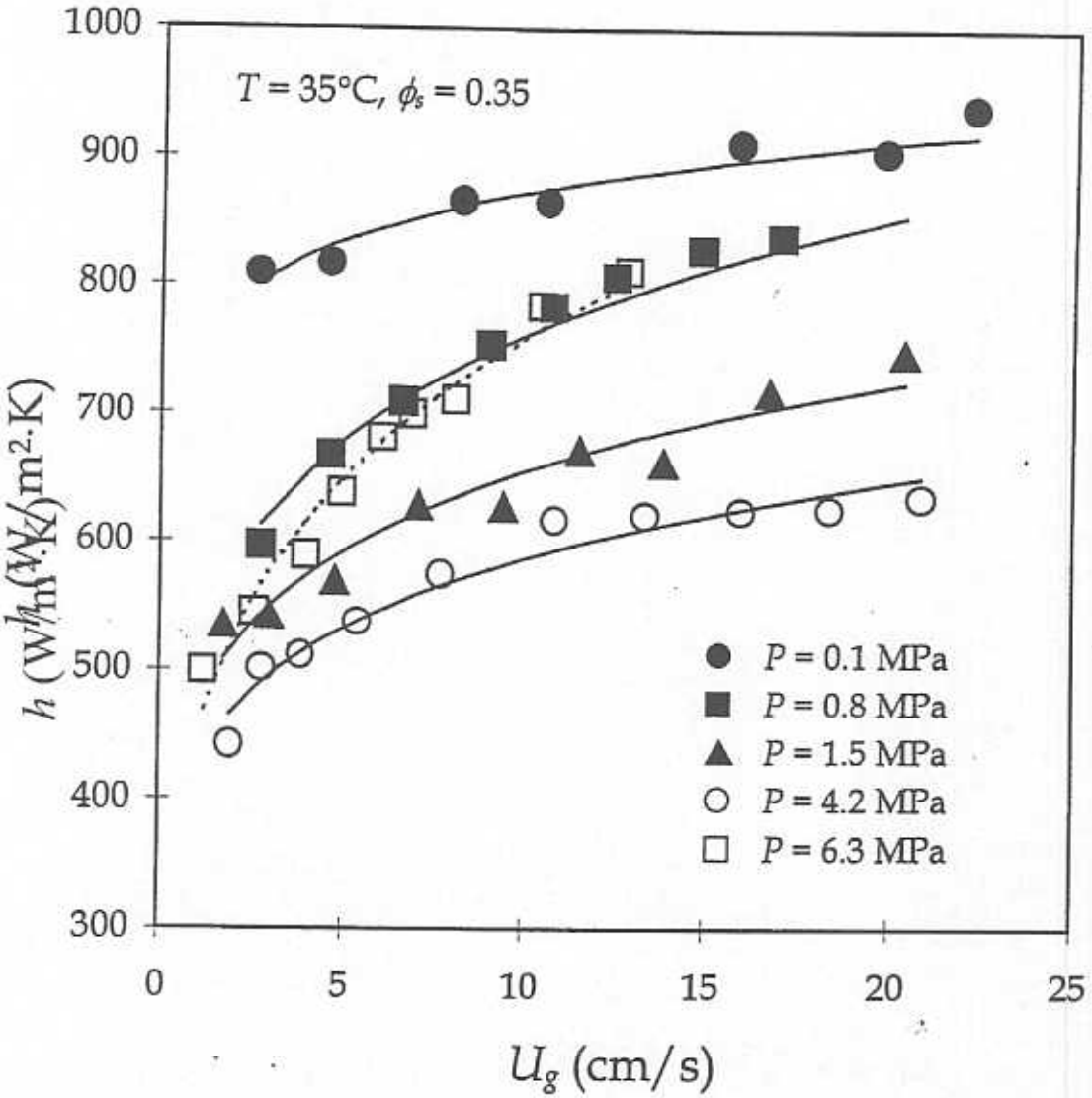
T = 35°C, ϕ_s = 0.35
h (W/m²·K)
U_g (cm/s)
P = 0.1 MPa
P = 0.8 MPa
P = 1.5 MPa
P = 4.2 MPa
P = 6.3 MPa
1000
900
800
700
600
500
400
300
0
5
10
15
20
25

Figure 21